CDOT-CU-R-94-8

A CASE STUDY OF CONCRETE DECK BEHAVIOR IN A FOUR-SPAN PRESTRESSED GIRDER BRIDGE: CORRELATION OF FIELD TESTS AND NUMERICAL RESULTS

by

Li Cao
John H. Allen
P. Benson Shing
University of Colorado

Dave Woodham
Colorado Department of Transportation

Report to the Sponsor:
Colorado Department of Transportation

April 1994
Department of Civil, Environmental,
& Architectural Engineering
University of Colorado
Boulder, CO 80309-0428
Research Series No. CU/SR-94/4

Colorado Department of Transportation

Technical Report Documentation Page

1. Report No.	2. Government Accession No.	3. Recipient's Catalog No.
CDOT-CU-R-94-8		

4. Title and Subtitle	5. Report Date
A Case Study of Concrete Deck Behavior in a Four-Span Prestressed Girder Bridge: Correlation of Field Tests and Numerical Results	April 1994
	6. Performing Organization Code: CU/SR-94/4
7. Author(s): Li Cao, John H. Allen, P. Benson Shing, and Dave Woodham	8. Performing Organization Rpt.No.: CDOT-CU-R 94-8
9. Performing Organization Name and Address: Department of Civil, Environmental, and Architectural Engineering, University of Colorado at Boulder, Boulder, CO. 80309-0428	10. Work Unit No. (TRAIS)
	11. Contract or Grant No.
12. Sponsoring Agency Name and Address: Colorado Department of Transportation, 4201 E. Arkansas Ave., Denver, CO. 80222	13. Type of Rpt. and Period Covered: Final Report
	14. Sponsoring Agency Code

15. Supplementary Notes

Prepared in Cooperation with the U.S. Department of Transportation Federal Highway Administration

16. Abstract

Cracking at the top of bridge decks exposes the top mat of reinforcing bars to chloride attack, which is a major cause of the deterioration of bridge decks. The top mat of reinforcement is required by the current AASHTO design code, in which the influence of girder flexibility on deck behavior is not considered. However, it has been observed that girder deflection reduces the tensile stresses developed at the top of bridge decks. As a result, the need for top reinforcing bars is questionable. To explore the possibility of eliminating top reinforcing bars and, thereby, reducing the vulnerability to deterioration, the behavior of a four-span highway bridge is being investigated.

In the four-span bridge deck studied, one span has an experimental deck which has no top reinforcement, while the remainder has both top and bottom reinforcement, which conforms to AASHTO Specifications and serves as a control. The response of the bridge deck under a test truck, which was 47% heavier than a standard HS20 truck, was monitored with imbedded strain gages. It was found that the peak transverse tensile strains developed at the top of the deck were less than 30% of the cracking strain. The behavior of the bridge deck under the test truck has also been analyzed with the finite element method. The numerical results correlate well with the test results.

The response of the deck under general truck loads has been analyzed with the validated numerical model, and the numerical results show that the tensile stresses developed at the top of the deck always tend to be much less than the modulus of rupture of the deck concrete. This study confirms the feasibility of eliminating most of the top reinforcement in bridge decks.

17. Key Words		18. Distribution Statement
Bridge Decks	Strain Gauges	No Restrictions: This report is available to the public through the National Technical Info. Service. Springfield, VA 22161
Corrosion	Finite Element Analysis	
Reinforced Concrete		

19.Security Classif. (report)	20.Security Classif. (page)	21. No. of Pages	22. Price
Unclassified	Unclassified	103	

Acknowledgments

The writers gratefully acknowledge the financial support and technical cooperation provided by the Colorado Department of Transportation for this study. The verification of the gage mounting techniques reported in Section 2.3.3 of this report was conducted by undergraduate assistants, Rebecca Matkins and Daniel Ott. However, opinions expressed in this report are those of the writers and do not necessarily represent those of the sponsor.

Contents

List of Figures

List of Tables

Chapter 1

INTRODUCTION

The deterioration of bridges in the United States is a serious problem. As bridges age, repair and replacement needs accrue. Forty percent of all bridge decks on the Federal-Aid System are between 15 and 35 years old. Most of the decks in these bridges were built without adequate cover or corrosion protection systems. Many of these decks need rehabilitation or replacement. It has been estimated that 41% of the nation's 578,000 bridges are either structurally deficient or functionally obsolete (USDOT 1989). An estimated investment of $51 billion is needed to bring all the nation's bridges to an acceptable and safe standard by either rehabilitation or replacement. It has also been estimated that an investment of $93 billion is required to eliminate existing and accruing bridge deficiencies through 2005 (USDOT 1989). Therefore, it is necessary to find a solution to prevent bridge decks from deterioration.

In North America, most short and medium span bridges are constructed as slab-on-girder bridges, where a reinforced concrete slab is supported by several steel or precast prestressed concrete girders. The slab is often connected to the girders by shear connectors. Most of these bridge decks were

designed according to AASHTO specifications, where the same design bending moment is used for the top and bottom transverse reinforcing bars of a slab. The required area of the top transverse bars is usually greater than the area of bottom transverse bars since greater top cover reduces the effective depth. In summary, the current bridge deck reinforcing practice is to place both an upper and a lower mat of reinforcing bars. The upper mat contains a top layer of transverse reinforcing bars over a longitudinal layer of bars.

Recently, it has been observed that shrinkage cracks often occur over the upper transverse bars, permitting increased exposure to deleterious substances such as de-icing chemicals. However, longitudinal cracks are not prevalent over the girders. Investigations on the behavior of bridge decks by Beal (1982) and Fang et al. (1990) have shown that the negative bending moments in bridge decks and the resulting top tensile stresses are usually very low, much less than the positive bending moments and the resulting bottom tensile stresses. Analysis of their work and other empirical evidence by Allen (1991) indicates that the tensile strength of deck concrete greatly exceeds the top tensile stresses that could be induced by truck loads. This can be attributed to the deflection of girders, which can greatly reduce the negative bending moments in the slab over the supporting girders and, thereby, the top tensile stresses in the slab.

With the above observations, one may choose to eliminate the entire upper mat of reinforcing bars in a deck. This can reduce maintenance problems and prolong the service life of a deck, as the top reinforcing bars are generally most susceptible to corrosion. To explore this new design concept, a collaborative research project has been initiated by the Colorado Department of Transportation, the University of Colorado, and Allen Research & Development, Corp. In this study, an experimental bridge deck was designed and

constructed without top reinforcement for an end span of a four-span bridge on Colorado State Route 224 over South Platte River. The main objective of this project is to assess the maximum tensile stresses that can be developed in such a deck and the durability of a deck that has no top reinforcement.

The investigation is divided into two parts. The first part consists of the development of a finite element model of the prototype bridge deck for evaluating the response of the deck under truck loads. Results of this study have been documented in the report by Cao, Allen, and Shing (1993). The second part of the investigation involves the instrumentation of the experimental bridge deck and monitoring the response of the bridge under a test truck and normal traffic load conditions, as well as the correlation of the field test results with the finite element model.

This report describes the instrumentation of the bridge deck and the response of the deck to a test truck. The response of the bridge deck under a test truck was monitored with embedded strain gages. The test truck was placed at nineteen different locations on the bridge to simulate the critical loading conditions for the deck. The test results were compared to numerical results obtained with the finite element models developed in the first phase of the study.

Chapter 2

DESCRIPTION OF BRIDGE DECK AND FIELD TESTS

2.1 Bridge Deck Configuration and Material Properties

The bridge selected for this project is located on Colorado State Route 224 over South Platte River near Commerce City. It is a 420-ft-long and 52-ft-wide bridge. The superstructure consists of four equal continuous spans. The supporting girders are standard precast Colorado Type G-54 girders spaced at approximately eight feet on center. The thickness of the bridge deck is 8.0 inches, which complies with the new design requirement adopted by the Colorado Department of Transportation. The configuration of the four-span bridge is shown in Fig. 2.1.

In the four-span deck, the west span is the experimental deck which has no top reinforcement. The remaining three spans have both top and bottom reinforcement, conforming to AASHTO Specifications (AASHTO 1989). The deck in the east span is the control deck. Both the experimental and control decks are instrumented with strain gages.

In the control deck, the top and bottom transverse reinforcement consists of No.5 bars with a 5.5-in center-to-center spacing. The top longitudinal reinforcement consists of No.5 bars with an 18-in center-to-center spacing, and the bottom longitudinal reinforcement consists of No.5 bars with a 9.5-in center-to-center spacing. The clear covers over the top and bottom reinforcing steel are 2.5 and 1.0 inches, respectively.

The experimental deck consists of the entire west span and 38-ft of the adjacent span. The reinforcement of the experimental deck is based on a new design approach, in which the top reinforcement is eliminated. As a result, no top reinforcing steel was placed in the experimental deck, except that there are short transverse bars placed in the cantilever overhangs supporting the railings. Furthermore, in both the experimental and control decks, longitudinal reinforcing bars are placed across the piers with a 9-in center-to-center spacing and a 3-in minimum cover. The reinforcing details of the control and experimental decks are shown in Fig 2.2.

The bridge was constructed in two phases to facilitate the flow of traffic. The phase-one portion of the deck consists of a 34-ft-wide slab supported over five girders. It was cast in January, 1993. The phase-two portion of the deck was cast in July, 1993.

Before the phase-one portion of the bridge was open to traffic, a load test was conducted. But the data collection system did not function properly during this test and the results were abandoned. The second test was conducted in September, 1993 with the complete bridge temporarily closed to traffic. At the time of the second load test, cracking in the deck was noted and marked prior to the test. After the test, the cracking patterns marked earlier with paint were checked, and no changes were noted. In December, 1993, the crack patterns in the deck were checked again. Unfortunately, most

of the marking had been worn away by traffic, and changes in the spacing, length, and width of cracks could not be accurately assessed.

A small amount of fiber was added to the deck concrete to reduce temperature and shrinkage cracks. The specified design strength for the deck concrete was 4,500 psi. The concrete mix consisted of the following ingredients per cubic-yard: 507 lb of cement (Type I/II), 56 lb of fly-ash, 1800 lb of intermediate aggregate (0.75 in), 1240 lb of sand, 1.5 lb of fiber (polypropylene), with a water-cement ratio of 0.47.

With the lab-cured specimens of deck concrete, the average 28-day compressive strength and the modulus of rupture obtained are 5,740 psi and 590 psi, respectively, and the 33-day split-cylinder strength is 350 psi. The average 28-day compressive strength of lab-cured specimens of girder concrete is 8,500 psi. The results of material tests conducted on deck concrete are summarized in Tables 2.1 and 2.2.

To determine the elastic modulus of the deck concrete, two 4" $\times$ 8" field-cured cylinders were tested in the laboratory in accordance with the specifications of ASTM-C469. The average compressive strength of the two cylinders is 5,100 psi, but the measured modulus of elasticity is much lower than that evaluated with the formula given in ACI 318-89 (which is $E_c = 57,000\sqrt{f'_c}$). Therefore, these test results were abandoned.

For the stress analysis of the deck, the ACI formula is used to estimated the modulus of elasticity for both the deck and girder concrete. The elastic modulus is 4,230 ksi for the deck concrete, with the compressive strength assumed to be 5,500 psi. The elastic modulus of the girder concrete is calculated to be 5,260 ksi, with the compressive strength assumed to be 8,500 psi.

Table 2.1: Compressive Strength of Lab-Cured Concrete (psi)

Samples	7-day Deck Conc.	28-day Deck Conc.	28-day Girder Conc.
1	4350	5650	9400
2	4390	5330	9300
3	4270	5570	8890
4	4280	5060	8200
5	4960	5180	8010
6	5010	5270	8380
7	4710	5890	8630
8	4740	6050	8840
9	4920	5870	7610
10	5000	5920	7220
11		6030	7740
12		5870	7870
13		5980	8740
14		6240	8400
15		6110	8700
16			8620
17			8930
18			8820
19			8600
20			9240
Average	4663	5735	8507
Std. Deviation	295	357	568

Table 2.2: Tensile Strength of Lab-Cured Deck Concrete (psi)

Samples	Modulus of Rupture Tests		Split-Cylinder Tests	
	7-day	28-day	33-day	56-day
1	483	542	340	530
2	534	591	345	600
3	524	639	360	555
Average	514	591	348	562
Std. Devi.	22	40	9	29
ACI Formula	512	568	–	–

2.2 Test Truck and Truck Load Positions

As shown in Fig. 2.3, the test truck used for the field tests included a front axle transmitting a force of 16.5 kips. The total force transmitted by the rear tandem axles of the test truck was 56.65 kips and the total forces exerted by the trailing axles was 32.75 kips. The total weight of the test truck was 106 kips, which is 47% more than a conventional HS20 truck. The axle and wheel spacings of the test truck were similar to those of a standard HS20 truck.

To investigate the maximum tensile stresses that could be developed in the transverse direction at the top of the deck, it was decided that the test truck should be positioned at three different locations along the longitudinal direction of the bridge. The first truck position was close to the abutment at the west end, with the resultant rear tandem axle load approximately 8-ft away from the abutment. The deflection of the girders was small when the truck was at this position. The trailing axles and the front axle were not used in this load case, since it is expected that these axle loads will increase the

girder deflection and, thereby, decrease the top transverse tensile stresses. The wheels of the test truck were positioned at six different locations along the transverse direction, as illustrated in Fig. 2.4. This is identified as Load Group 1.

The second truck position in the longitudinal direction was near the mid-span of the deck at the west span, with the resultant rear tandem axle load approximately 44-ft away from the abutment. This induced differential deflections among the girders. The test truck was placed transversely in seven different positions, as illustrated in Fig. 2.5. This is identified as Load Group 2.

The third truck load position in the longitudinal direction was in the vicinity of the pier at the west span, with the resultant rear tandem axle load approximately 6-ft away from the pier. Along the transverse direction, the wheels of the test truck were positioned at six different locations, as shown in Fig. 2.6. This is identified as Load Group 3.

The above truck load positions were determined from the results of finite element analysis (Cao, Allen and Shing 1993). In addition to these three positions, the test truck was also placed on the control deck. Load Groups 4 and 5 correspond to the mid-span and abutment positions in the east span, which are similar to Load Groups 2 and 1, respectively.

2.3 Instrumentation

2.3.1 Strain Gages

The response of the bridge deck under the test truck was monitored by strain gages embedded at different locations in the deck. These locations were determined from the results of finite element analysis (Cao, Allen and Shing

1993). From the finite element analysis, it was found that when the model truck is close to the abutment as shown in Fig. 2.4, the maximum transverse tensile stress at the top of the deck occurs between the two tandem axles at a section which is about 6-ft away from the abutment. As indicated by the analysis, from the truck position which produces the maximum transverse stress, moving the truck back and forth by 2 feet does not increase the maximum transverse tensile stress at the top of the deck.

When the model truck is near the mid-span of the deck as shown in Fig. 2.5, the maximum transverse tensile stress at the top of the deck occurs between the two rear tandem axles at a section which is 42-ft away from the abutment. When the model truck is in the vicinity of the pier as shown in Fig. 2.6, the maximum transverse tensile stress at the top of the deck occurs beneath the second axle of the rear tandem axles at a section which is 8-ft away from the pier.

The above analysis provided guidelines for determining the locations of the strain gages to be installed in the bridge. As a result, five gage lines were selected, as shown in Fig. 2.7. The first three gage lines are located in the experimental deck and the other two gage lines are located in the control deck. In the experimental deck, the first and second gage lines are 6-ft and 44-ft away from the abutment, respectively. The third gage line is 8-ft away from the pier. Gage Lines 4 and 5 are identical to Gage Lines 2 and 1, but are located in the control deck.

There are seven gage points (A through G) along each of the above transverse gage lines, as shown in Fig. 2.7. Each gage point usually has top and bottom gages, which are oriented in either the transverse or longitudinal direction of the deck. The top and bottom gages are about 1-in away from the top and bottom surfaces of the deck. The strain gages were welded on

21-in-long No.4 bars with anchoring hooks, which were embedded in deck concrete, as shown in Fig. 2.8.

The actual positions of the strain gages were measured before deck concrete was cast. The distances from the center of an embedded bar to the surface of the concrete finish machine and to the bottom of the form supporting the concrete slab were measured. It was found that the elevations of the gages are not uniform. In the west span, the average distance from top transverse and longitudinal gages to the top surface of the deck is 1.42 in, and the standard deviation is 0.33 in. The average distance from bottom transverse gages to the bottom surface of the deck is 1.23 in, and the standard deviation is 0.13 in. The average distance from bottom longitudinal gages to the bottom surface of the deck is 1.81 in, and the standard deviation is 0.42 in. The gage locations measured are listed in Appendix A.

2.3.2 Data Acquisition System

The data acquisition system (DAS) used on this project is a Megadac Series 3000 produced by Optim Electronics Corporation. The Megadac DAS is of modular design and consists of a chassis and plug-in modules to read a variety of sensors. A block diagram of the Megadac is shown in Fig. 2.9.

The Megadac was configured, for this project, as follows. Four SCI 88C modules are used to provide constant current excitation for up to 32 channels of 120Ω resistance strain gages. Four AD 885D analog input modules offer gains of 1~500 and filtering options for each of the 32 channels. The analog-to-digital conversion is handled by the ADC 3016 module which is capable of a maximum of 25,000 samples per second at 16-bit resolution. Post conversion gains of 1, 2, 4, 8, 16, 32, and 128 are software selectable on a channel-by-channel basis.

During attended bridge testing, the Megadac is typically connected to an IBM compatible personal computer via an IEEE-488 interface. The computer software (TCS 3000) allows the user to set sampling frequencies, label channel output, select gains, and observe sensor values either in digital or graphical form. In this configuration, the test results can be stored on the computer's fixed disk drive and the recording of data can be controlled from the computer's keyboard.

During stand-alone monitoring of the test bridge, the Megadac will monitor a "trigger" strain gage and start the recording of all gages when a threshold value has been exceeded. Since the Megadac initially stores all readings in its own memory, it is possible to record data that occurred several seconds prior to the trigger. During unattended monitoring of the bridge, data will be recorded to an external 1-Gbyte rewritable laser drive.

The DAS is installed at the bridge in a recycled traffic controller cabinet. The cabinet has been stripped of the controller circuits and insulated to minimize temperature variations. Commercial 120V AC service has been supplied to the cabinet and an uninterrupted power supply will run the DAS for approximately 30 minutes if electrical service is disrupted. Two cabinets were used in order to minimize the lead lengths of the strain gages and the DAS will be moved to each end of the bridge for monitoring the experimental and control decks. The strain gage leads are routed into each cabinet using PVC pipe fittings.

Sample rates are currently set at 60 samples per second. An external trigger device has been fabricated to sample at 60 Hz to be synchronized with the electrical supply. This device reduces system noise by always triggering at the same instance in the 60 Hz sinusoid. Lower sampling rates are being contemplated for the extended monitoring of the bridge in order to reduce

the volume of collected data.

2.3.3 Verification of Gage Mounting Techniques

The performance of strain gages welded on embedded bars was investigated in the laboratory with a reinforced concrete beam subjected to four-point loads. The clear span of the beam was 96 inches, and the height and width of its section was 8 and 12 inches, respectively. The compressive strength of the concrete was 3,660 psi, which was obtained from standard cylinder tests conducted on the 28th day. The modulus of elasticity and modulus of rupture of the concrete were calculated to be 3,450 ksi and 454 psi, respectively, based on ACI formulas. There were six strain gages welded on two 18-in-long No.4 bars, with their locations and numbering shown in Fig. 2.10. One bar was placed beneath a point load, and the other was placed at the mid-span of the beam. It must be pointed out that, unlike the bars in the bridge deck, these bars had no hooks. There were three additional strain gages, #7, #8 and #9, welded on a longitudinal reinforcing bar in the beam. These locations are identical to those of gages #1, #2 and #3. It was expected that readings from the strain gages welded on the embedded bars would be slightly less than those from the strain gages welded on the longitudinal reinforcing bar due to possible bond-slip. The details of the beam specimen are illustrated in Fig. 2.10.

The cracking load of the beam and the corresponding strain at the gage points were estimated with the simple beam theory. The ratio of flexural reinforcement in the beam was 1.54% and the modulus of elasticity of the bars was assumed to be 29,000 ksi. The moment of inertia of the beam was 569 in^4 for an uncracked section and 224 in^4 for a cracked section. Hence, the beam is expected to develop the first crack at $P = 2.86$ kips. At this

point, the strain at a gage point is expected to jump from 79 μs to 350 μs. However, the strain readings obtained from the test vary from 110 μs to 170 μs when $P = 2.86$ kips.. In addition, all gage readings were slightly greater than the predicted values before cracking and substantially smaller than the predicted values after cracking. The former is probably due to the fact that the elastic modulus of concrete calculated with the ACI formula is higher than the actual value. The latter could be due to the fact that flexural cracks occurred sporadically in the beam and may not be right at the gage points. It can be seen from Fig. 2.11 that the difference in readings obtained from the gages welded on embedded bars and those on longitudinal reinforcing bars before cracking is less than 60 μs. Based on these results, it was decided hooks would be added at the ends of embedded bars to be used in the field tests as mentioned before. With this precaution and the fact that the measured E_c tends to be smaller than the value calculated with the ACI formula, it is expected that the stresses in the bridge deck evaluated with the strain measurements from the embedded bars should fall on the conservative side.

2.4 Pre-Test Crack Observation

The substructure numbering starts from the west end in accordance with the convention adopted by the Colorado Department of Transportation, as shown in Fig. 2.1. The girder numbering starts from the north side of the bridge, with numbers 1 through 7, as shown in Fig. 2.4.

Before the load test, it was observed that some longitudinal cracks developed at the top of the experimental deck adjacent to Abutment 1, as shown in Fig. 2.12(a). These cracks were located near the edges of the flanges of

the girders below. The longest crack extended about 20 ft in the longitudinal direction of the bridge. This crack was difficult to see at the time of the load test. In December, 1993, this crack was readily detected and was measured to be approximately 0.02-in wide. This crack was over the interior edge of the flange of Girder 6. Shorter longitudinal cracks were noted over one or both flanges of Girders 3, 4 and 5. No transverse or longitudinal cracks were noted in the middle part of the west span of the phase-one portion of the deck. There was a longitudinal crack running the full length of the bridge along the construction joint between the phase-one and phase-two portions of the bridge. This crack was over the center of Girder 3.

In Span 1, transverse cracks were noted only in the phase-two portion of the deck, which were spaced at approximately 15 ft and were typically 0.025-in wide. Cracks at similar spacing were noted at the bottom of the deck. These cracks were highlighted by efflorescence, which indicated that they extended through the depth of the deck. No longitudinal cracks were visible at the bottom of the deck. The observations of the cracks at the bottom of the deck were made from the ground with naked eyes. At this distance, only wide cracks (0.02 in) or cracks highlighted with efflorescence can be detected with naked eyes.

At the top of the deck above Pier 2, there were transverse cracks approximately at the edges of the pier diaphragm. There were also two longitudinal cracks at the top of the deck over the pier diaphragm. These cracks were in the vicinity of Girders 4 and 5.

At the middle part of Span 2, there were no longitudinal or transverse cracks at the top of the phase-one portion of the deck. Along the full length of the phase-two portion of the deck of this span, transverse cracks were spaced at about 4~12-ft at the top of the deck, and spaced at about 6-ft at

the bottom of the deck, as shown in Fig. 2.12(b). No longitudinal cracks were visible at the bottom of the deck.

At the top of the deck above Pier 3, there were transverse cracks at the edges of the pier diaphragm and longitudinal cracks over the pier diaphragm, similar to those observed at Pier 2. A diagonal crack was also noted at the top of the deck above this pier.

No transverse cracks were visible at the top of the deck in the phase-one portion of Span 3. However, transverse cracks in the phase-two portion were spaced more closely together than those noted in the first two spans, spaced at about 3~6 ft, as shown in Fig. 13(a). At the bottom of the deck, transverse cracks highlighted by efflorescence were visible at approximately the same spacing. In some instances, longitudinal cracks over the flange of Girder 3 were also visible. No cracks were visible at the bottom of the phase-one portion of the deck, however.

Cracking at the top of the deck above Pier 4 was similar to those noted at the other piers. At the bottom of the deck near this pier, transverse and diagonal cracks with efflorescence were visible in the phase-two portion of the deck.

No transverse cracks were visible at the top of the phase-one portion of the deck adjacent to Pier 4, but the phase-two portion exhibited transverse cracks spacing at about 4~8 ft, as shown in Fig. 2.13(b). The width of a typical transverse crack was measured to be 0.025 in with a crack gage. The crack spacing increased to about 16 ft near Abutment 5. At the bottom of the deck, the crack spacing was about 4~8-ft along the full length of the span. In the phase-two portion of the deck adjacent to the abutment, there were also a few transverse and diagonal cracks at the bottom of the deck. No longitudinal cracks were visible at the top of the deck adjacent to

Abutment 5.

In summary, extensive wide transverse cracks have occurred in the phase-two portion of the deck, but not in the phase-one portion of the deck. This transverse cracking was much more prevalent in the control deck than in the experimental deck of the bridge, although the same concrete mix was used for the whole bridge deck and the concrete placement was performed continuously starting from the west end to the east end of the bridge. Transverse and longitudinal cracking in the vicinity of the piers is similar for both the experimental deck and the control deck of the bridge. Short longitudinal cracks have developed over the flanges of the girders beneath the traffic lanes at Abutment 1. Similiar cracks were not noted in the deck at Abutment 5.

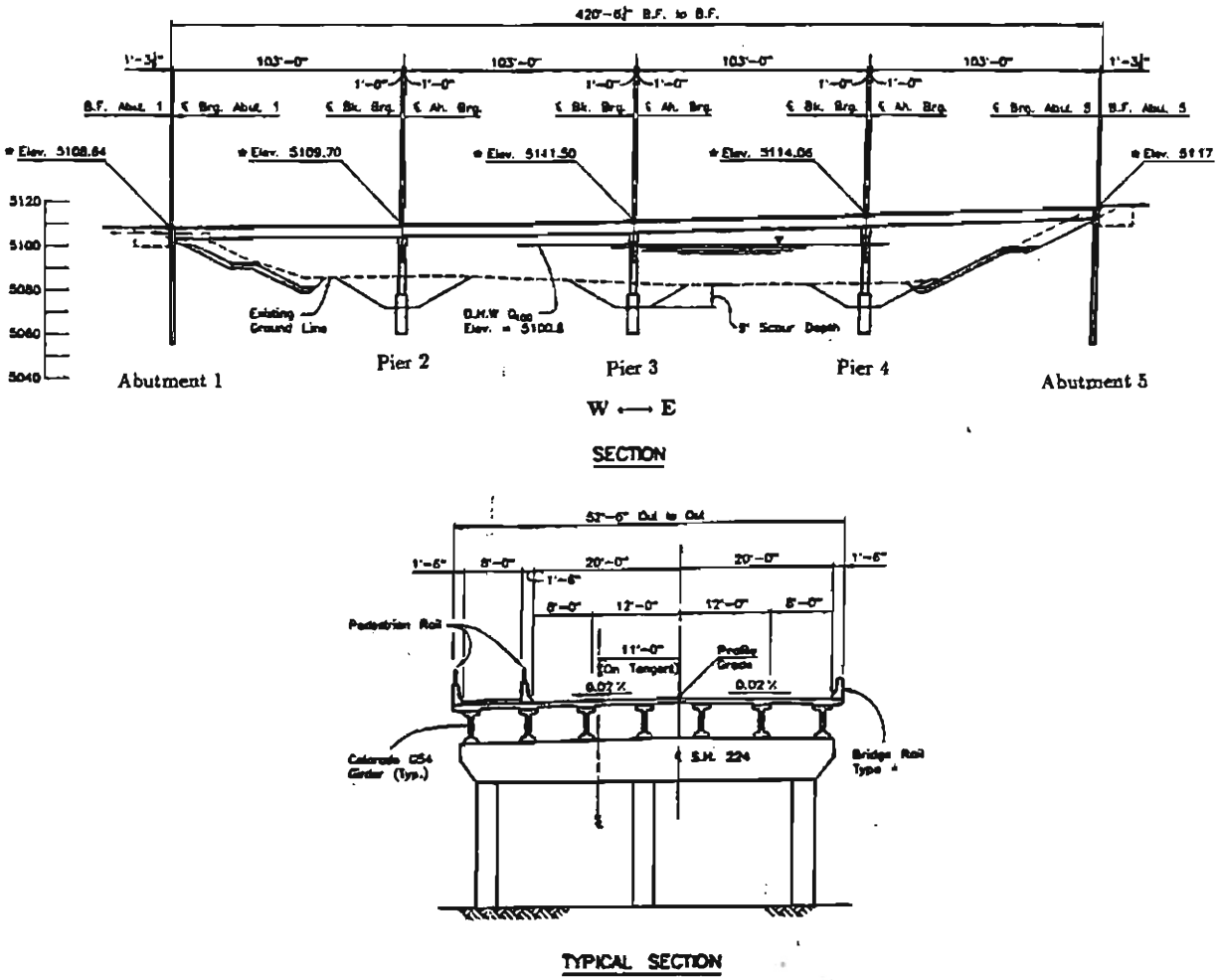

Figure 2.1: Configuration of the Bridge Deck

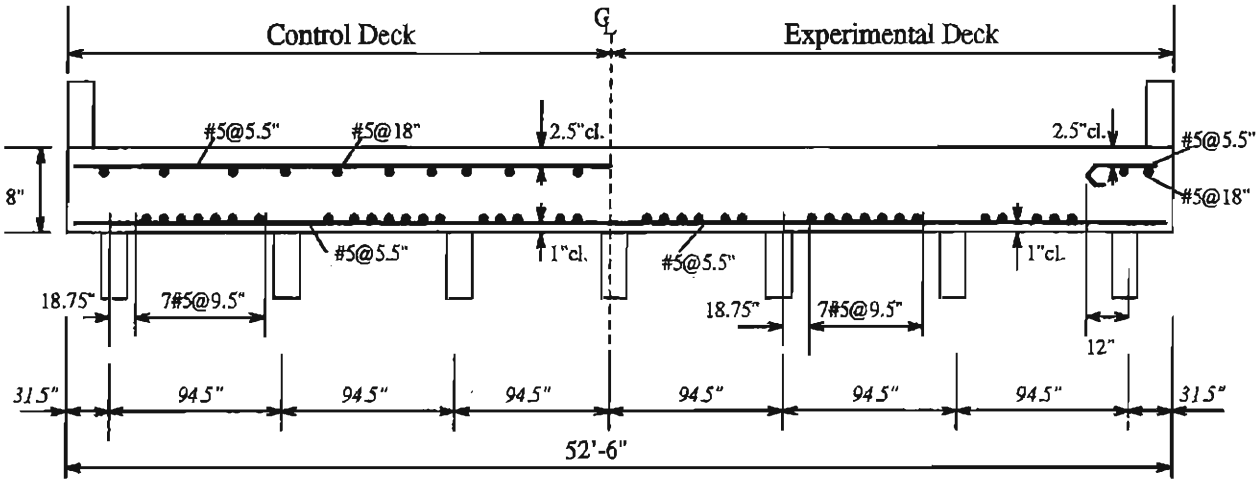

(a) Near Mid-Span

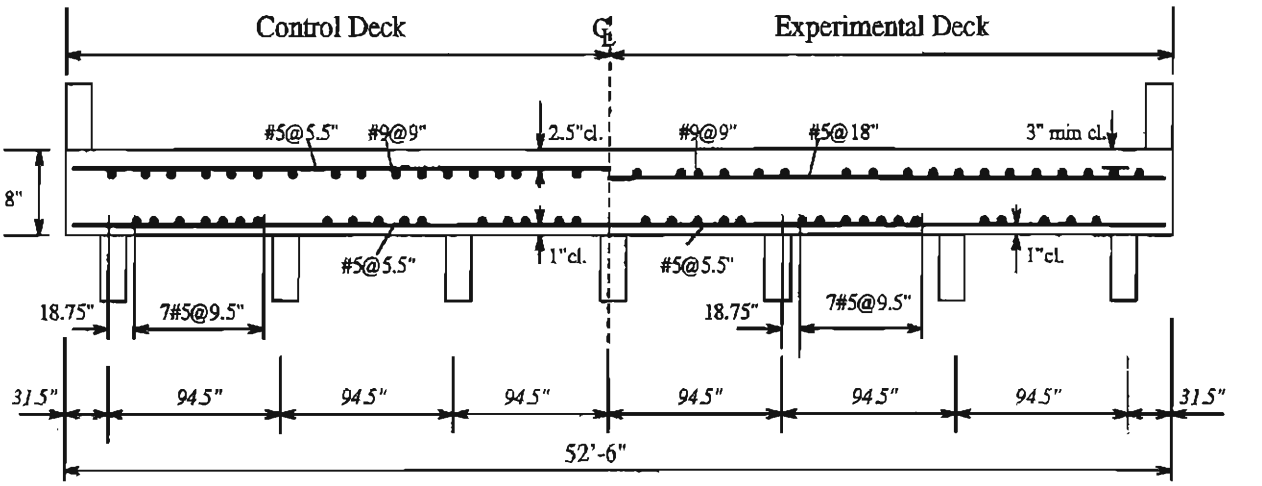

(b) Near Pier

Figure 2.2: Details of the Reinforcement in the Bridge Deck (Not to Scale)

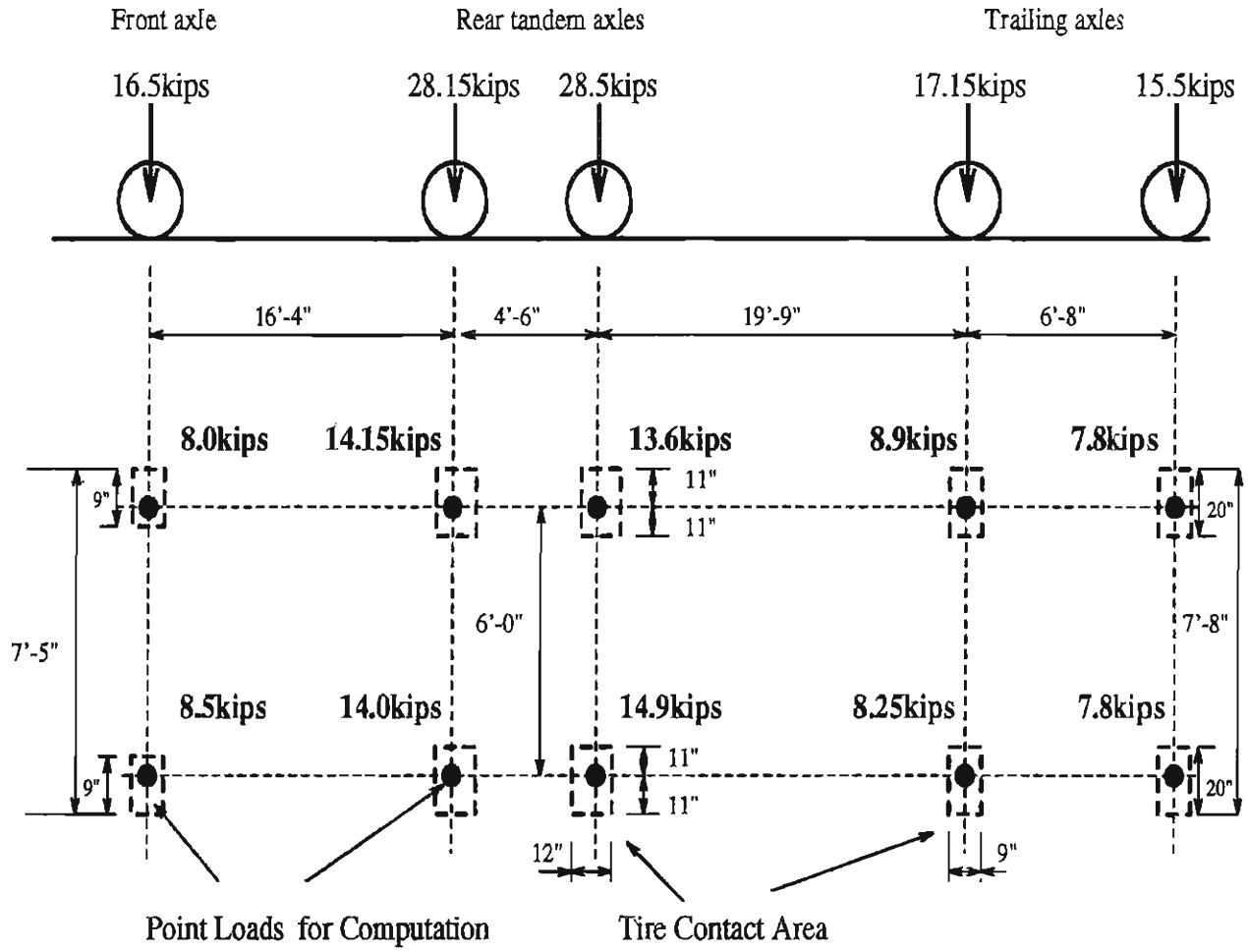

Figure 2.3: Test Truck

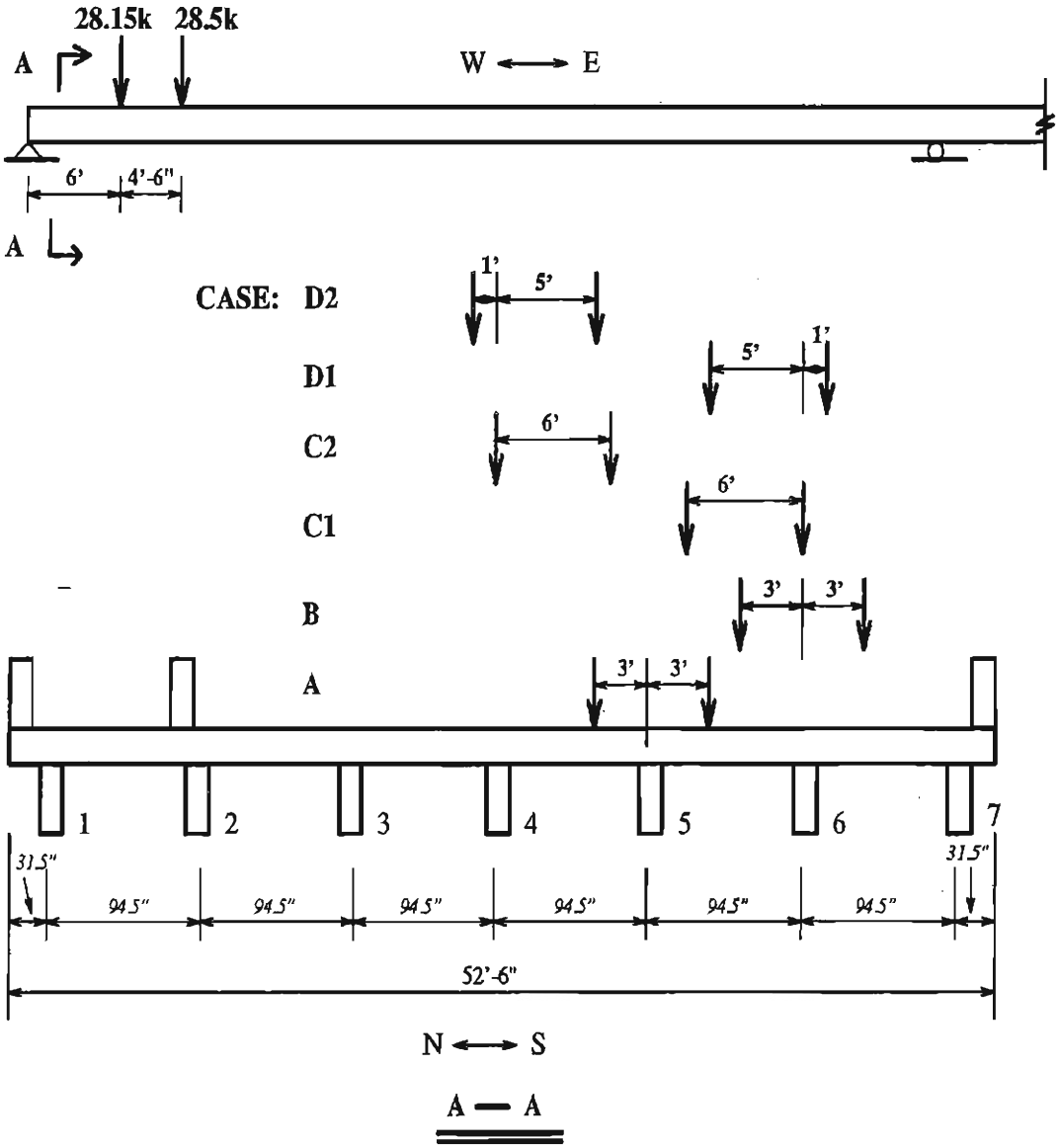

Figure 2.4: Test Truck Positions in Load Group 1 (and Load Group 5)

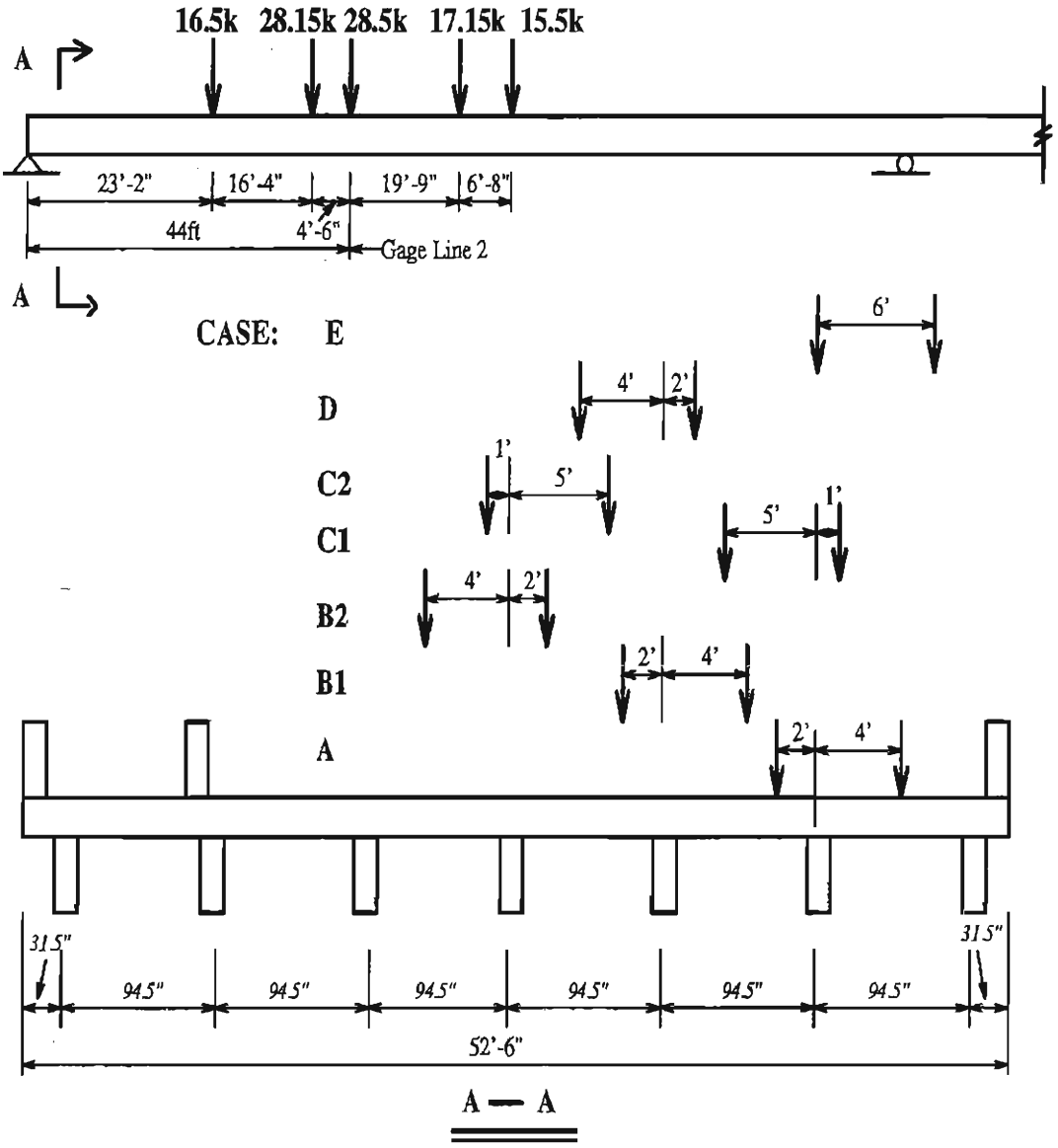

Figure 2.5: Test Truck Positions in Load Group 2 (and Load Group 4)

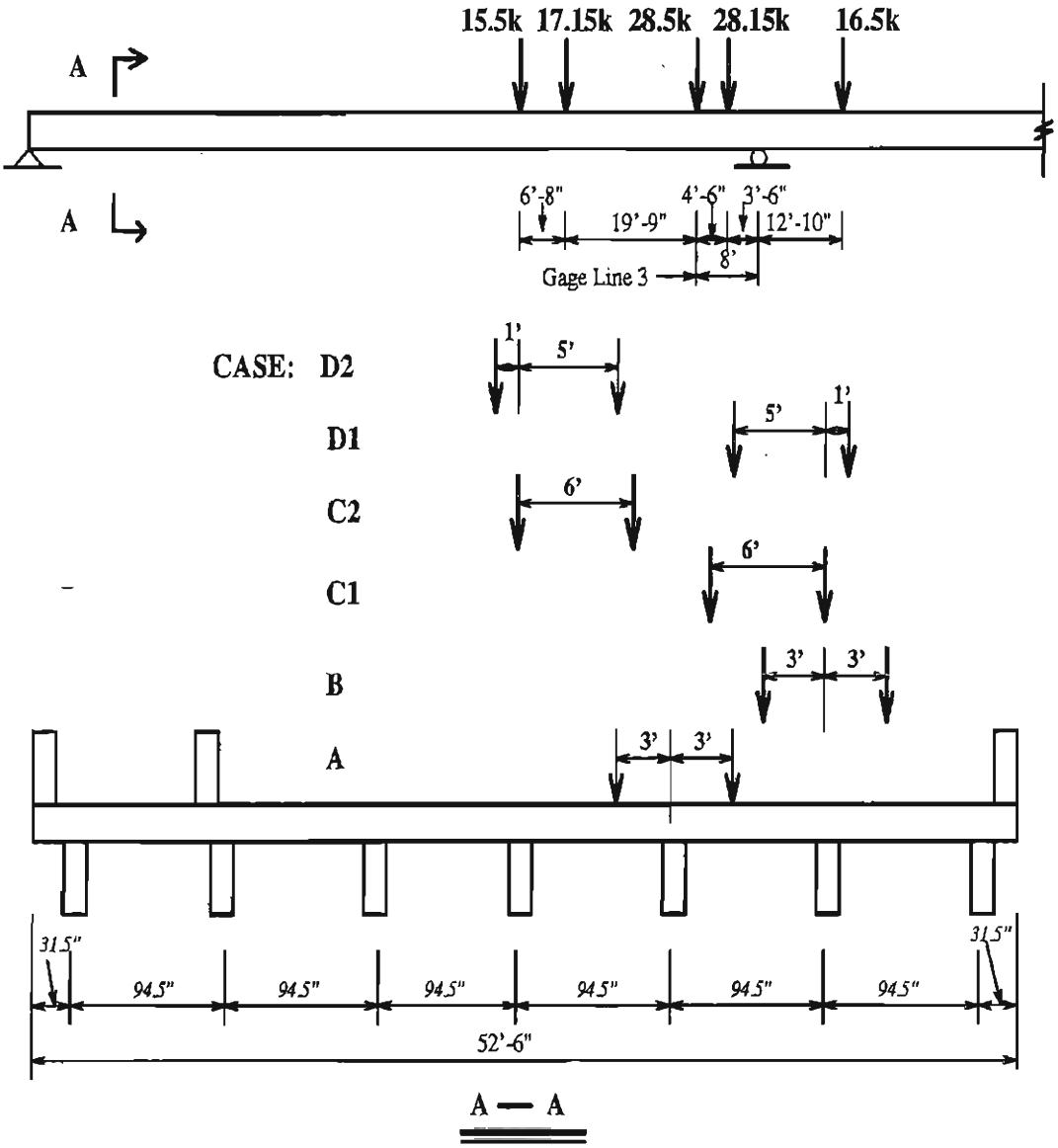

Figure 2.6: Test Truck Positions in Load Group 3

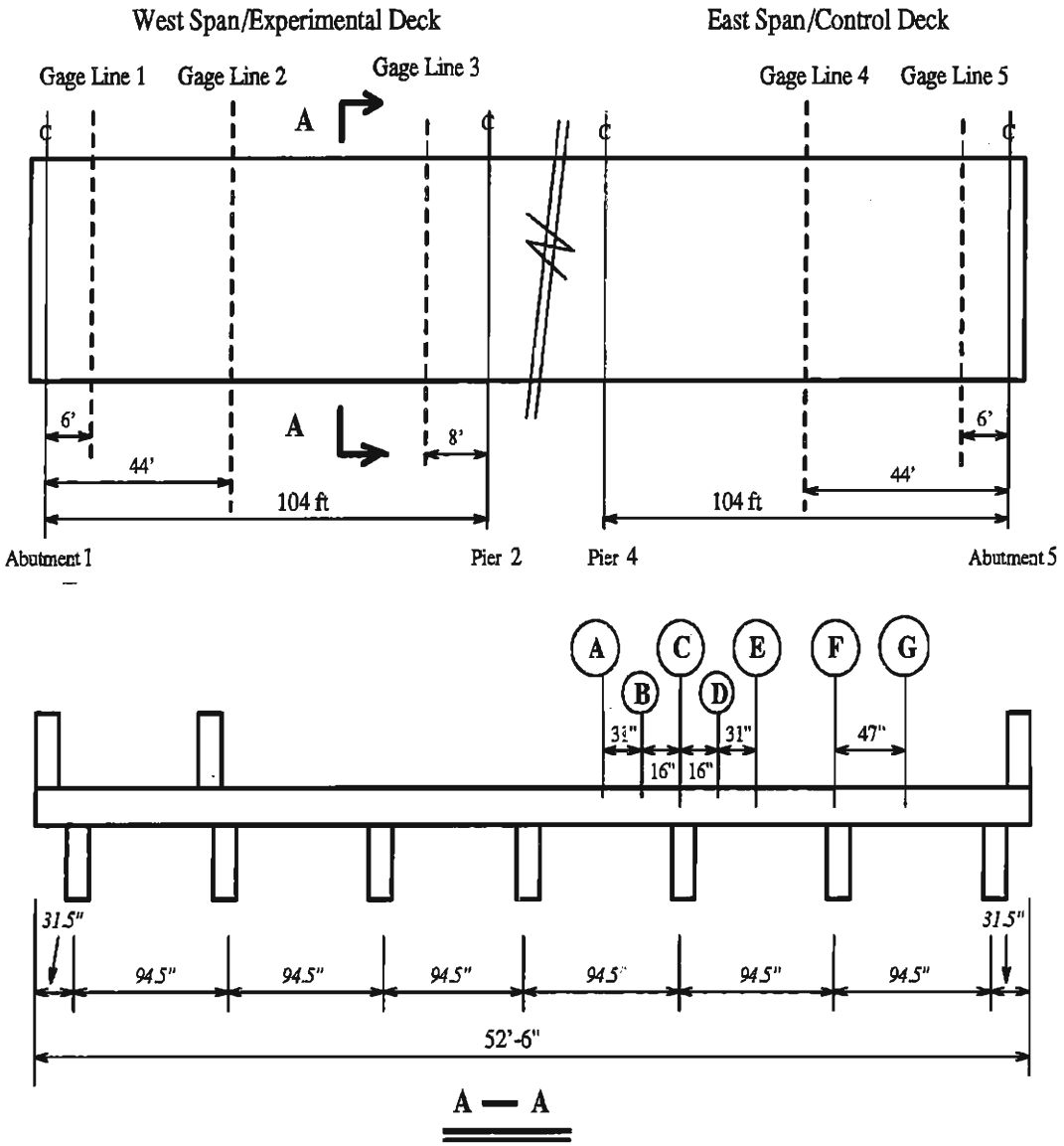

Figure 2.7: Locations of Strain Gages along the Bridge Deck

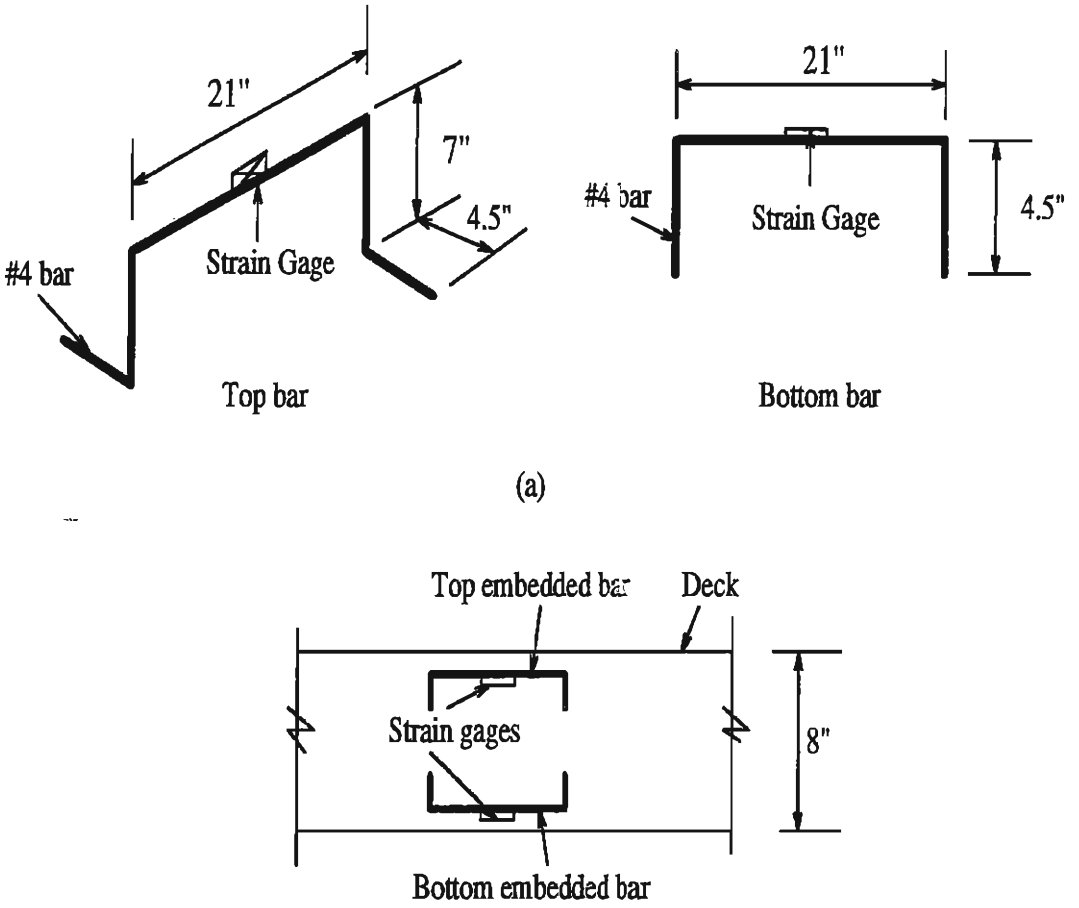

Figure 2.8: Embedded Bars and Strain Gages: (a) Embedded Bars; (b) Locations of Strain Gages

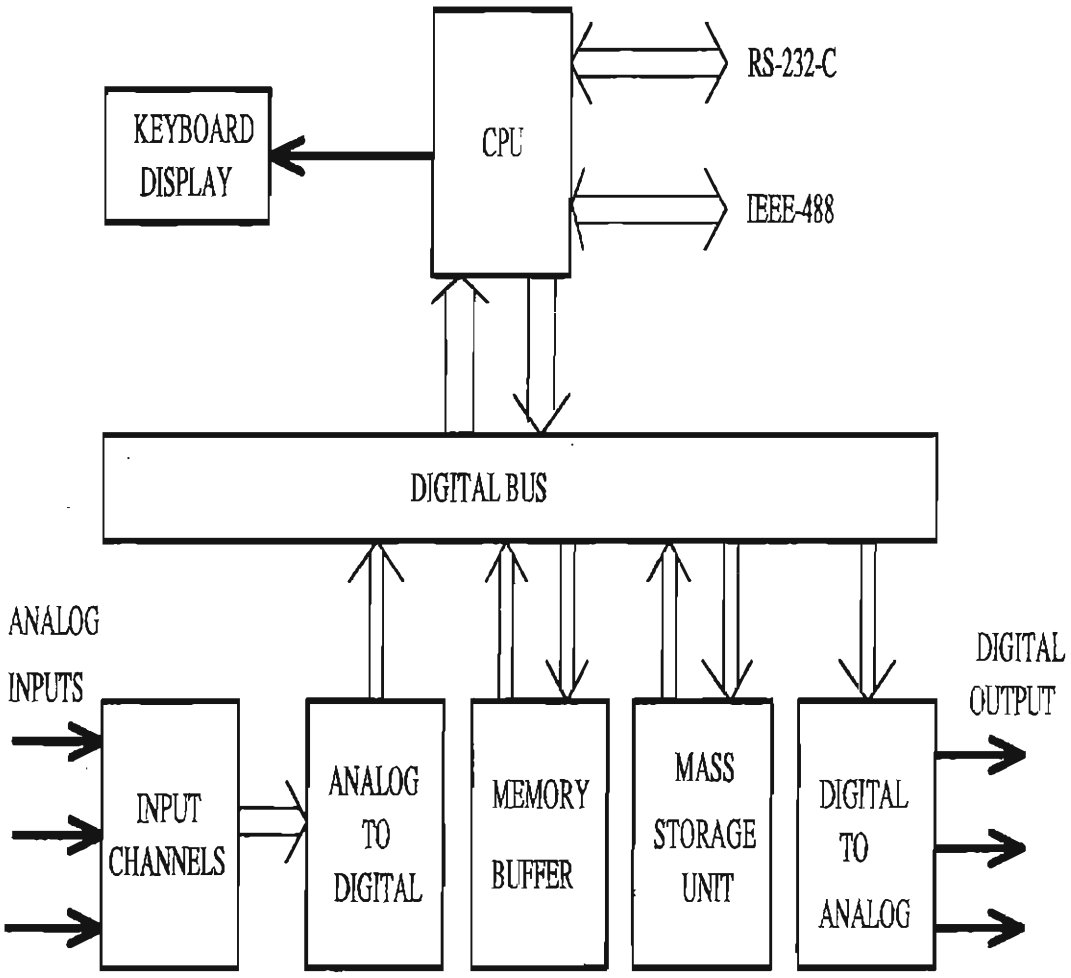

Figure 2.9: Logical Block Diagram of the MEGADAC

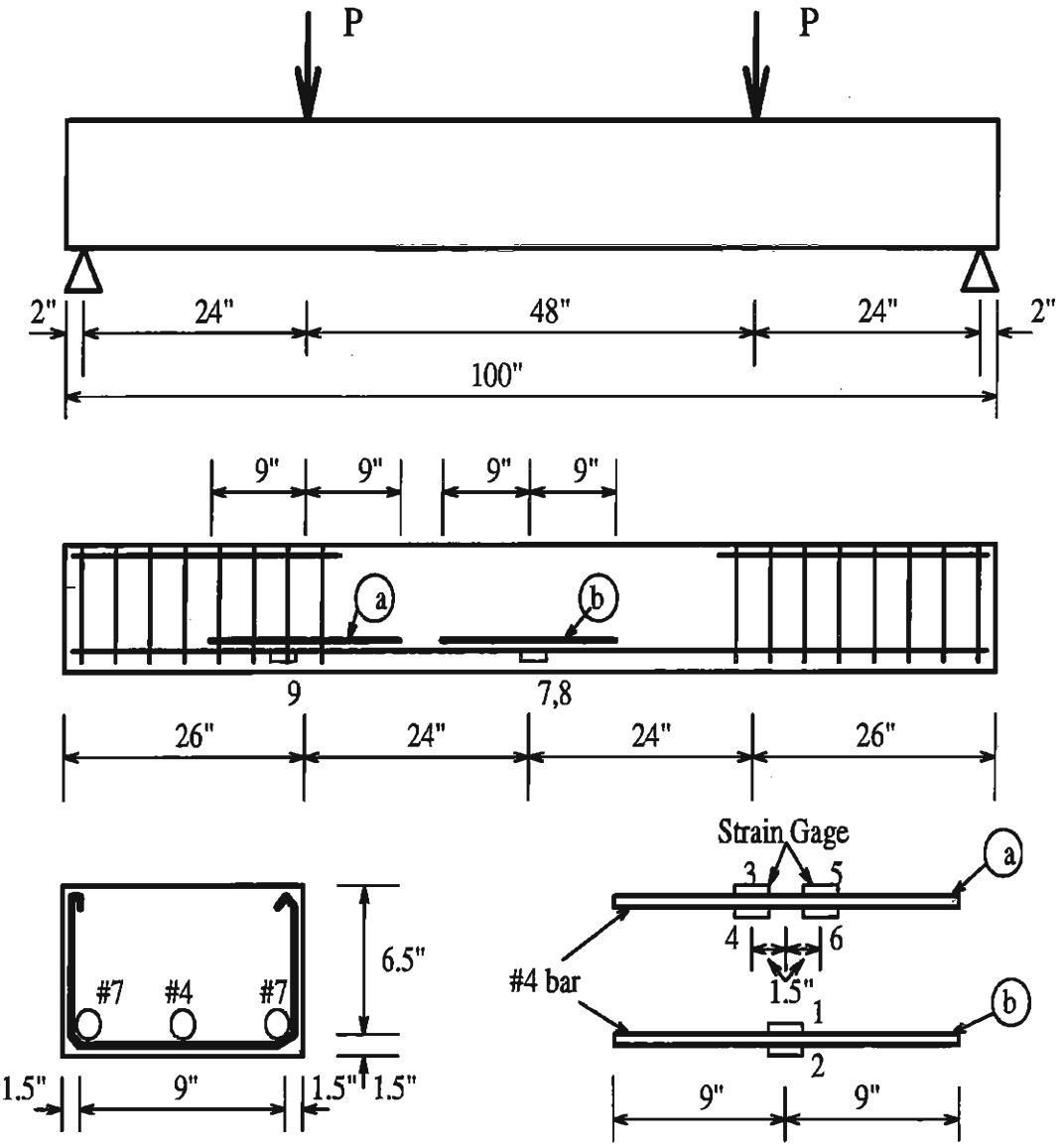

Figure 2.10: Verification of Gage Mounting Techniques

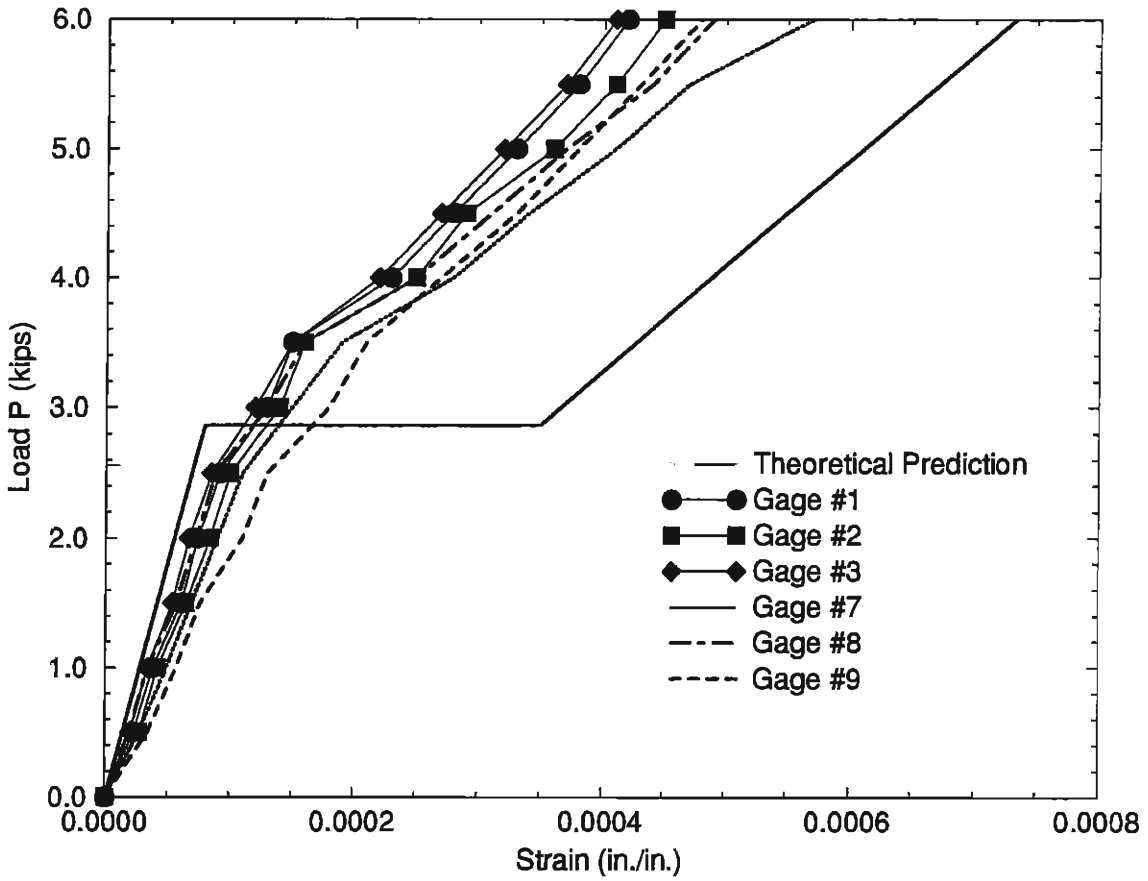

Figure 2.11: Strain Readings from Four-Point Bending Test

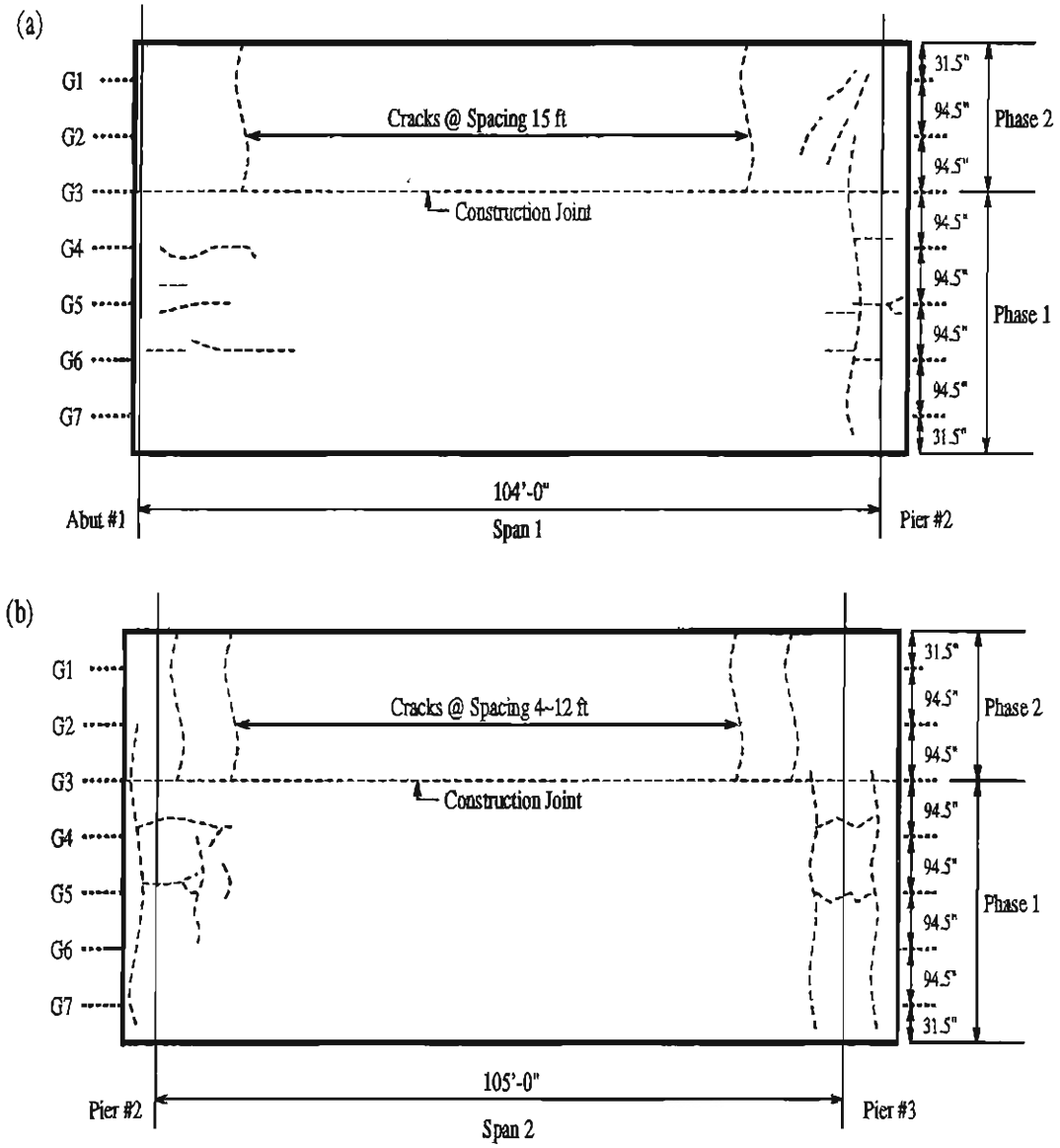

Figure 2.12: Approximate Sketch of the Pre-Test Cracking Pattern at the Top of the Deck: (a) Span 1; (b) Span 2.

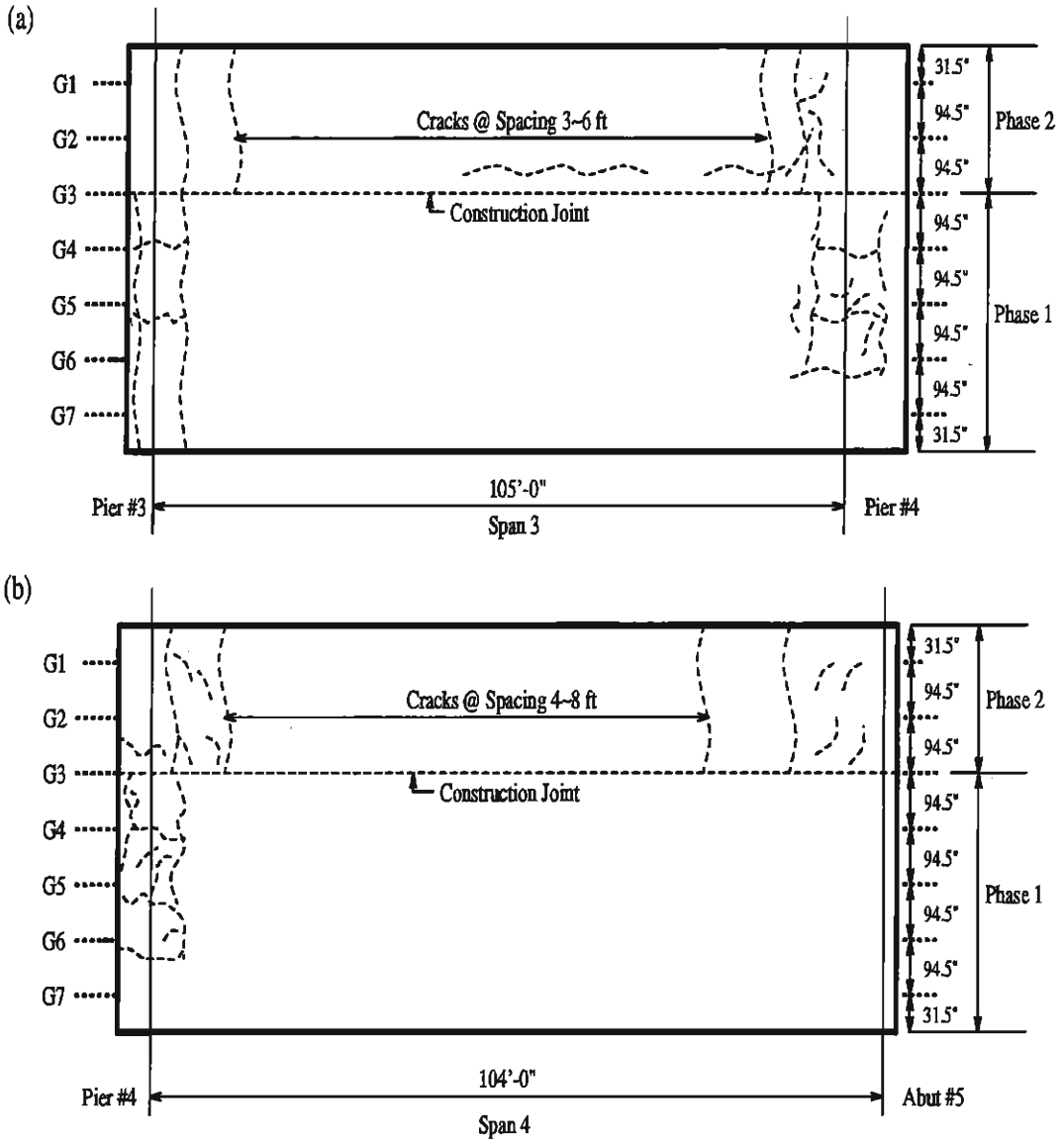

Figure 2.13: Approximate Sketch of the Pre-Test Cracking Pattern at the Top of the Deck: (a) Span 3; (b) Span 4.

Chapter 3

FINITE ELEMENT MODELING OF BRIDGE DECK

3.1 General Considerations

For the elastic stress analysis of a four-span bridge deck, it is impossible to use solid elements to model both the concrete slab and the girders due to the limitation of the computer capacity. Hence, in the finite element model adopted here, two layers of solid elements are used to model the concrete slab and rigid links are used to connect the nodes at the bottom of the slab to the centroids of the girders which are represented by 3-D beam elements. The cross-sectional area and moment of inertia of each girder of the bridge are 631 in^2 and 242,585 in^4, respectively. This modeling approach has been validated in a previous study (Cao, Allen and Shing 1993).

Furthermore, since only a single end span of the four-span bridge is considered at a time, the remaining three spans are modeled by equivalent beam elements only. Each equivalent beam has a 54-in-high and 43.45-in-wide rect-

Table 3.1: Moment of Inertia of the Equivalent Beam

Components	$A_i(\text{in}^2)$	$I_i(\text{in}^4)$	$y_i(\text{in})$	$A_i y_i$	$Y_i(\text{in})$	$A_i Y_i^2$	$I_i + A_i Y_i^2$
Slab	756	4,032	4.0	3,024	13.95	147,120	151,152
Girder	631	242,585	34.67	21,877	16.72	176,401	418,986
Total	1,387	—	—	24,901	—	—	570,138

Note:
A_i — Area of the ith component of the composite section;
I_i — Moment of inertia of the ith component of the section;
y_i — Distance between the centroid of the ith component of the section and the top of the slab;
Y_i — Distance between the centroid of the ith component of the section and the neutral axis of the equivalent beam.

angular section, whose moment of inertia is equal to that of a fully-coupled composite T-beam section consisting of a girder and a concrete slab. The effective width of the flange is equal to the center-to-center distance between the girders, in accordance with ACI recommendations. The moment of inertia of the equivalent beam is 570,138 in^4, as shown in Table 3.1.

In this study, the most important consideration is the maximum tensile stresses produced by transverse negative moments in the slab. These stresses are thought to occur at the top of the deck in the vicinity of supporting girders. Therefore, a suitable mesh should be chosen to obtain accurate stresses at these sites. The strategy used here to select a mesh is to vary element sizes in the longitudinal and transverse directions independently, and a suitable element size is determined by looking at the convergence of the stresses. The study on mesh refinement is documented in detail by Cao, Allen and Shing (1993), and is briefly summerized in the following paragraphs.

The mesh refinement study was carried out with a simply supported

Table 3.2: Maximum Transverse Tensile Stresses with Different Meshes

Longitudinal Divisions	Element Aspect Ratio	Max. Tensile Stress (ksi)	% Error with Respect to 30 Elements
10 Elements	10.64	0.467	17.54
20 Elements	5.32	0.545	3.73
30 Elements	3.55	0.566	0.0

bridge deck that had a span length of 399 inches and seven equally spaced girders. The concrete slab was modeled with two layers of solid elements. The concrete slab between two girders is discretized into seven solid elements in the transverse direction of the deck. Furthermore, with the mesh in the transverse direction fixed, the slab was divided into 10, 20 and 30 elements, respectively, in the longitudinal direction. Such arrangements lead to element aspect ratios (length/thickness) of 10.64, 5.32 and 3.55, respectively.

With two 50-kip point loads applied at the mid-span of the deck, stresses were computed with the aforementioned meshes. The maximum transverse tensile stresses at the top of the deck obtained with the different meshes are compared in Table 3.2, where the maximum transverse tensile stress obtained with 30 elements is used as the comparison standard. Based on the results in Table 3.2, it is estimated with a quadratic interpolation that using an element aspect ratio not greater than 7.0 leads to an error less than 10%.

Furthermore, the simply supported bridge deck was discretized with two different meshes in the transverse direction. In both cases, there were 30 solid elements in the longitudinal direction of the deck. In the coarse mesh, there is only one solid element between a wheel load and a girder, and in the fine mesh, two solid elements were used.

Analysis results obtained with the coarse mesh appear unrealistic in that the maximum stresses in the transverse direction do not occur under the point loads or above the girders. This means that stresses at these sites are greatly distorted. When the fine mesh is used, this distortion virtually disappears. Hence, it is apparent that there should be at least two solid elements between a wheel load and a girder for stress analysis. Based on these considerations, a mesh of eight elements in the transverse direction between each pair of girders has been chosen.

3.2 Finite Element Models

Based on the above considerations, only one end span is modeled in a refined fashion at a time. A total of 50 solid elements is used in the transverse direction of the bridge deck, with eight solid elements used between two girders. The span length between two girders is adjusted to be 96 in, which is 1.5-in longer than the actual span length, to fit the different wheel load positions along the transverse direction. The mesh along the transverse direction remains the same for all three load groups. The mesh along the longitudinal direction is adjusted in accordance with the locations of the axle loads of the test truck. The dimensions of the test truck are slightly modified to fit the meshes. The distance between the rear tandem axles is changed from 54 to 48 in. The length of the truck is modified to be 9-in shorter for Load Group 2, and 2-in shorter for Load Group 3 than the actual length of the test truck. A total of 24 solid elements is used in the longitudinal direction of a single span. For all three load groups, a fine mesh is used in the vicinity of the rear tandem axle loads. In this region, the length of each element is 24 in, which leads to an element aspect ratio (length/thickness) of 6.0. In the model, the

span length of the bridge is 104 ft for the two end spans and 105 ft for other spans, which are equal to the actual span lengths of the bridge. The vertically supported joints are located along the central line of the diaphragm above the abutment or the pier.

The mesh used for the stress analysis of the deck under Load Group 1 is shown in Fig. 3.1(a). From the left side of the mesh, the first solid element has a length of 15 inches. This element accounts for the stiffness of the concrete diaphragm above the abutment. This effect is simulated by using equivalent solid elements which have the same in-plane bending stiffness as that of the diaphragm. The depth and width of the diaphragm are 62 and 30 inches, and those of the equivalent solid elements are 8 and 15 inches. Since the modulus of elasticity of the diaphragm is calculated to be 4,230 ksi, that of the equivalent solid elements is determined to be 279,560 ksi. In the longitudinal direction, six small solid elements are used in the region of the fine mesh, and the rest of the deck is modeled by seventeen solid elements.

The mesh used for the stress analysis of the deck under Load Group 2 is shown in Fig. 3.1(b). In the longitudinal direction, six small solid elements are used in the region of the fine mesh, and the rest of the deck is modeled with eighteen solid elements. The lengths of these elements vary so that the axle loads can be located at the desired nodes.

The mesh used for the stress analysis of the deck under Load Group 3 is shown in Fig. 3.1(c). There are two solid elements with a high modulus of elasticity (32,760 ksi) used to account for the stiffness of the diaphragm above the pier. The depth and width of the diaphragm are 62 and 51 inches, and those of the equivalent solid elements are 8 and 25.5 inches. The approach used to determine the modulus of elasticity for the equivalent solid elements is the same as that for Load Group 1. In the longitudinal direction, twelve

small solid elements are used in the region of the fine mesh, including two solid elements for the diaphragm, and the rest of the deck is modeled with twelve solid elements.

In the finite element analysis of the bridge, the elastic modulus for deck concrete is assumed to be 4,230 ksi and that for girder concrete is 5,260 ksi. The Possion's ratio is assumed to be 0.2 for both the deck and girder concrete. There is a steel diaphragm (C15X33.9) at the mid-span of each span, whose cross-sectional area is 9.96 in^2. The diaphragm is modeled by bar elements which are connected to the girders. The elastic modulus of the bars is assumed to be 29,000 ksi.

The bridge deck has an eight-degree angle of skew. However, because the angle of skew is small, it is ignored in the stress analysis. The wheel loads of the test truck are treated as concentrated point loads, which are applied at appropriate nodes of the finite element mesh. The finite element program SAP90 (Wilson 1989) is used for the stress analysis. Non-conforming solid elements are used to eliminate possible shear locking.

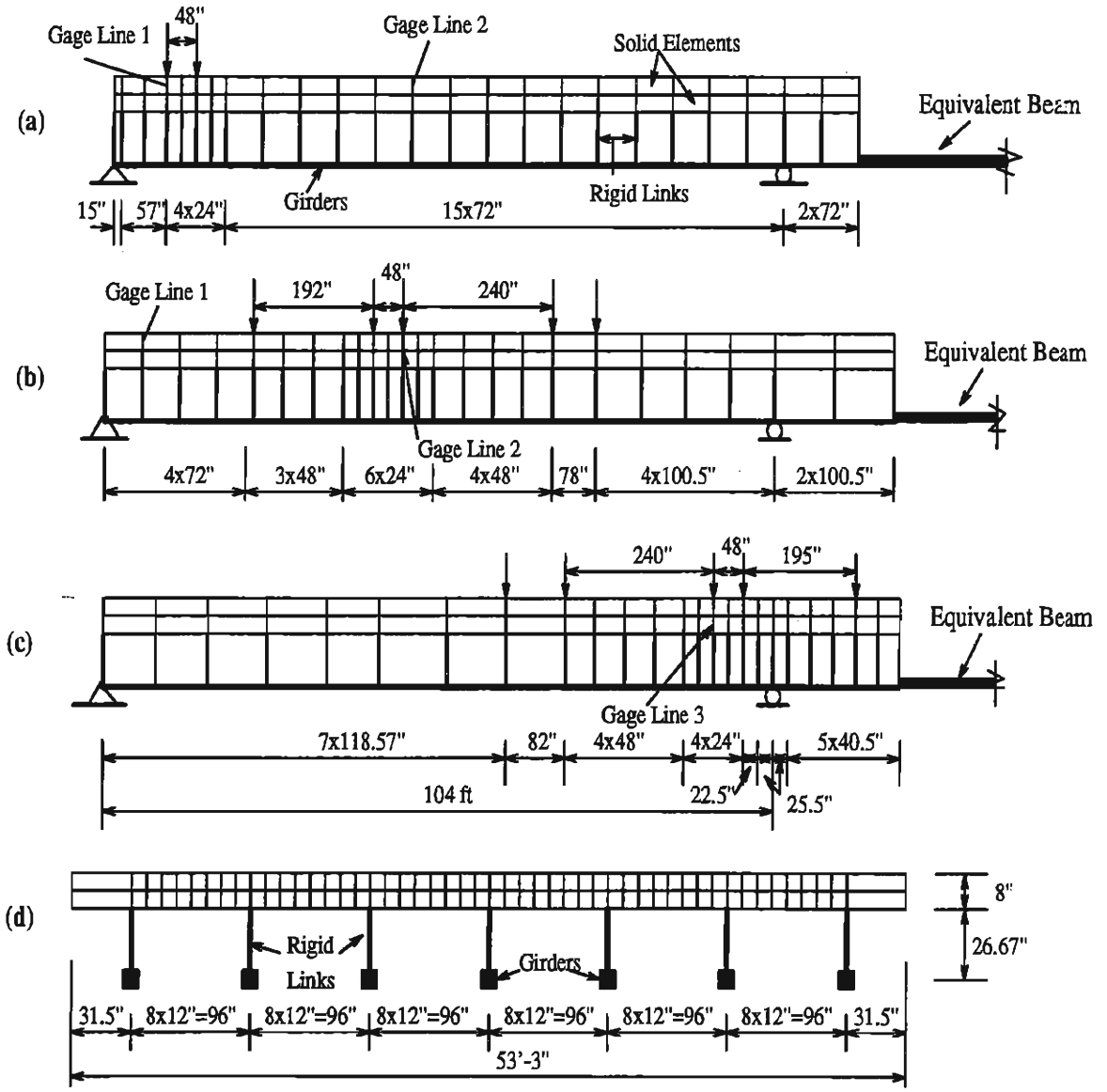

Figure 3.1: Finite Element Meshes: (a) Longitudinal Section for Load Group 1; (b) Longitudinal Section for Load Group 2; (c) Longitudinal Section for Load Group 3; (d) Transverse Section for All Three Load Groups.

Chapter 4

TEST AND NUMERICAL RESULTS

4.1 Results of Field Tests

The response of the bridge deck to a test truck positioned at different locations was monitored by embedded strain gages, whose arrangement is presented in Chapter 2. These strain readings are tabulated in Appendix B. The maximum values of transverse and longitudinal strain readings at the top and bottom of the deck are separately summarized in Tables 4.1 and 4.2.

Based on the results of material tests described in Chapter 2, the modulus of elasticity of the deck concrete is determined to be 4,230 ksi and the modulus of rupture of the deck concrete is 590 psi, which were obtained with the 28-day lab-cured specimens. The cracking strain of the deck concrete corresponding to the aforementioned modulus of rupture is 140 μs. Based on the plane-section assumption, the strain at the top or bottom of the deck can be determined with the strain at a gage point. Since the distance from an embedded gage to the top or bottom of the deck is about 1$\sim$2 inches and the thickness of the deck is 8 inches, it is expected that the strain at the top

or bottom of the deck will reach the cracking strain (140 μs) when the strain at an embedded gage is about 70~105 μs.

It can be seen from Table 4.1 that when the test truck was close to the abutment, the transverse tensile strains at the top gage positions of the deck along Gage Line 1 were less than 20 μs and those at the bottom gage positions of the deck were about 60~80 μs. When the test truck was near the mid-span, the transverse tensile strains at the bottom gage positions of the deck along Gage Line 2 became very large, and were about 110~180 μs. At the same time, the transverse tensile strains at the top gage positions of the deck were less than 15 μs. This indicates that the deflection of girders increases the transverse tensile stresses at the bottom of the deck and reduces those at the top of the deck. When the test truck was close to the pier, the transverse tensile strains at the top gage positions of the deck along Gage Line 3 were less than 20 μs, and those at the bottom gage positions of the deck were about 50~80 μs.

It can be seen from Table 4.2 that the longitudinal tensile strains developed at gage positions in the deck under the test truck are small, and are less than 28 μs for all three load groups. It is also noted from the test results that the behavior of the experimental and control decks is similar.

In summary, when the test truck was close to the abutment and the pier, the transverse tensile strains at the bottom of the deck were close to the cracking strain of deck concrete. When the test truck was near the mid-span, the transverse tensile strains at the bottom of the deck exceeded the cracking strain. For all three load groups, the transverse tensile strains at the top of the deck were much less than the cracking strain.

Table 4.1: Max. Values of Transverse Strain Readings (Top/Bottom) (μs)

Gage Point	Gage Line				
	1	2	3	4	5
A	+3.1/+66.5	-52.3/+117.9	-53.3/+54.9	−/−	−/−
B	−/-31.5	-24.5/−	−/−	−/−	−/−
C	+20/−	+6.8/−	+19.2/−	+5.6/−	+13.8/−
D	+18.3/−	−/+50.7	−/−	−/−	−/−
E	-32.6/+76.7	-53.9/+173.8	-51.1/+73.4	-46.5/+133.2	-39.6/+30.2
F	+15.4/−	+13.0 /−	+18.7/−	−/−	+15.7/−
G	-14.8/+30.8	−/+176.2	−/−	−/−	−/−

Note: The plus and minor signs refer to the tensile strains and compressive strains, respectively. The locations of gage lines and gage points are illustrated in Fig. 2.6. The strain readings of each column are obtained under a load group which has an identical number as the gage line.

Table 4.2: Max. Values of Longitudinal Strain Readings (Top/Bottom) (μs)

Gage Point	Gage Line				
	1	2	3	4	5
A	−/+0.4	-61.8/+1.0	-10.9/+10.7	−/-30.2	−/−
C	+6.2/−	-41.9/−	−/−	−/−	+10.0/−
E	-24.3/+27.5	-35.7/-23.4	−/−	−/-21.9	−/−
F	-17.3 /−	-51.7/−	−/−	−/−	−/−

Note: The plus and minor signs refer to the tensile strains and compressive strains, respectively. The locations of gage lines and gage points are illustrated in Fig. 2.6. The strain readings of each column are obtained under a load group which has an identical number as the gage line.

4.2 Comparison of Test and Numerical Results

The behavior of the bridge deck under the nineteen load cases is analyzed with the finite element models presented in Chapter 3. The corresponding normal stresses along the transverse and longitudinal directions of the bridge deck are determined.

Since two layers of solid elements are used to model the bridge deck, the stresses are computed at three nodes along the depth of the deck. The stresses at the gage locations are projected from the nodal stresses with a quadratic interpolation. However, it happens that these nodal stresses fit into a linear interpolation. Ignoring the scattering in field measurements, it is assumed that all strain gages are 1-in away from the top or bottom of the deck. The normal stresses developed in the deck during the field test are calculated by multiplying the strain readings by the calculated elastic modulus of deck concrete (4,230 ksi). They are compared to the numerical results.

The comparisons of the test and numerical results on the normal stresses developed under different load groups are summarized in Appendices C through G. Results of selected load cases are shown in Figures 4.1 through 4.6. These are Case A of Load Groups 1 and 3, and Case D of Load Group 2. In Case A of Load Groups 1 and 3, the wheel load positions along the transverse direction of the deck are similar to those in Case D of Load Group 2, as shown in Figures 2.3 through 2.5. These three load cases demonstrate the effect of girder deflection on the normal stresses in the transverse direction of the deck. It can be seen from the figures that the numerical results are quite close to the test results for all these load cases. Nevertheless, the tensile

stresses developed at the bottom of the deck in the field tests are about twice as large as the numerical predictions. This can be attributed to the cracking at the bottom of the deck, which is not accounted for in the analysis.

It can seen from Fig. 4.1 that when the truck was close to the abutment and each of the wheel loads was near the mid-span between two girders, the transverse normal stresses obtained from the tests at the top of the girders are only about 50% of the numerical predictions. This difference is also found in other load cases where the truck was close to an abutment or a pier, as shown in Appendices C, E and G. This is probably caused by the flange of the girders, which is not considered in the computations. This effect is not significant when truck loads are near the mid-span, since the transverse normal stresses at the top of the girders are dominated by the deflection of the girders. It can also be seen from Fig. 4.2 that the normal stresses obtained from the tests in the longitudinal direction of the bridge deck are close to the numerical results. Similar results are obtained for the case where the test truck was close to the pier, as shown in Figures 4.5 and 4.6.

It can be seen from Fig. 4.3 that when the test truck was near the middle of the west span of the bridge deck, the transverse tensile stresses at the bottom of the deck were relatively high. This phenomenon can be observed from both numerical predictions and test results. It can also be seen from Fig. 4.4 that the numerical predictions of the normal stresses in the longitudinal direction of the bridge deck are very close to the test results.

In summary, the numerical predictions of the deck response under the test truck are close to the test results. When the test truck was near the middle of the experimental deck of the bridge, the transverse tensile stresses at the top of the deck was very low due to girder deflections.

4.3 Concluding Remarks

It is found from the test results that when a truck load was close to an abutment or a pier, the transverse tensile strains at the bottom of the deck were close to the cracking strain of deck concrete. When a truck load was near a mid-span, the maximum transverse tensile strains at the bottom of the deck usually exceeded the cracking strain. For all the load cases considered here, the maximum transverse tensile strains at the top of the deck were less than 30% of the cracking strain.

The behavior of the bridge deck under the three load groups has been analyzed with the finite element method. The numerical results have been compared with the test results. It is found that the numerical predictions of the deck response under the test truck are close to the test results. Therefore, it can be concluded that the finite element model used here is a suitable model for the stress analysis of bridge decks. The same finite element model was used in a previous study to investigate the deck stresses under more severe truck load conditions (Cao, Allen and Shing 1993). In this study, the response of the bridge deck under one and two trucks was investigated. It has been found that the maximum transverse tensile stresses at the top of the bridge deck are 286, 222 and 239 psi when the truck loads are close to the abutment, the mid-span and the pier, respectively. These stresses are much less than the modulus of rupture (590 psi) of the deck concrete.

A highway bridge is normally subjected to about 100,000 to 10,000,000 cycles of repeated loadings during its life time (Hsu 1981). It is observed from test results that the fatigue strength of plain concrete is about 60% of its rupture strength when concrete specimens were subjected to 10 million load cycles (Ballinger 1972, Tepfers 1979, Oh 1986). If the experimental

bridge deck will be subjected to about 10 million load cycles, the tensile strength of the deck concrete is expected to be reduced from 590 psi to 355 psi. As discussed above, the maximum tensile stresses developed at the top of the deck under truck loads are about 280 psi, which are less than the reduced tensile strength of the deck concrete (355 psi). Since the designated truck loads used in the stress analysis of the deck were greater than the standard truck loads, it is expected that normal traffic loads will not cause greater stresses at the top of the deck. Hence, it can be expected that the transverse tensile stresses developed at the top of the deck under traffic loads will not induce cracking.

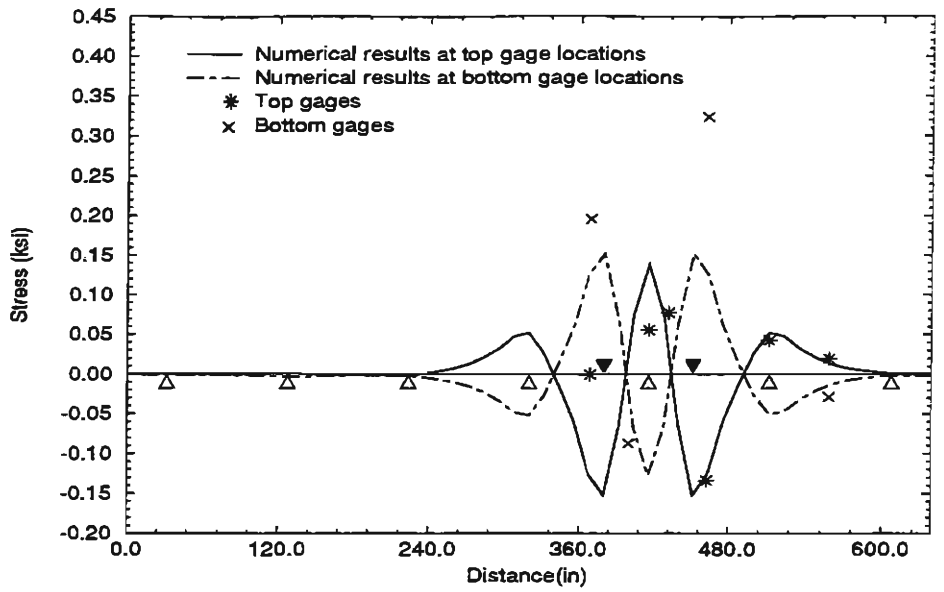

Figure 4.1: Normal Stress in Transverse Direction along Gage Line 1 (Case 1A)

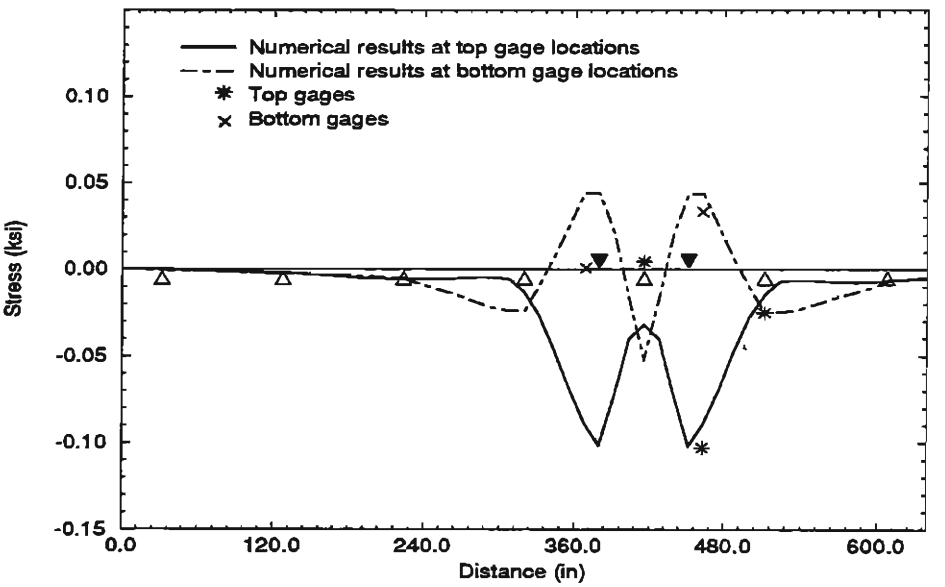

Figure 4.2: Normal Stress in Longitudinal Direction along Gage Line 1 (Case 1A)

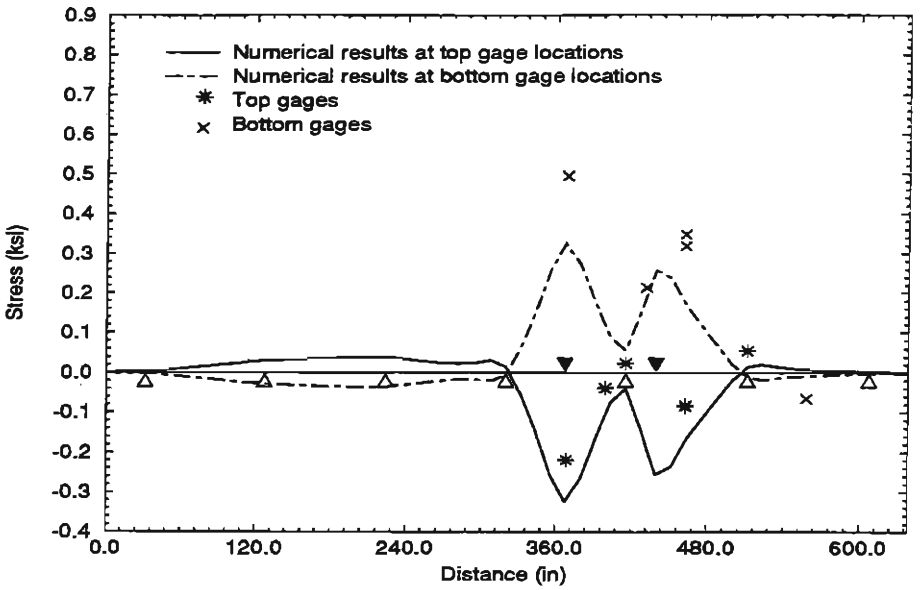

Figure 4.3: Normal Stress in Transverse Direction along Gage Line 2 (Case 2D)

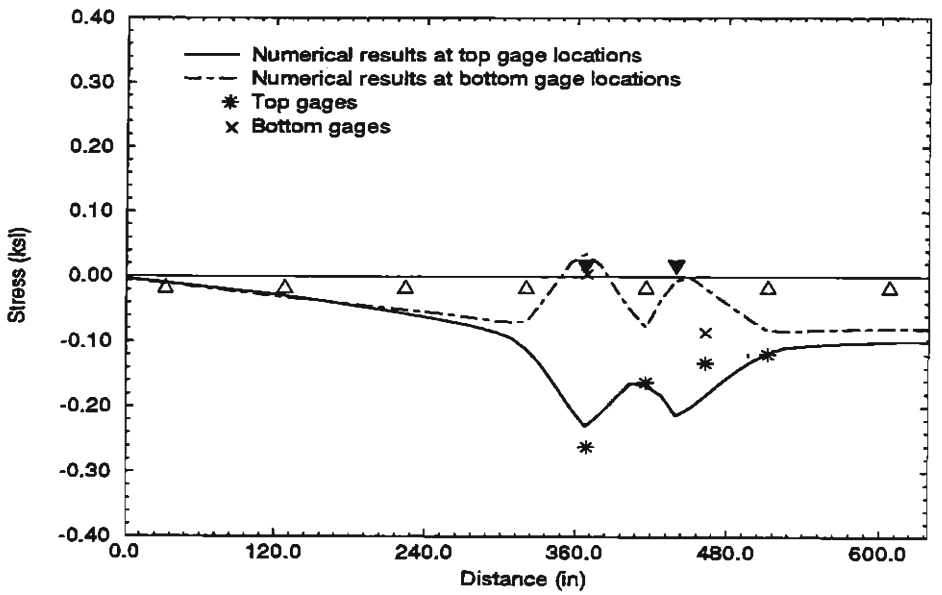

Figure 4.4: Normal Stress in Longitudinal Direction along Gage Line 2 (Case 2D)

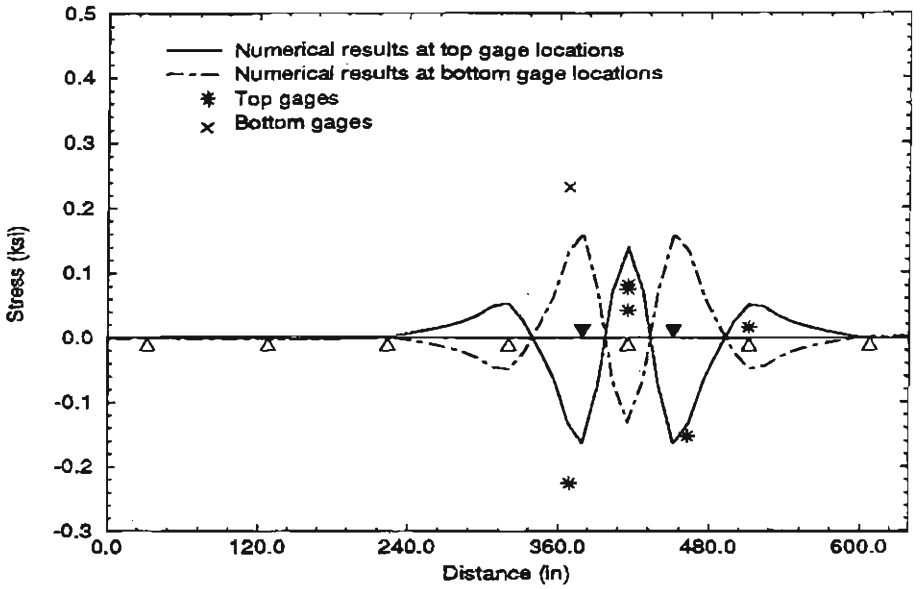

Figure 4.5: Normal Stress in Transverse Direction along Gage Line 3 (Case 3A)

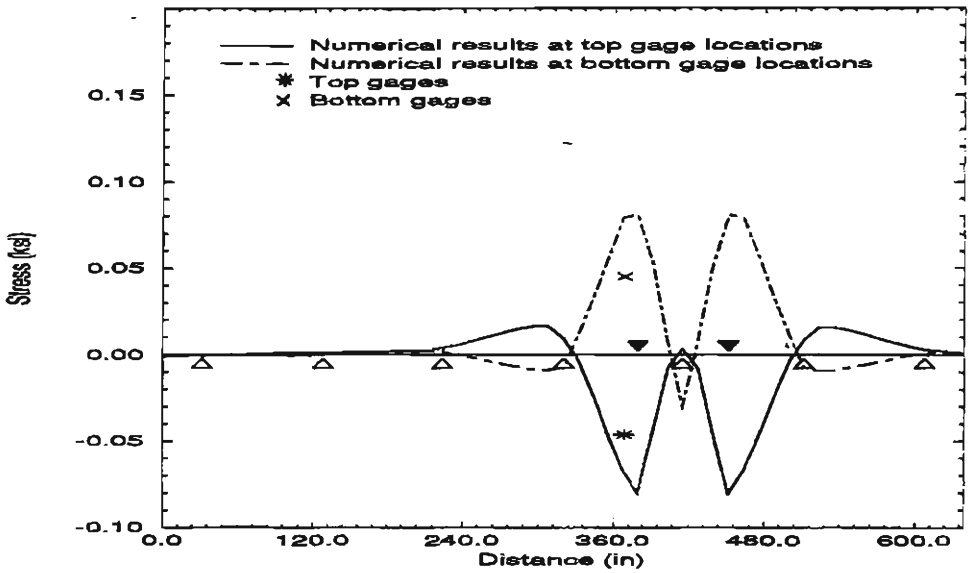

Figure 4.6: Normal Stress in Longitudinal Direction along Gage Line 3 (Case 3A)

Chapter 5

SUMMARY AND CONCLUSIONS

5.1 Summary

The deterioration of a bridge deck due to the corrosion of top reinforcing bars could be prevented by eliminating the top reinforcement in the deck. This new concept was implemented in the design of an experimental deck in a four-span bridge, in which the top reinforcement was eliminated. The reinforcement in the control deck conforms to the specifications of AASHTO (AASHTO 1989). To assess the maximum tensile stresses developed at the top of the deck under traffic loads, the behavior of the bridge deck was investigated with a test truck positioned at different locations.

The test truck chosen for the field test consisted of a front axle of 16.5 kips and a rear tandem axle of 56.65 kips as well as a trailing tandem axle of 32.75 kips. The total weight of the test truck was 106 kips, which is 47% more than a conventional HS20 truck. The test truck was placed at three different longitudinal positions along the bridge. They were near the abutment, mid-span, and pier. When the test truck was near the abutment

and the pier, the test truck was placed at six positions along the transverse direction. When the test truck was near the mid-span, the test truck was placed at seven positions along the transverse direction. Therefore, there were totally nineteen truck positions on the bridge deck.

The response of the bridge deck under the test truck was monitored with embedded strain gages. There were five designated gage lines along the longitudinal direction of the bridge. Three gage lines were located in the experimental deck of the bridge, and the other two gage lines were located in the control deck of the bridge. Along each gage line, there were seven gage points where gages were placed at the top and bottom of the deck along the transverse and longitudinal directions of the bridge.

It is found from the test results that when a truck load was near an abutment or a pier, the transverse tensile strains at the bottom of the deck were close to the cracking strain of deck concrete (140 μs). When a truck load was near a mid-span, the transverse tensile strains at the bottom of the deck exceeded the cracking strain. For all the load cases considered here, the transverse tensile strains at the top of the deck were always less than 40 μs which are much less than the cracking strain.

The behavior of the bridge deck under the three load groups has been analyzed with the finite element method. The numerical results have been compared with the test results. It is found that the numerical predictions of the deck response under the test truck are close to the test results. When the test truck is near a mid-span of the bridge deck, the transverse tensile stresses at the top of the deck is very small due to girder deflections. For all three load groups considered here, the transverse tensile stresses at the top of the deck are only 30% of the modulus of rupture of deck concrete (590 psi), and are even less than the fatigue strength of deck concrete (355 psi).

5.2 Conclusions

From the experimental and numerical investigations of the response of a four-span slab-girder deck subjected to truck loads, the following conclusions have been reached.

1) A finite element model consisting of solid and 3-D beam elements is suitable for the stress analysis of slab-girder bridge decks. The numerical results correlate well with the test results. Hence, this numerical model can be used to investigate the response of a bridge deck under different load conditions.

2) From the test and numerical results, it has been found that the tensile stresses developed at the top of the deck are much less than the modulus of rupture of the deck concrete. They are also less than the fatigue strength of the deck concrete. Hence, it can be concluded that traffic loads alone are not sufficient to cause cracking at the top of the deck, since the normal truck loads are smaller than the designated truck loads used in the field tests and numerical analysis.

3) Results of this and prior studies indicate that top reinforcement is not necessary, except for the longitudinal reinforcement near an abutment or a pier. This can possibly slow down the deterioration of a deck due to the corrosion of top reinforcement.

For further studies, it will be informative to conduct non-linear stress analysis of the bridge deck, considering the cracking of concrete. Such studies will provide a better understanding of the behavior of concrete bridge decks under extreme traffic loads, as well as the effects of shrinkage and temperature cracks.

REFERENCES

ACI (1989), Building Code Requirements for Reinforced Concrete (ACI 318-89), American Concrete Institute.

Allen, J. H. (1991). "Cracking, Serviceability and Strength of Concrete Bridge Decks", Third Bridge Engineering Conference, *Transportation Research Record No. 1290*, Transportation Research Board, National Research Council, Washington, D.C., 152-171.

Ballinger, C. A. (1972), "Cumulative Fatigue Damage Characteristics of Plain Concrete", *Transportation Research Board Report No. 372.*

Beal, D. B. (1982), "Load Capacity of Concrete Bridge Decks", *Journal of the Structural Division*, ASCE, Vol. 108, No. ST4, 814-832.

Cao, L., Allen, J. H. and Shing, P. B. (1993), "A Case Study of Elastic Concrete Deck Behavior in a Four-Span Prestressed Girder Bridge: Finite Element Analysis", *Research Series No. CU/SR-93/1 (National Technical Information Service, #CDOT-DTD-CU-93-7)*, CEAE Department, University of Colorado at Boulder, January.

Fang, I. K., Worley, J. A., Burns, N. H. and Klingner, R. E. (1990). "Behavior of Isotropic R/C Bridge Decks on Steel Girders", *Journal of Structural Engineering*, ASCE, Vol. 116, No. 5, 659-678.

Hsu, T. T. C. (1981), "Fatigue of Plain Concrete", *ACI Journal*, July-August, 292-305.

Oh, B. H. (1986), "Fatigue Analysis of Plain Concrete in Flexure", *Journal of Structural Engineering*, ASCE, Vol. 112, No. 2, 273-288.

Standard Specifications for Highway Bridges (1989), 14th ed., AASHTO, Washington, D.C..

Tepers, R. and Kutti, T. (1979), " Fatigue Strength of Plain, Ordinary, and Lightweight Concrete", *ACI Journal*, May, 635-652.

USDOT (1989), " The Status of the Nation's Highways and Bridges: Conditions and Performance – *Highway Bridge Replacement and Rehabilitation Program*", U.S. Department of Transportation, Federal Highway Administration.

Wilson, E. L. et al. (1989). *SAP90 Program User's Manual*, Computers & Structures, Inc.

Appendix A

LOCATIONS OF STRAIN GAGES

The actual positions of the strain gages were measured with respect to two reference points, which are the distance from the top of an embedded bar to the surface of the concrete finish machine, and the distance from the top of an embedded bar to the bottom of the form for the concrete slab. These measurements are then converted to distances with respect to the centroidal axis of an embedded bar. They are summarized in Tables A.1 through A.4.

The label of a strain gage as shown in the tables consists of four characters, which indicates its location and orientation. The first character of a gage label refers to the gage line number of the gage. The second character of a gage label refers to a gage point, which is the transverse position along a gage line. The third character of a gage label refers to the top or bottom position in a slab, with T denoting the top and B the bottom. The fourth character of a gage label refers to the gage orientation, with T denoting the transverse direction and L the longitudinal direction. An "X" appending to a label refers to an additional gage at the same location. For example, gage 2EBT refers to the strain gage located at gage point E of gage line 2, which is oriented in the transverse direction of the bridge and is at the bottom of the slab. The locations of gage lines and gage points are illustrated in Fig. 2.6.

Table A.1: Positions of Top Strain Gages in the West Span

Strain Gage	Distance to Top of the Deck (in)	Distance to Bottom of the Deck (in)	Deck Thickness (in)
1ATTX	1.31	6.75	8.06
1ATLX	1.38	6.38	7.76
1BTT	1.75	6.31	8.06
1CTTX	1.38	6.12	7.50
1CTL	1.25	6.63	7.88
1DTT	1.44	5.88	7.31
1ETTX	1.31	6.38	7.69
1ETLX	1.31	6.25	7.56
1FTT	1.13	6.69	7.81
1FTL	1.50	6.25	7.75
1GTT	1.31	6.31	7.62
2ATTX	1.81	6.63	8.44
2ATLX	1.31	6.63	7.94
2BTT	2.06	6.69	8.75
2CTTX	1.56	6.25	7.81
2CTL	1.81	6.63	8.44
2DTT	2.06	6.69	8.75
2ETTX	1.56	6.25	7.81
2ETLX	1.62	6.63	8.25
2FTT	1.31	6.50	7.81
2FTL	1.07	6.37	7.44
2GTT	2.12	6.44	8.56
3ATLX	1.12	6.69	7.81
3ATT	1.12	6.63	7.75
3CTT	0.87	6.44	7.31
3CTTX	1.25	5.75	7.00
3ETT	0.75	6.44	7.19
3FTT	1.25	5.88	7.13
Average	1.42	–	7.83
Std. Deviation	0.33	–	0.46

Table A.2: Positions of Bottom Strain Gages in the West Span

Strain Gage	Distance to Top of the Deck (in)		Distance to Bottom of the Deck (in)		Deck Thickness(in)
	T	L	T	L	
1ABTX	7.12	–	1.38	–	8.50
1ABLX	–	6.00	–	2.19	8.19
1BBT	6.88	–	1.31	–	8.19
1DBT	6.25	–	1.13	–	7.38
1EBTX	6.31	–	1.00	–	7.31
1EBLX	–	5.62	–	1.94	7.56
1GBT	6.25	–	1.50	–	7.75
2ABTX	7.00	–	1.19	–	8.19
2ABLX	–	6.25	–	1.88	8.13
2BBT	7.13	–	1.31	–	8.44
2DBT	7.12	–	1.19	–	8.31
2EBTX	6.50	–	1.19	–	7.69
2EBLX	–	5.75	–	1.00	6.75
2GBT	7.19	–	1.31	–	8.50
3ABTX	6.50	–	1.13	–	7.63
3ABL	–	5.81	–	2.06	7.87
3EBT	6.00	–	1.19	–	7.19
Average	–	–	1.23	1.81	7.86
Deviation	–	–	0.13	0.42	0.49

Note: T means transverse gages and L means longitudinal gages.

Table A.3: Positions of Top Strain Gages in the East Span

Strain Gage	Distance to Top of the Deck (in)	Distance to Bottom of the Deck (in)	Deck Thickness(in)
4ATT	1.75	5.75	7.50
4ATLX	1.88	6.44	8.32
4CTTX	1.75	6.69	8.44
4ETT	1.75	5.89	7.64
5CTTX	2.00	6.50	8.50
5CTL	1.88	6.63	8.51
5ETT	1.44	5.75	7.19
5FTT	2.06	5.88	7.94

Table A.4: Positions of Bottom Strain Gages in the East Span

Strain Gage	Distance to Top of the Deck (in)	Distance to Bottom of the Deck (in)	Deck Thickness(in)
4ABTX	7.25	2.19	9.44
4ABL	6.00	1.19	7.19
4EBT	6.25	1.25	7.50
4EBL	6.13	1.43	7.56
5EBTX	6.63	1.00	7.63

Appendix B

STRAIN GAGE READINGS FROM FIELD TESTS

Table B.1: Strain Gage Readings under Load Group 1 (μs)

Strain Gage	Load Case					
	A	B	C1	C2	D1	D2
1ATT	0.1	-3.1	-1.7	2.8	-2.8	2.8
1ABT	-46.2	-1.3	-0.3	-62.3	0.7	-66.5
1BBT	20.6	6.2	1.4	28.0	7.8	31.5
1CTT	-13.2	7.7	8.3	-20.0	5.6	-17.5
1DTT	-18.3	-7.0	6.6	-3.1	-6.8	-2.5
1ETT	31.6	32.6	13.7	0.2	28.3	-0.1
1EBT	-76.7	-72.8	-7.9	9.2	-69.0	8.3
1EBTX	-76.6	-72.9	-7.3	9.3	-68.2	8.3
1FTT	-10.0	-15.4	-11.2	-1.8	-9.4	-0.5
1GTT	-4.6	14.8	-8.6	-1.5	-4.8	-0.7
1GBT	6.8	-30.8	4.7	1.5	4.8	1.0
1ABL	-0.2	0.0	-0.1	-0.2	-0.1	-0.4
1CTL	-1.1	-6.2	-2.8	1.3	-5.5	1.6
1ETL	24.3	12.5	17.2	1.0	20.9	0.1
1EBL	-7.9	27.5	3.5	1.8	11.7	0.9
1FTL	5.9	15.5	17.3	-0.9	14.4	0.0
2CTT	-0.9	-5.1	-2.3	0.9	-4.3	0.5
2EBT	-11.1	-4.4	-12.5	-1.8	-9.1	-0.3
2ABL	-0.3	2.4	1.3	-0.3	1.8	-2.0
2EBL	-1.7	10.1	-4.5	1.1	-8.3	1.3
3CTT	-7.9	-12.9	-9.9	-3.6	-12.5	-2.8
3EBT	-1.1	3.3	-0.7	-0.4	1.8	-0.4
3ABL	-5.3	-6.9	-6.1	-3.1	-6.8	-3.0

Note: The labeling of strain gages is explained in Appendix A. The load cases are illustrated in Figures 2.3 to 2.5. The negative strain readings refer to tensile strains, and the positive strain readings refer to compressive strains.

Table B.2: Strain Gage Readings under Load Group 2 (μs)

Strain Gage	Load Case						
	A	B1	B2	C1	C2	D	E
1CTT	9.0	12.4	-3.1	10.2	2.2	10.8	3.6
1EBT	-1.0	-5.6	3.0	-7.8	1.8	-1.2	1.3
1EBL	-1.5	-9.1	-6.6	-8.7	-8.9	-6.6	-0.1
2ATTX	-8.9	22.8	20.4	-6.6	52.3	51.9	-8.8
2ABTX	17.3	-59.2	-46.7	4.3	-117.9	-117.0	19.8
2BTT	-7.6	24.5	-8.8	-4.1	3.1	9.4	-10.2
2CTT	-4.1	-3.9	-5.2	-6.8	-3.8	-5.5	-3.5
2DBT	15.0	-15.7	-1.3	-7.2	-12.0	-50.7	14.5
2ETT	24.4	53.9	-6.0	44.3	-1.9	20.3	-5.2
2ETTX	23.4	52.6	-6.3	43.1	-2.3	19.4	-4.9
2EBT	-66.2	-173.8	11.0	-142.1	-3.2	-82.3	5.3
2EBTX	-62.6	-160.8	9.4	-131.2	-3.9	-75.4	4.9
2FTT	-8.0	-10.0	-6.8	4.8	-7.4	-13.0	-1.4
2GBT	-176.2	5.8	21.0	-68.7	21.8	15.3	-93.3
2ATL	22.9	36.7	36.0	20.1	48.3	61.8	15.5
2ABL	0.0	0.0	-0.3	0.4	-0.3	-1.0	0.4
2CTL	26.1	41.9	28.6	23.2	36.5	38.4	18.3
2ETL	35.3	33.7	18.2	35.7	22.7	31.3	21.8
2EBL	21.0	22.6	13.7	14.3	14.3	20.3	23.4
2FTL	51.7	39.1	17.1	44.7	21.9	28.1	33.4
3CTT	-4.4	-8.4	-5.4	-8.5	-7.5	-9.3	-3.9
3EBT	-9.1	-14.4	8.0	-17.3	4.9	-10.3	-4.2
3ABL	-2.1	-8.0	-10.1	-6.3	-11.5	-10.4	-0.2

Table B.3: Strain Gage Readings under Load Group 3 (μs)

Strain Gage	Load Case					
	A	B	C1	C2	D1	D2
1EBT	0.4	0.0	-1.2	-2.1	0.3	-0.5
1EBL	2.0	1.4	1.5	-0.2	1.7	1.1
2CTT	2.7	1.7	2.3	0.0	2.6	0.3
2EBT	-12.0	-11.8	-13.5	-6.1	-13.9	-2.3
2ABL	0.0	-0.1	0.3	0.0	-0.3	0.5
2EBL	1.7	-2.2	3.7	-0.4	1.1	1.9
3ATT	53.3	-3.8	-3.5	36.8	-6.2	48.0
3ABTX	-54.9	6.1	7.1	-29.4	8.1	-43.1
3CTT	-19.2	-3.6	-1.4	-6.2	-6.7	-10.9
3CTTX	-17.6	-4.0	-1.5	-4.8	-7.2	-9.1
3ETT	36.0	51.1	24.8	-3.2	42.0	-1.7
3EBT	-66.3	-72.9	-33.0	16.4	-73.4	17.3
3FTT	-3.8	-18.7	3.6	1.2	-7.1	2.7
3ATL	10.9	-0.5	-0.9	8.9	-0.2	-1.0
3ABL	-10.7	-0.9	0.4	2.3	0.1	15.2

Table B.4: Strain Gage Readings under Load Group 4 (μs)

Strain Gage	Load Case						
	A	B1	B2	C1	C2	D	E
4CTTX	-2.7	-1.5	-5.6	-1.6	-5.2	0.2	-5.0
4ETT	28.2	46.5	-7.1	40.1	-4.3	25.3	-4.5
4EBT	-78.1	-133.2	11.3	-118.6	1.2	-79.8	0.7
4ABL	12.7	24.1	24.8	17.2	30.2	22.1	9.0
4EBL	18.2	18.3	18.4	13.6	21.9	17.0	16.8
5CTTX	-4.4	3.1	8.5	-2.9	9.3	7.7	-7.5
5ETT	5.8	9.8	1.1	8.5	3.1	8.4	-2.1
5EBTX	-5.1	-2.0	3.3	-3.9	3.6	-1.3	-4.6
5FTT	8.4	14.1	4.7	11.2	5.9	12.8	-0.6
5CTL	-0.2	-7.8	-6.2	-3.3	-8.1	-6.6	0.7

Table B.5: Strain Gage Readings under Load Group 5 (μs)

Strain Gage	Load Case					
	A	B	C1	C2	D1	D2
4CTTX	0.9	0.8	1.0	0.9	0.3	-0.2
4ETT	2.4	3.2	3.5	0.8	3.0	0.0
4EBT	-6.2	-5.2	-9.3	-3.8	-6.5	-2.7
4ABL	2.5	3.1	1.7	1.0	3.3	1.7
4EBL	2.3	2.1	1.0	0.7	2.3	1.3
5CTTX	-13.8	-6.7	-9.4	0.0	-12.0	-1.5
5ETT	39.6	26.5	19.4	1.2	32.3	-0.5
5EBTX	-30.2	-15.2	-14.3	1.9	-24.7	2.6
5FTT	-3.5	-15.7	-2.1	3.5	-10.3	2.4
5CTL	6.4	1.7	5.1	10.0	2.7	8.0

Appendix C

COMPARISON OF TEST AND NUMERICAL RESULTS FOR LOAD GROUP 1

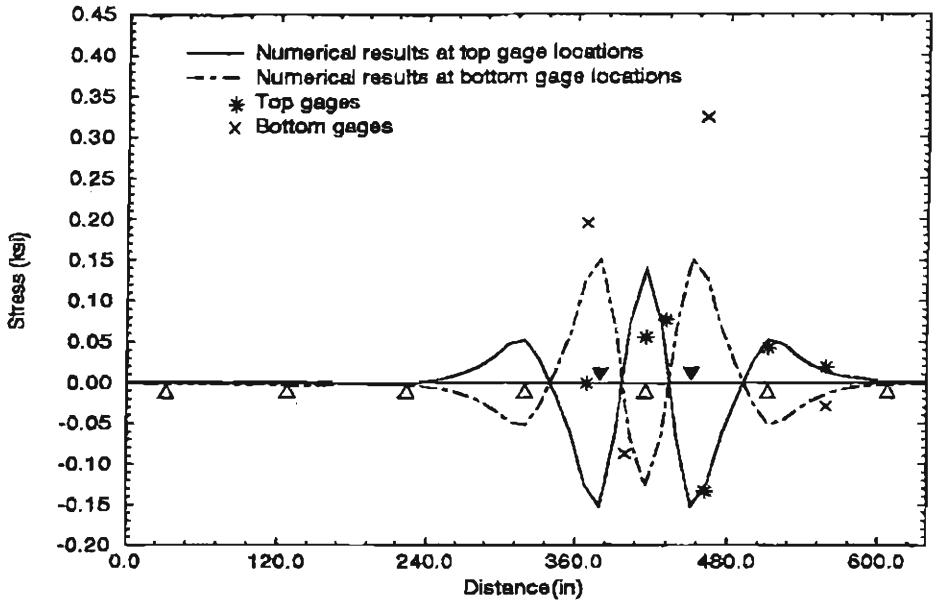

Figure C.1: Normal Stress in Transverse Direction along Gage Line 1 (Case 1A)

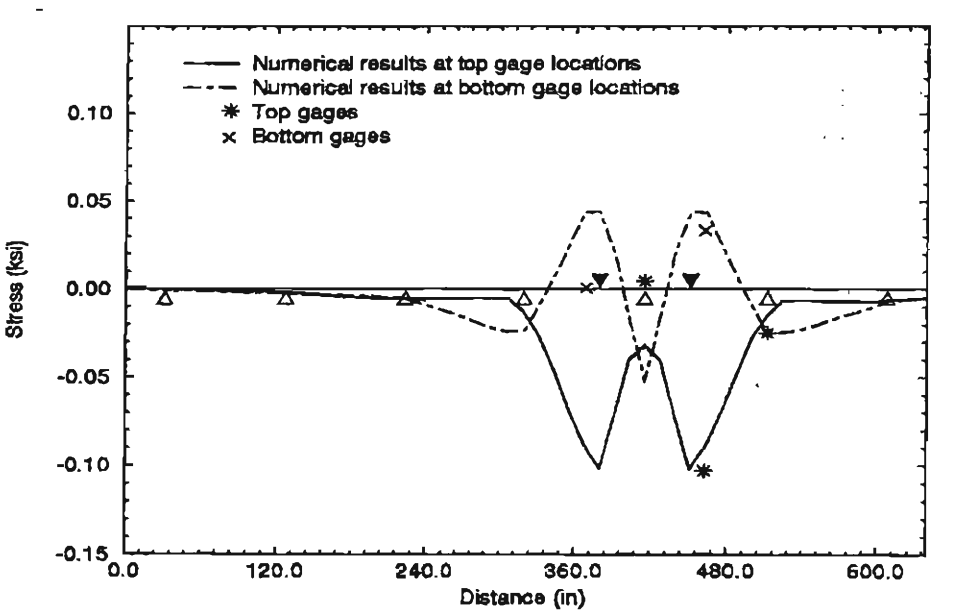

Figure C.2: Normal Stress in Longitudinal Direction along Gage Line 1 (Case 1A)

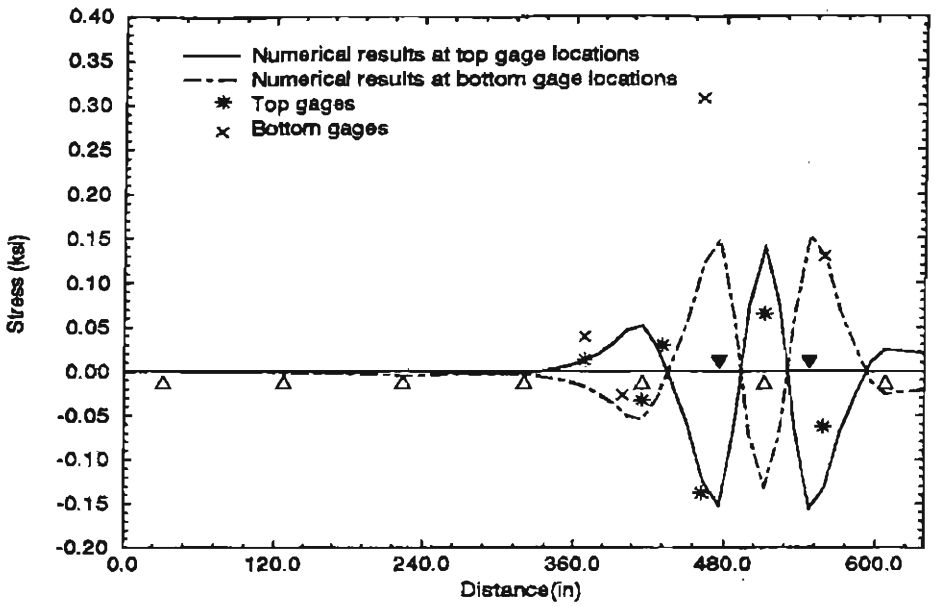

Figure C.3: Normal Stress in Transverse Direction along Gage Line 1 (Case 1B)

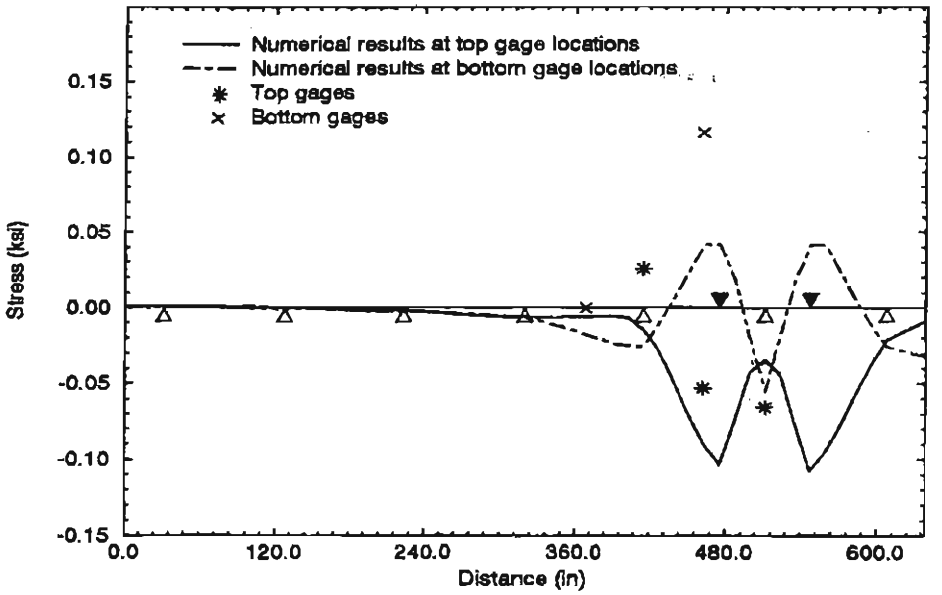

Figure C.4: Normal Stress in Longitudinal Direction along Gage Line 1 (Case 1B)

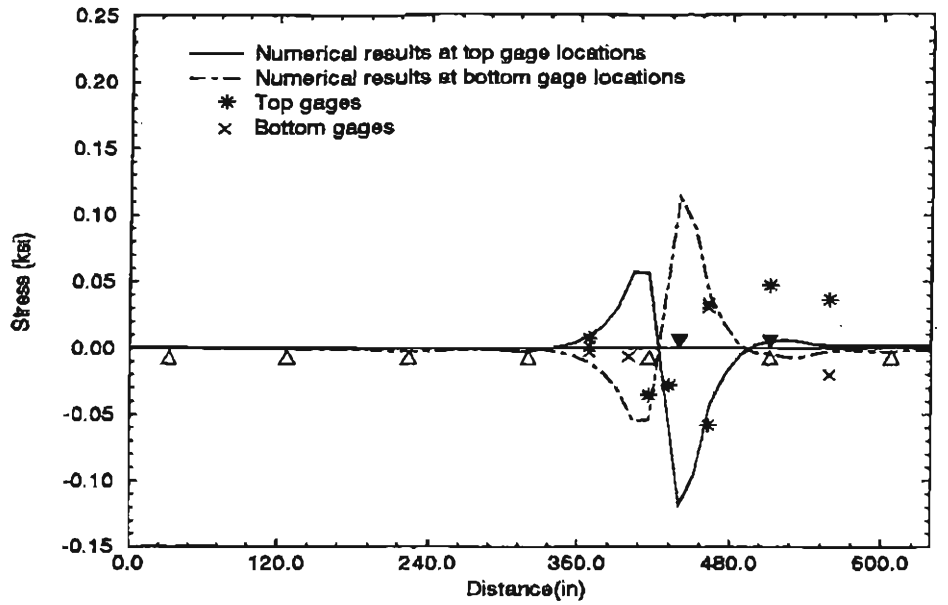

Figure C.5: Normal Stress in Transverse Direction along Gage Line 1 (Case 1C1)

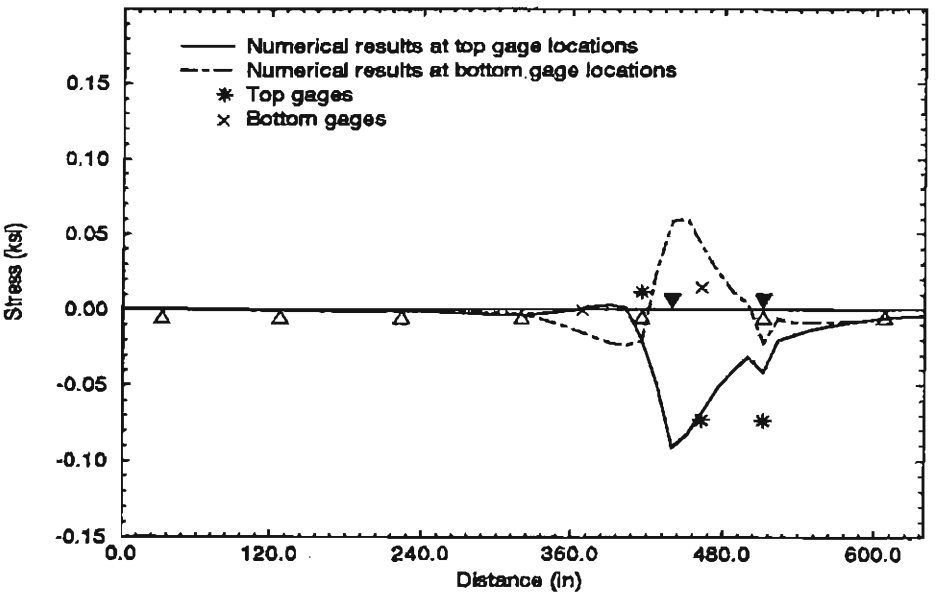

Figure C.6: Normal Stress in Longitudinal Direction along Gage Line 1 (Case 1C1)

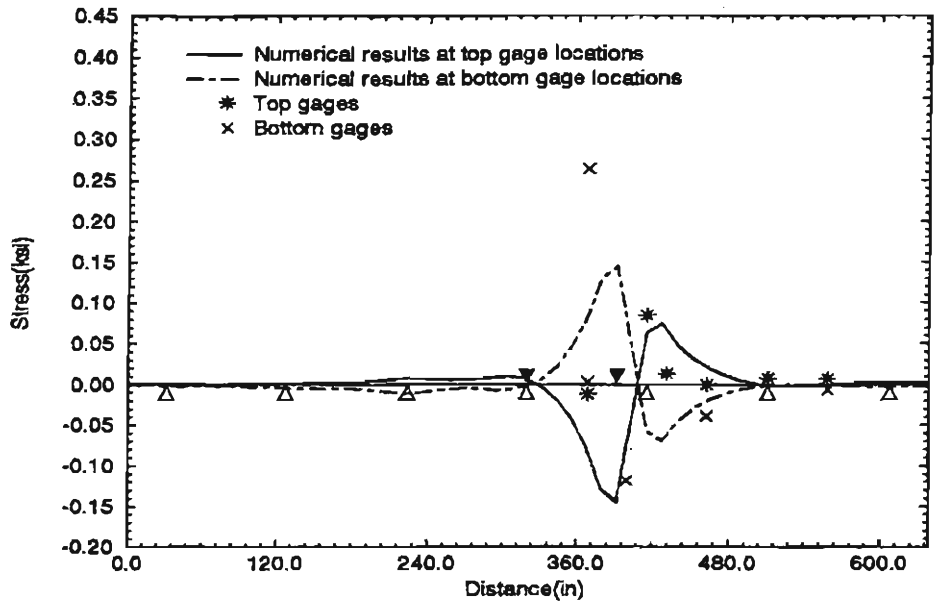

Figure C.7: Normal Stress in Transverse Direction along Gage Line 1 (Case 1C2)

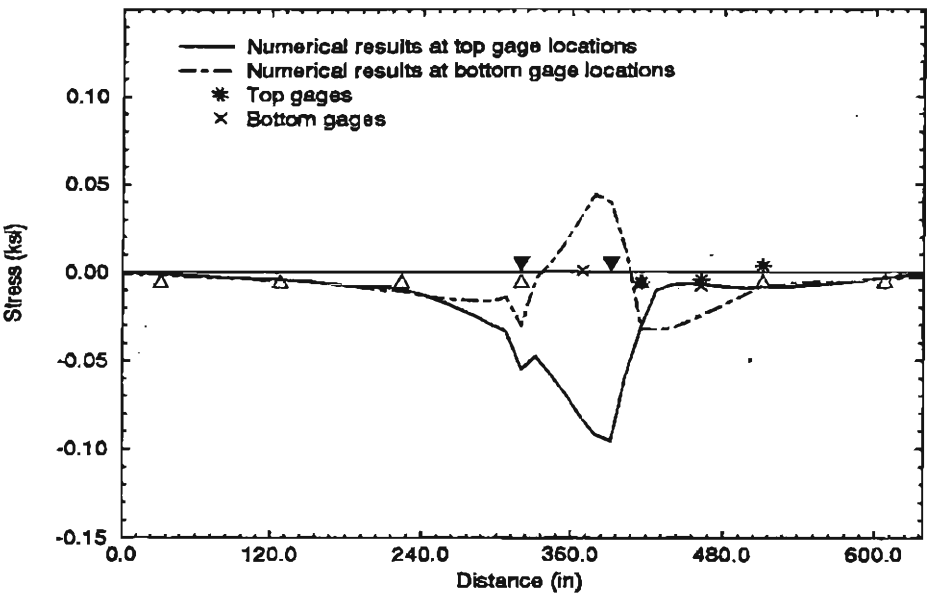

Figure C.8: Normal Stress in Longitudinal Direction along Gage Line 1 (Case 1C2)

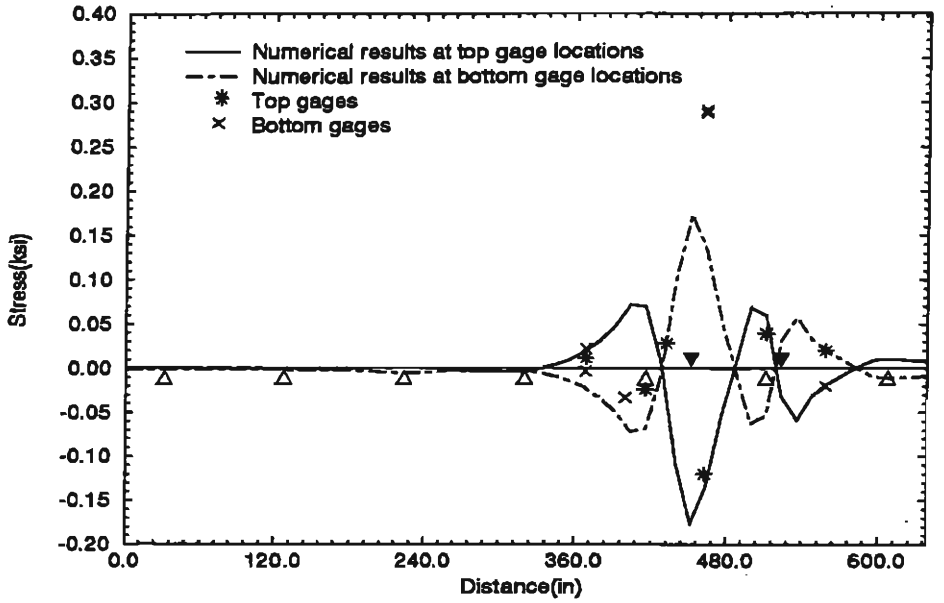

Figure C.9: Normal Stress in Transverse Direction along Gage Line 1 (Case 1D1)

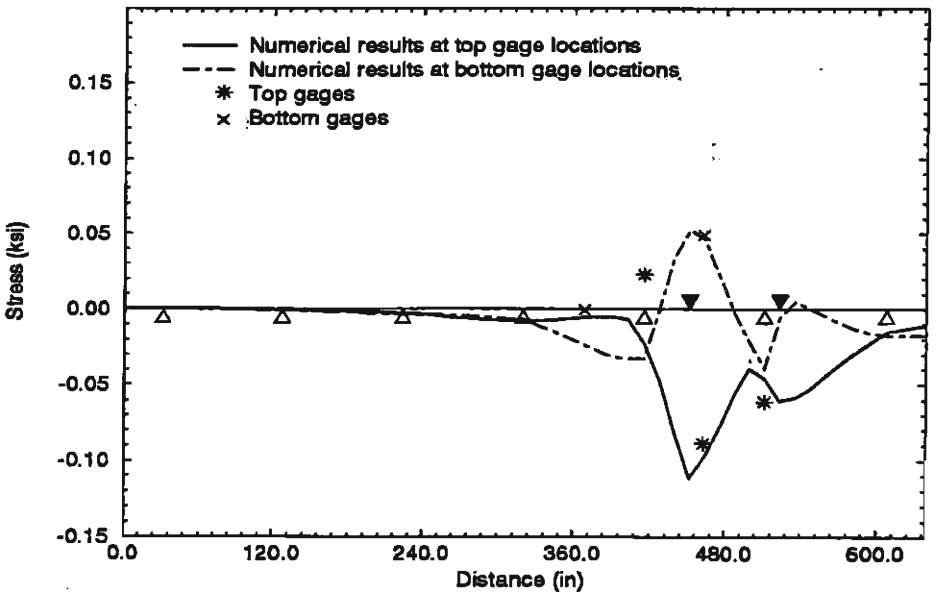

Figure C.10: Normal Stress in Longitudinal Direction along Gage Line 1 (Case 1D1)

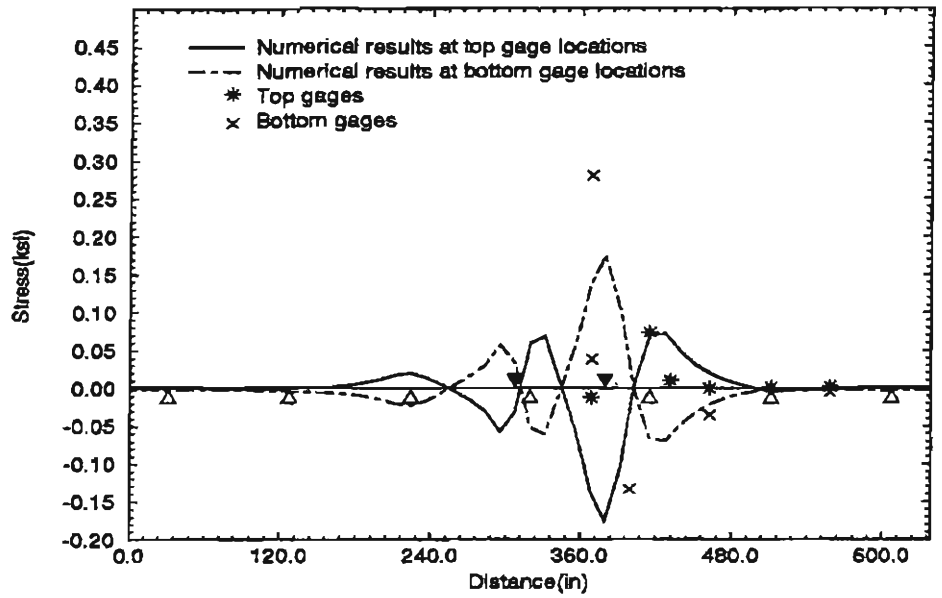

Figure C.11: Normal Stress in Transverse Direction along Gage Line 1 (Case 1D2)

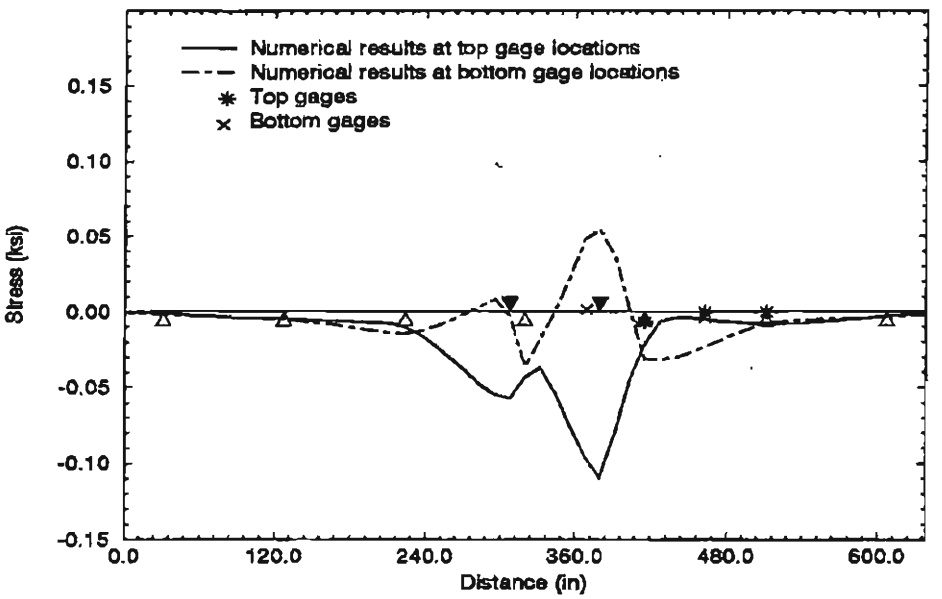

Figure C.12: Normal Stress in Longitudinal Direction along Gage Line 1 (Case 1D2)

Appendix D

COMPARISON OF TEST AND NUMERICAL RESULTS FOR LOAD GROUP 2

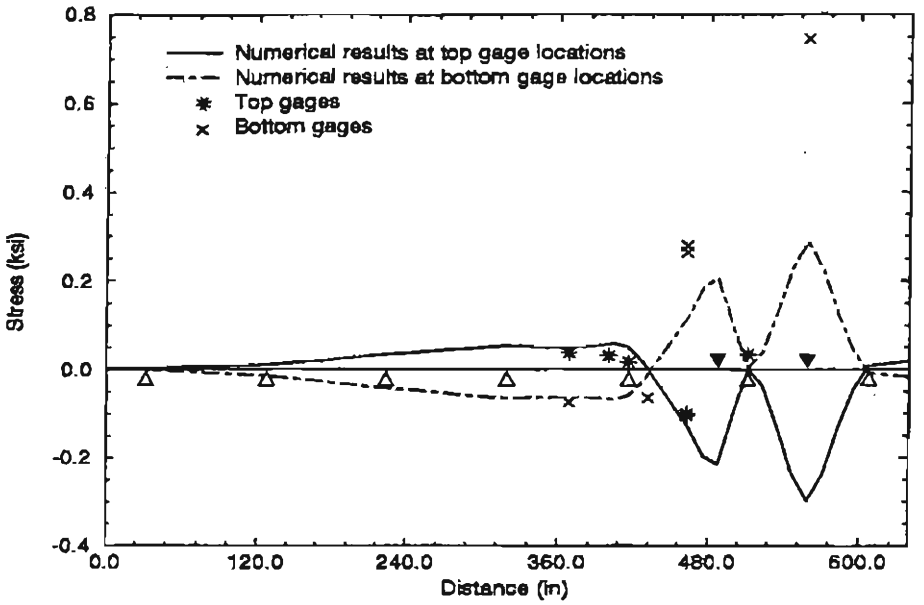

Figure D.1: Normal Stress in Transverse Direction along Gage Line 2 (Case 2A)

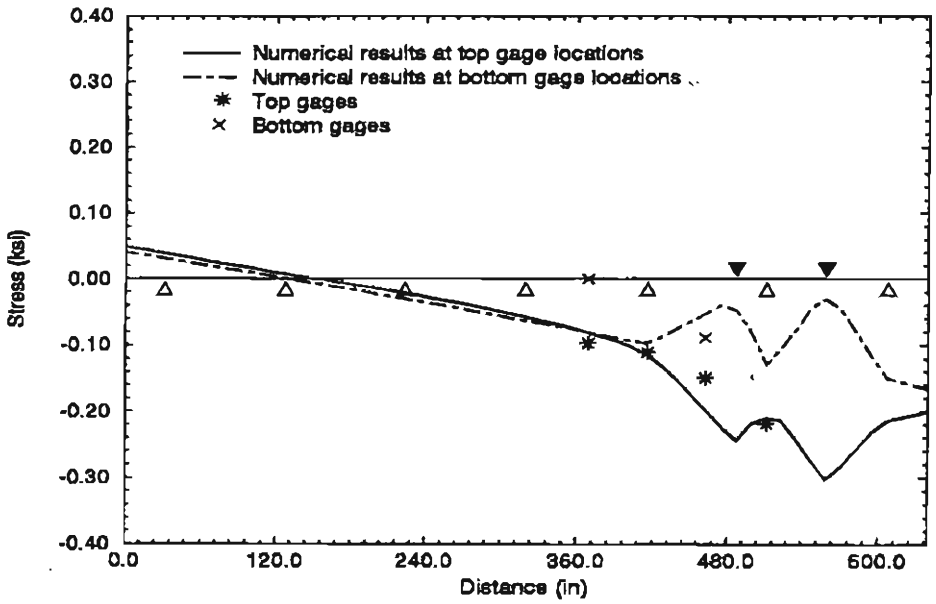

Figure D.2: Normal Stress in Longitudinal Direction along Gage Line 2 (Case 2A)

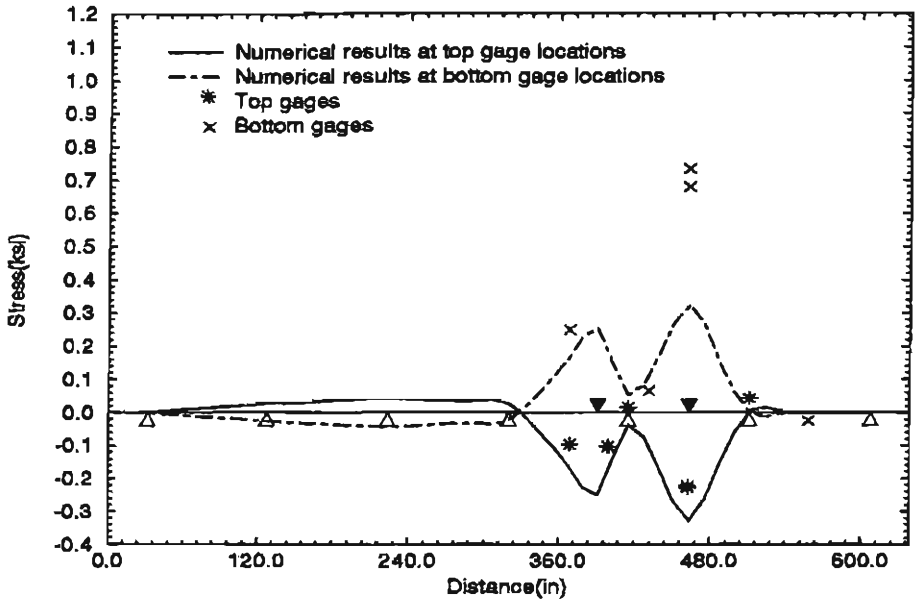

Figure D.3: Normal Stress in Transverse Direction along Gage Line 2 (Case 2B1)

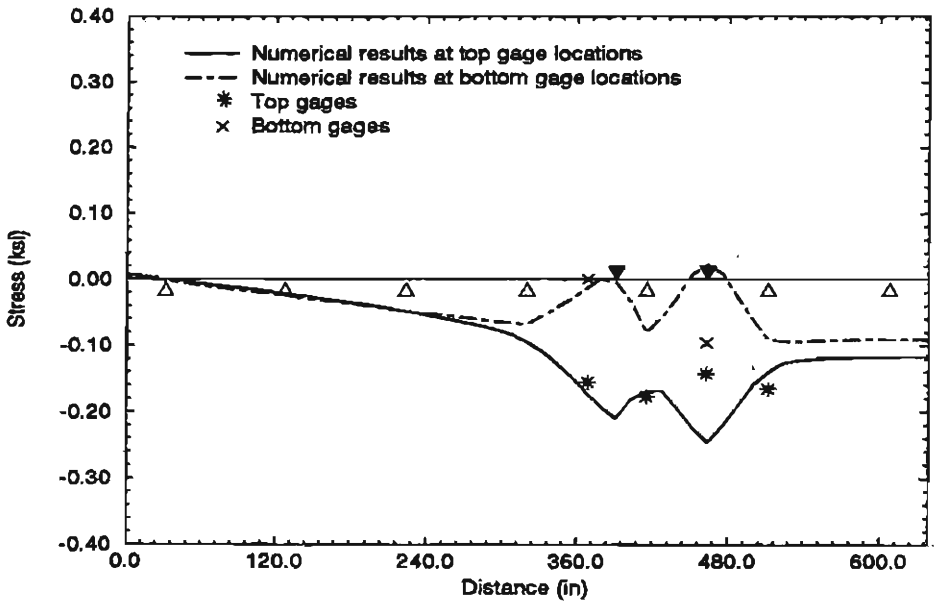

Figure D.4: Normal Stress in Longitudinal Direction along Gage Line 2 (Case 2B1)

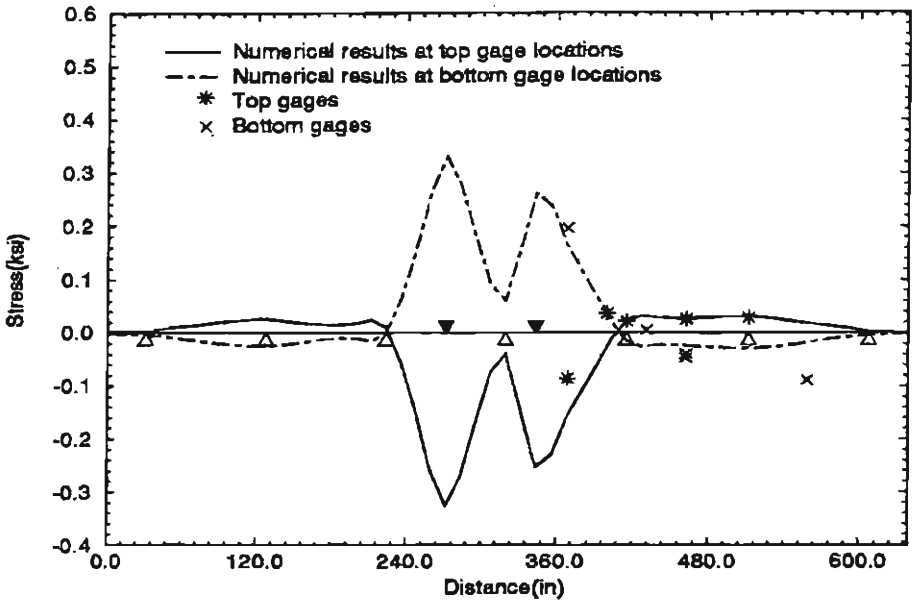

Figure D.5: Normal Stress in Transverse Direction along Gage Line 2 (Case 2B2)

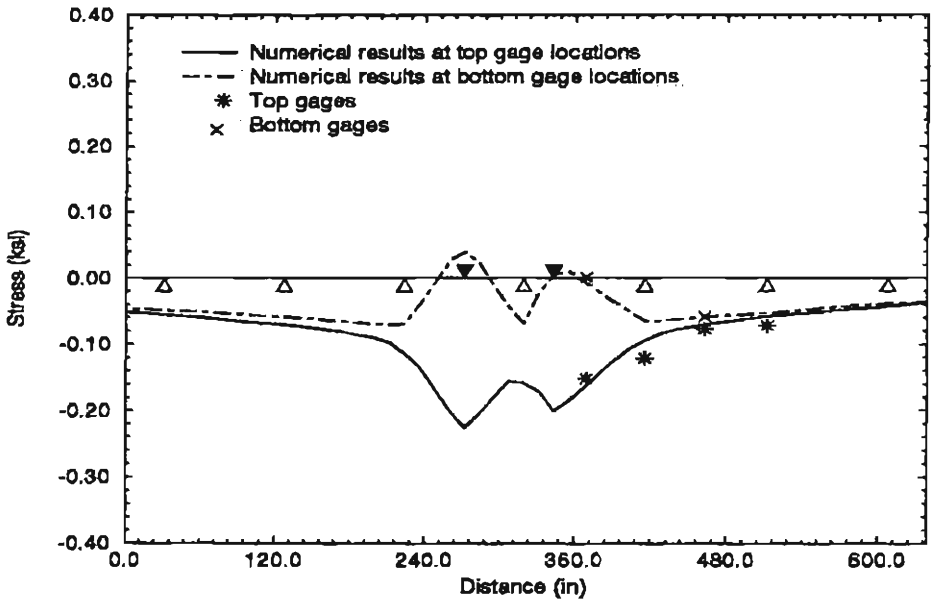

Figure D.6: Normal Stress in Longitudinal Direction along Gage Line 2 (Case 2B2)

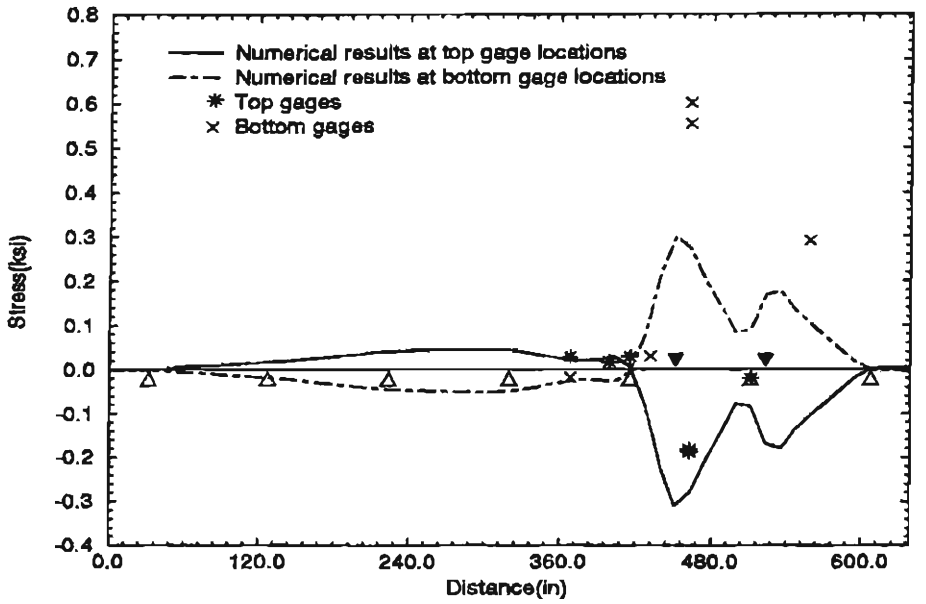

Figure D.7: Normal Stress in Transverse Direction along Gage Line 2 (Case 2C1)

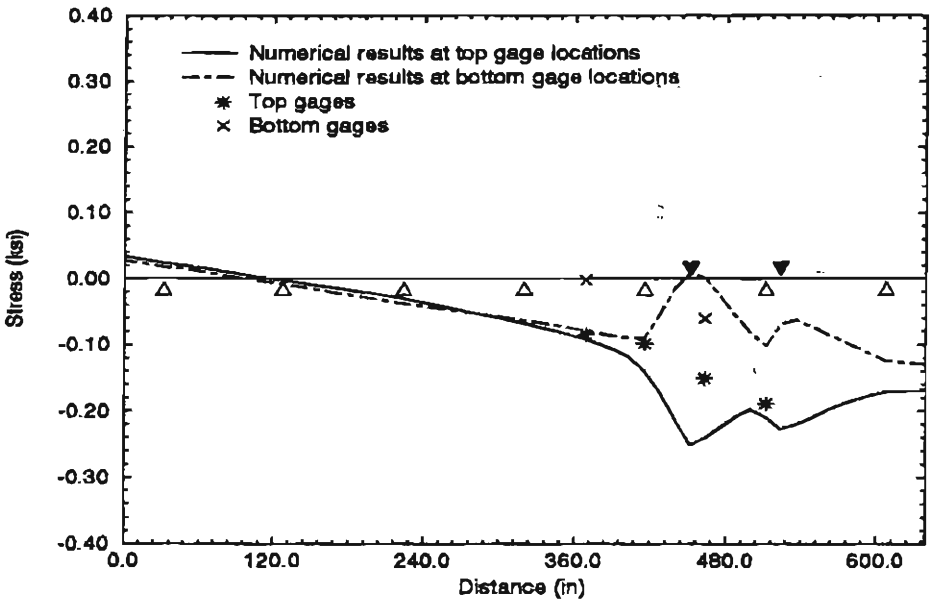

Figure D.8: Normal Stress in Longitudinal Direction along Gage Line 2 (Case 2C1)

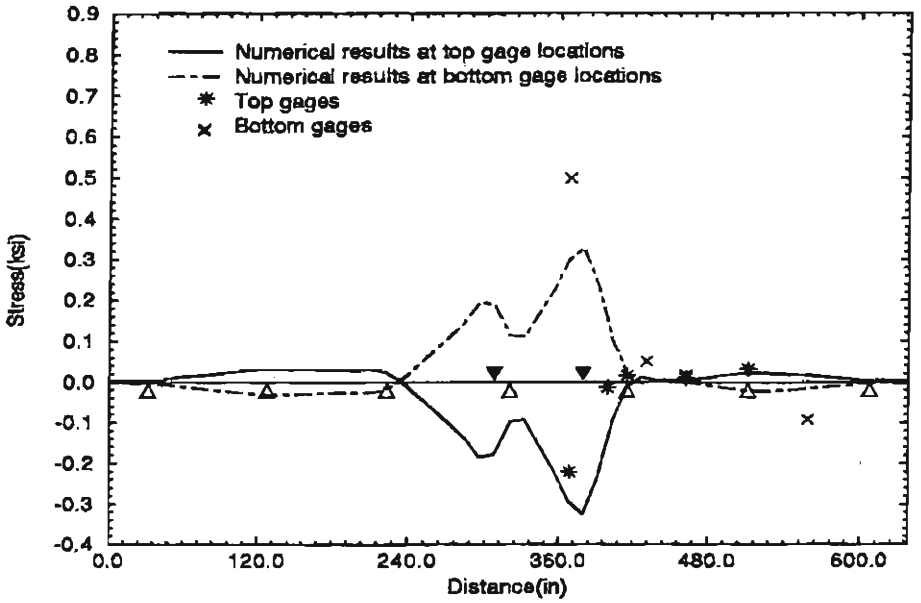

Figure D.9: Normal Stress in Transverse Direction along Gage Line 2 (Case 2C2)

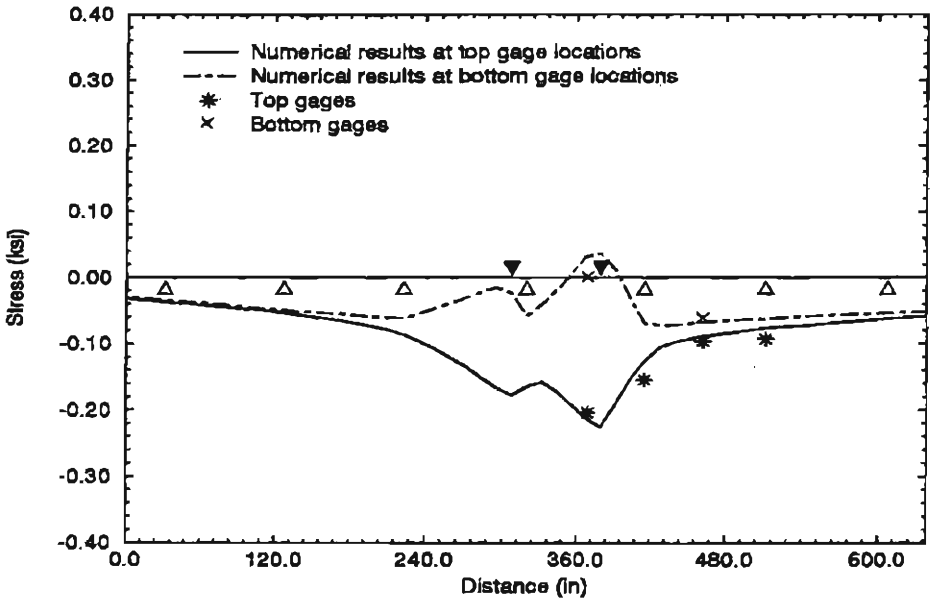

Figure D.10: Normal Stress in Longitudinal Direction along Gage Line 2 (Case 2C2)

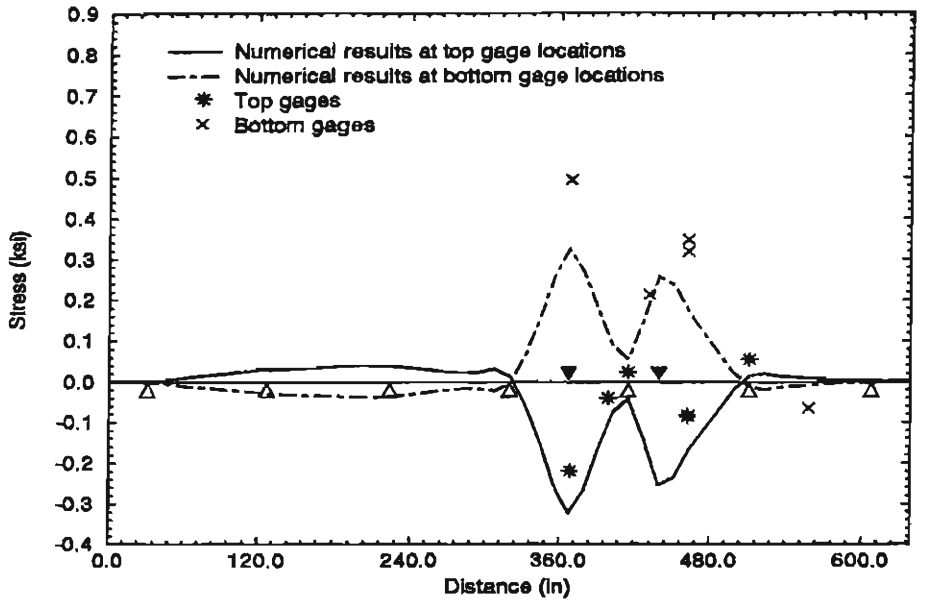

Figure D.11: Normal Stress in Transverse Direction along Gage Line 2 (Case 2D)

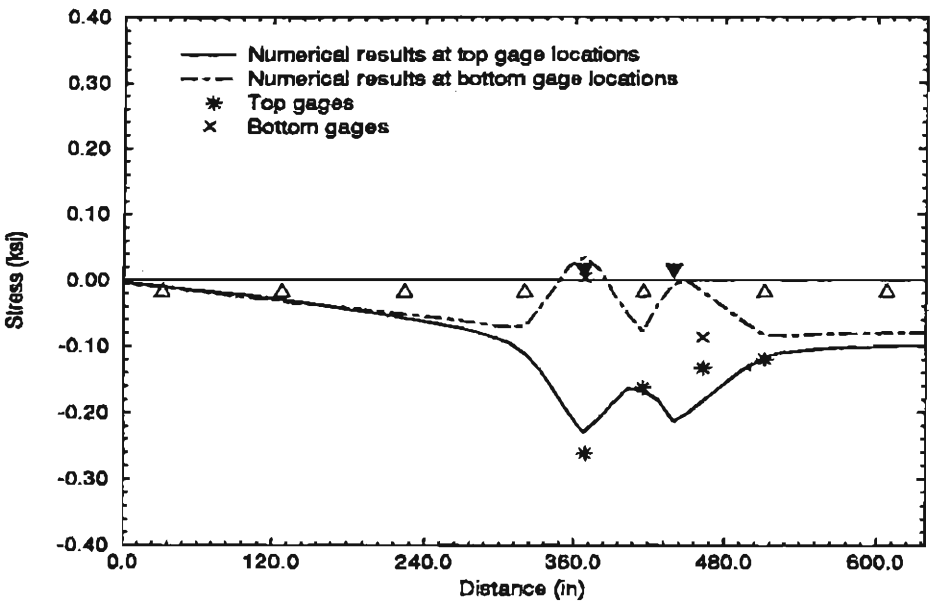

Figure D.12: Normal Stress in Longitudinal Direction along Gage Line 2 (Case 2D)

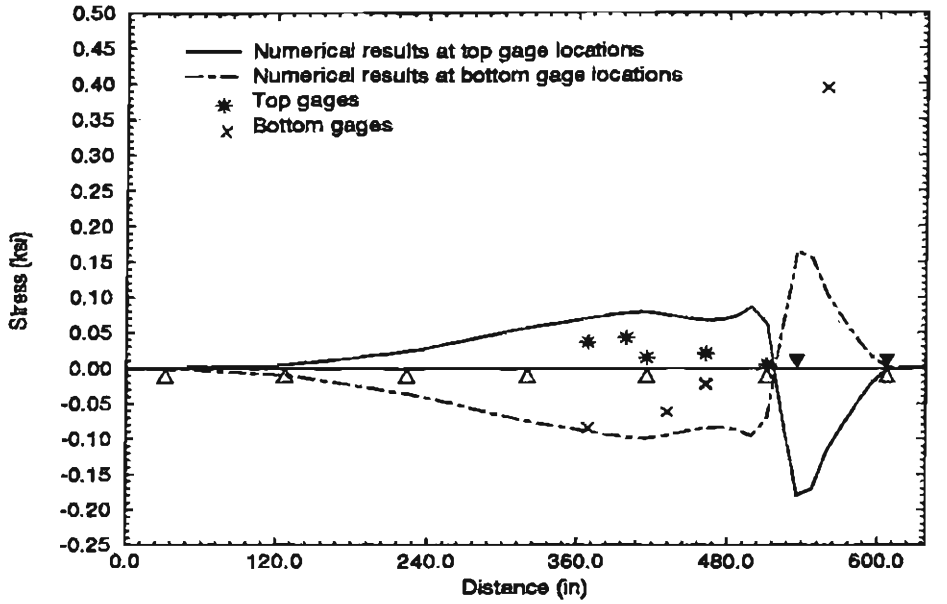

Figure D.13: Normal Stress in Transverse Direction along Gage Line 2 (Case 2E)

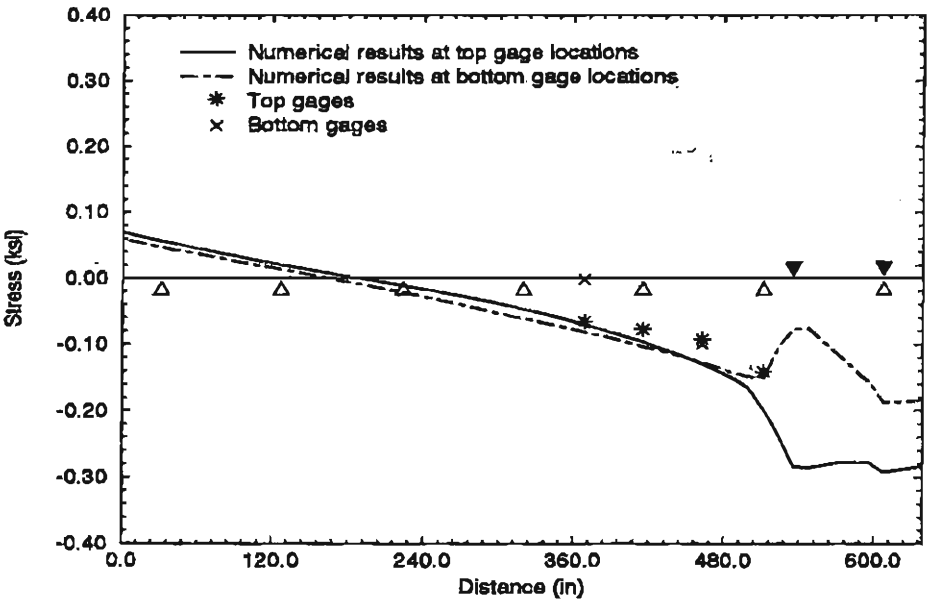

Figure D.14: Normal Stress in Longitudinal Direction along Gage Line 2 (Case 2E)

Appendix E

COMPARISON OF TEST AND NUMERICAL RESULTS FOR LOAD GROUP 3

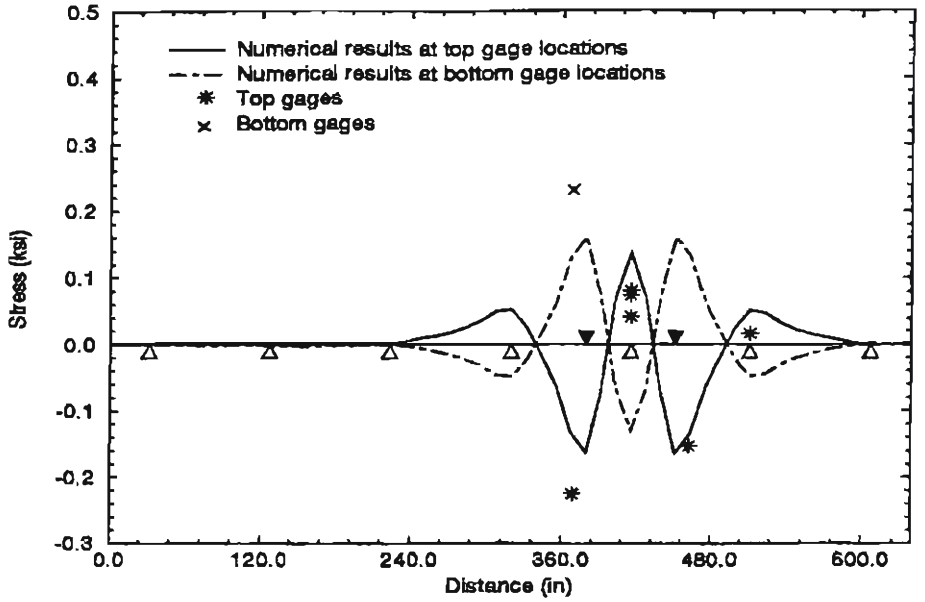

Figure E.1: Normal Stress in Transverse Direction along Gage Line 3 (Case 3A)

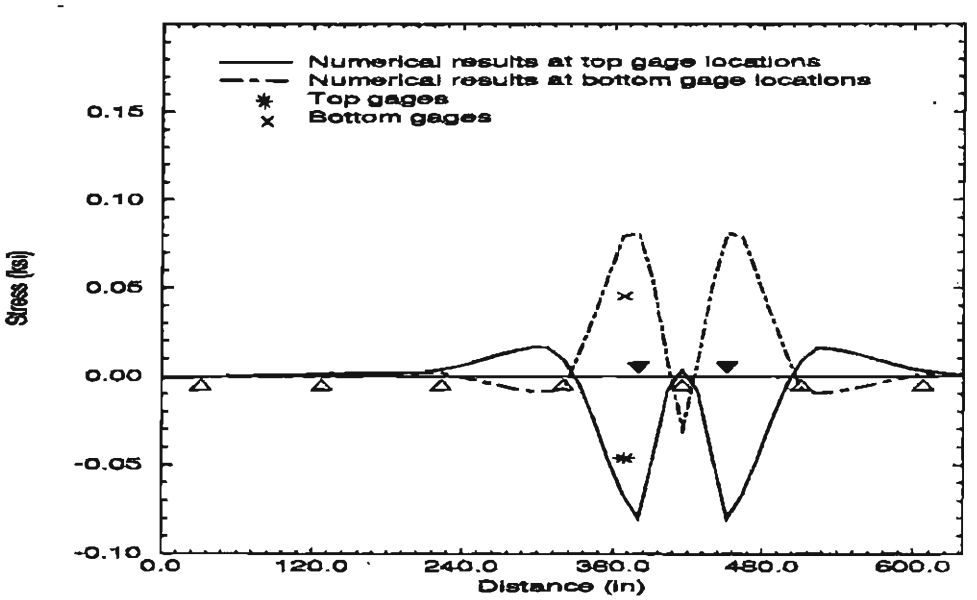

Figure E.2: Normal Stress in Longitudinal Direction along Gage Line 3 (Case 3A)

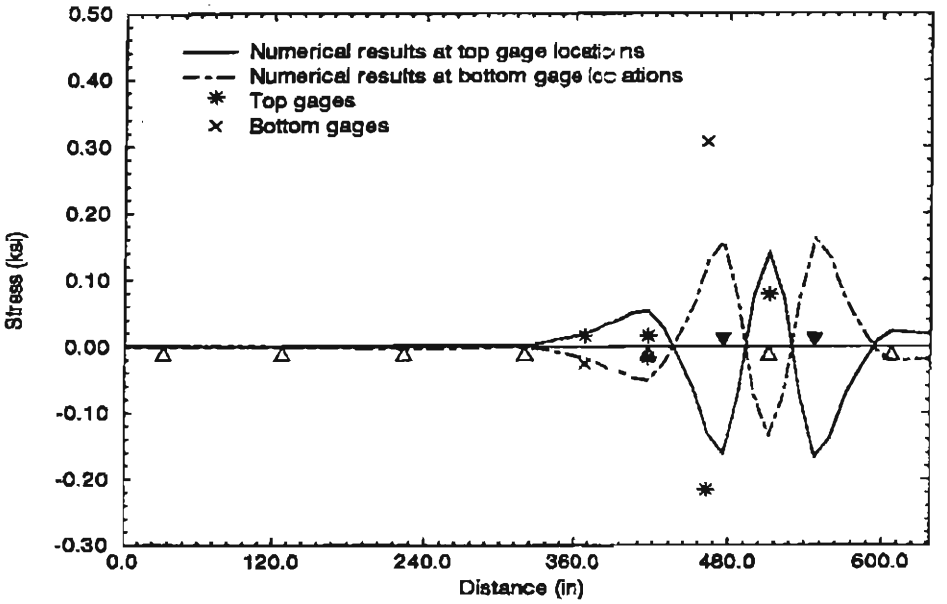

Figure E.3: Normal Stress in Transverse Direction along Gage Line 3 (Case 3B)

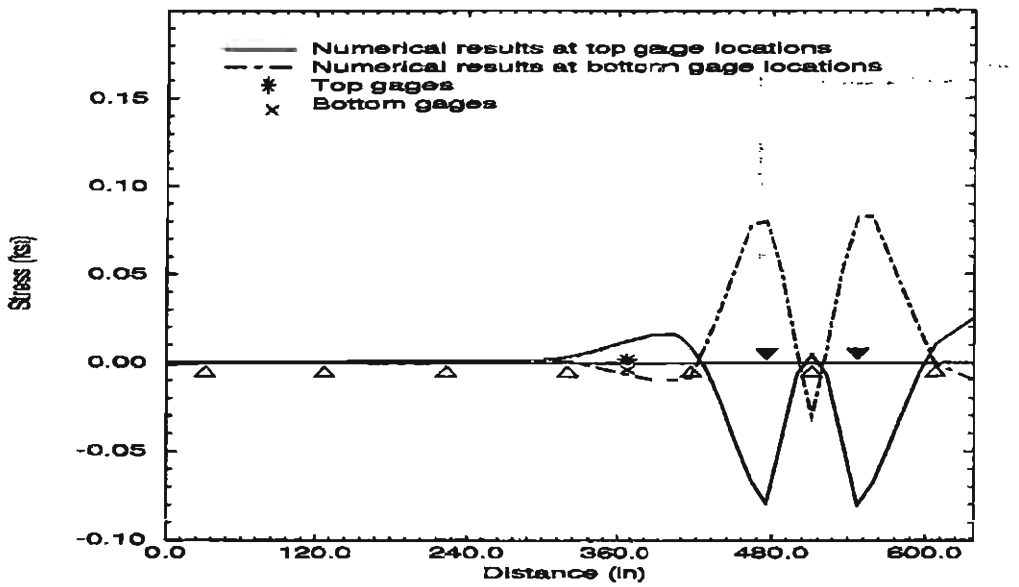

Figure E.4: Normal Stress in Longitudinal Direction along Gage Line 3 (Case 3B)

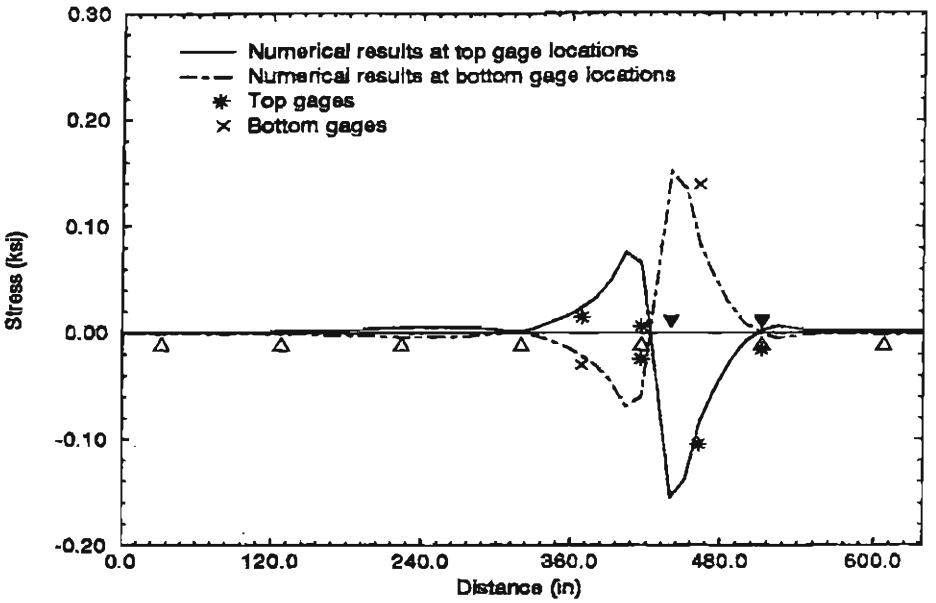

Figure E.5: Normal Stress in Transverse Direction along Gage Line 3 (Case 3C1)

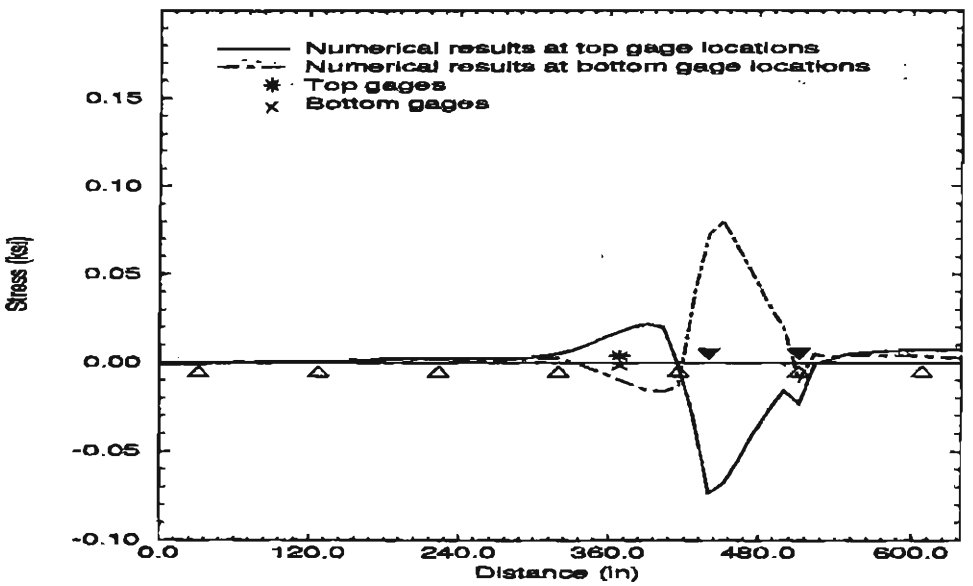

Figure E.6: Normal Stress in Longitudinal Direction along Gage Line 3 (Case 3C1)

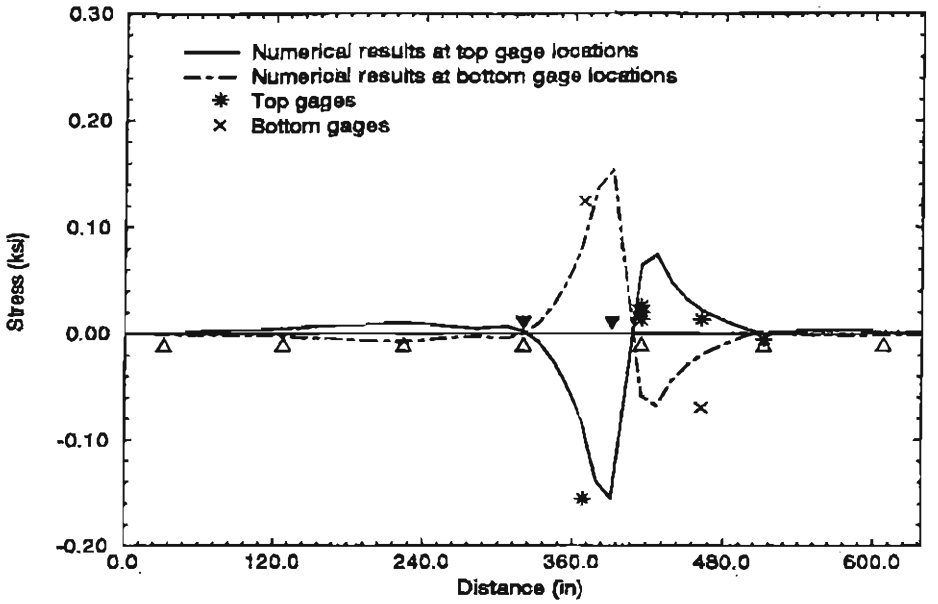

Figure E.7: Normal Stress in Transverse Direction along Gage Line 3 (Case 3C2)

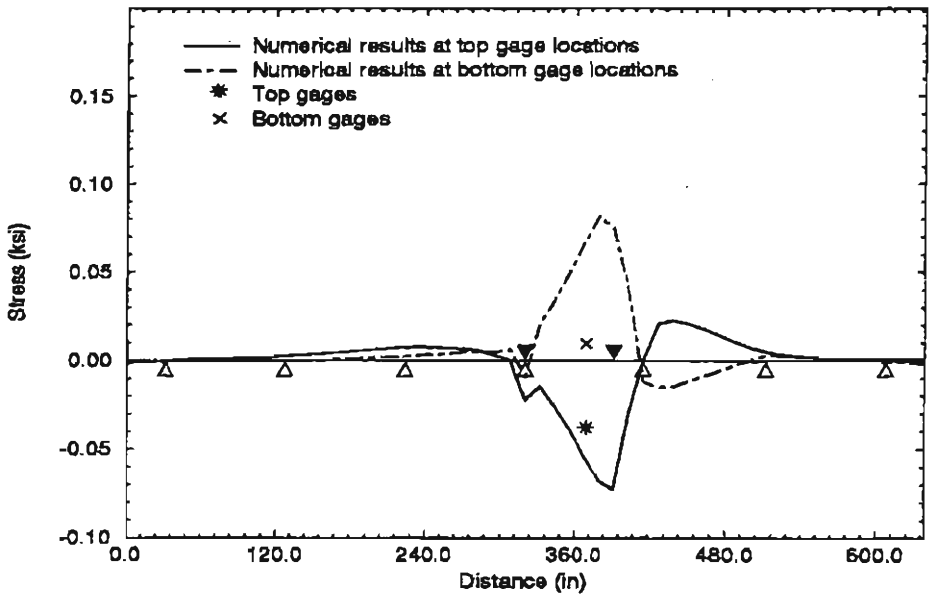

Figure E.8: Normal Stress in Longitudinal Direction along Gage Line 3 (Case 3C2)

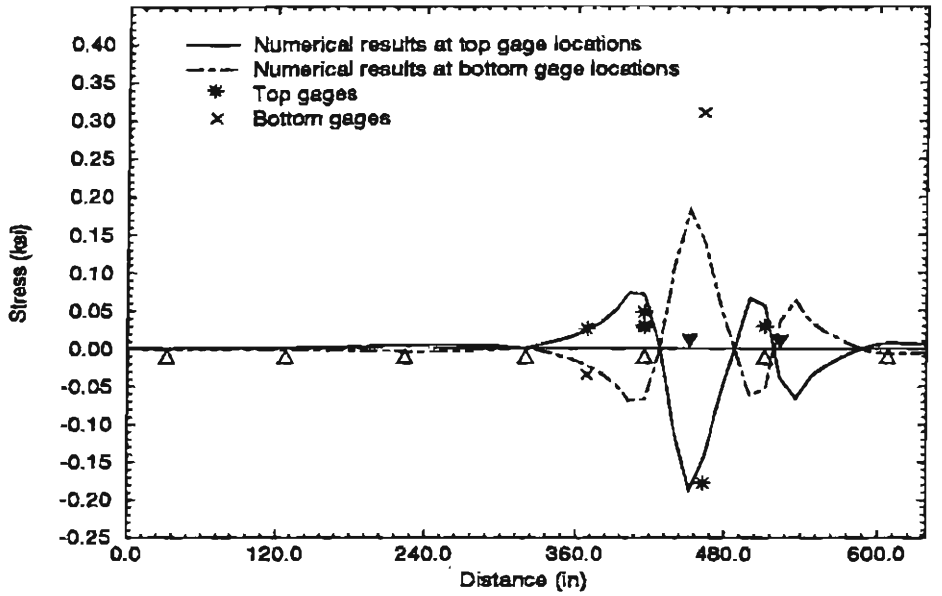

Figure E.9: Normal Stress in Transverse Direction along Gage Line 3 (Case 3D1)

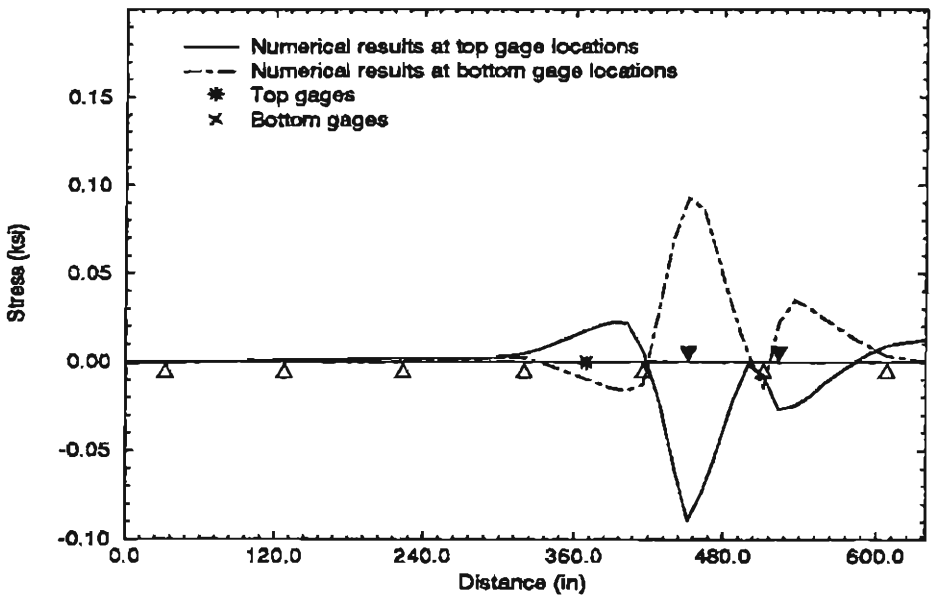

Figure E.10: Normal Stress in Longitudinal Direction along Gage Line 3 (Case 3D1)

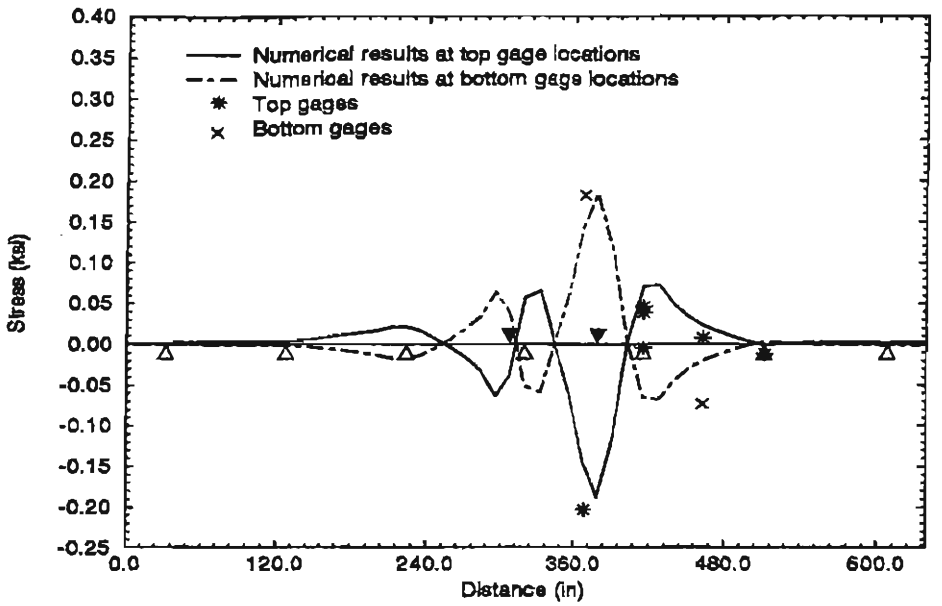

Figure E.11: Normal Stress in Transverse Direction along Gage Line 3 (Case 3D2)

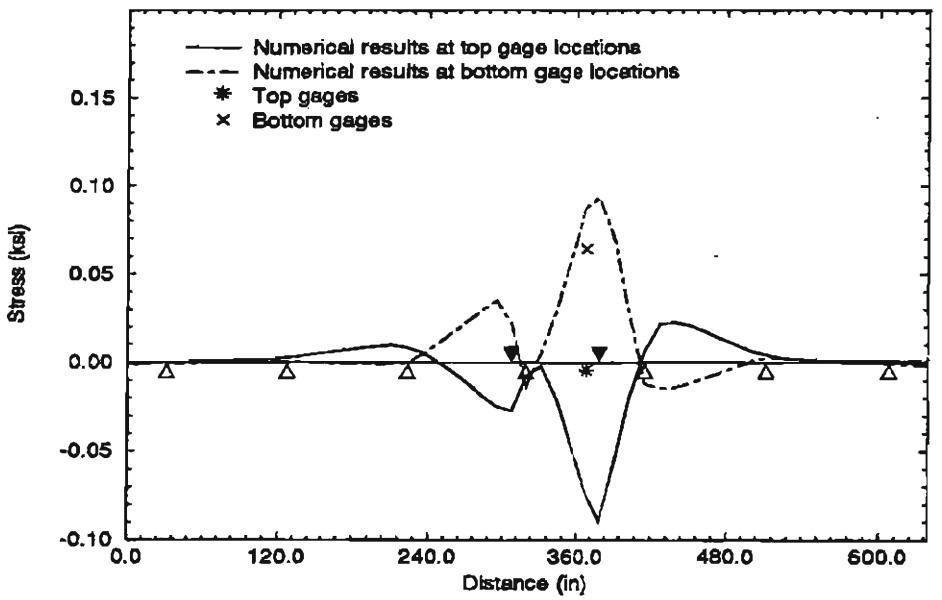

Figure E.12: Normal Stress in Longitudinal Direction along Gage Line 3 (Case 3D2)

Appendix F

COMPARISON OF TEST AND NUMERICAL RESULTS FOR LOAD GROUP 4

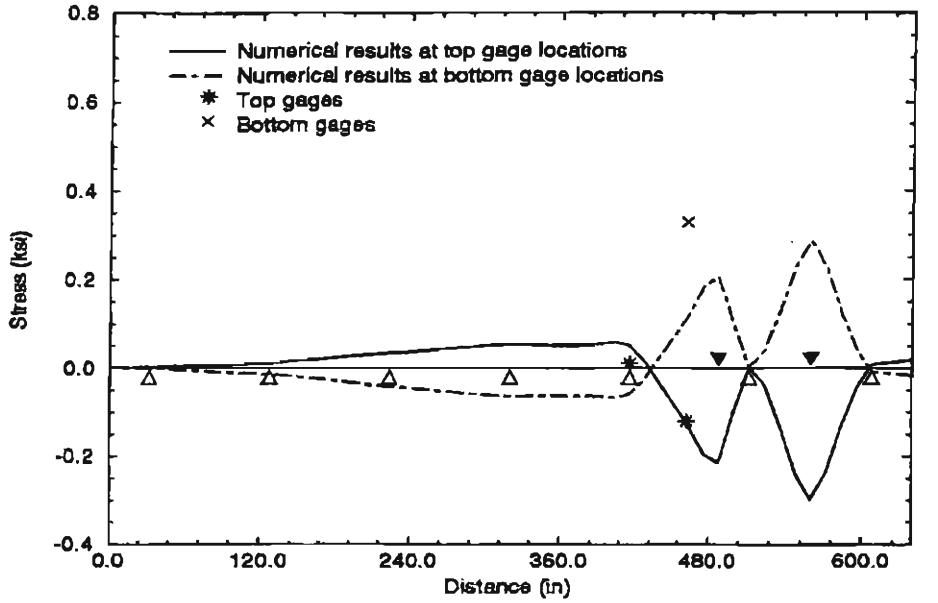

Figure F.1: Normal Stress in Transverse Direction along Gage Line 4 (Case 4A)

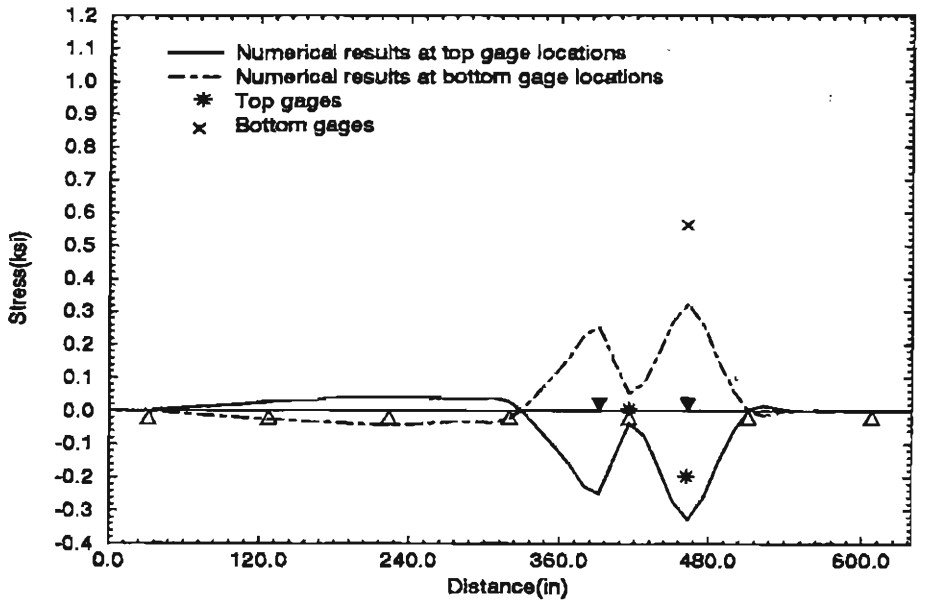

Figure F.2: Normal Stress in Transverse Direction along Gage Line 4 (Case 4B1)

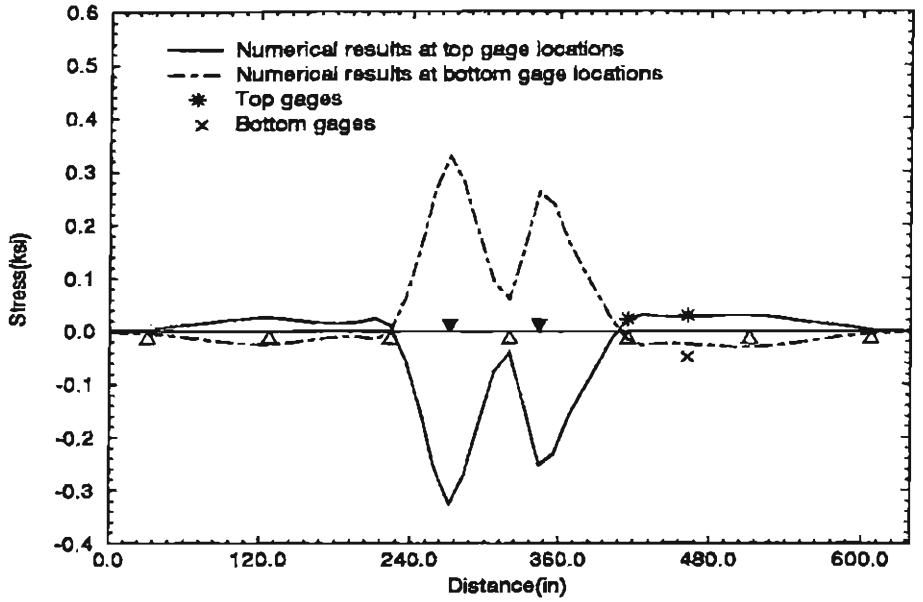

Figure F.3: Normal Stress in Transverse Direction along Gage Line 4 (Case 4B2)

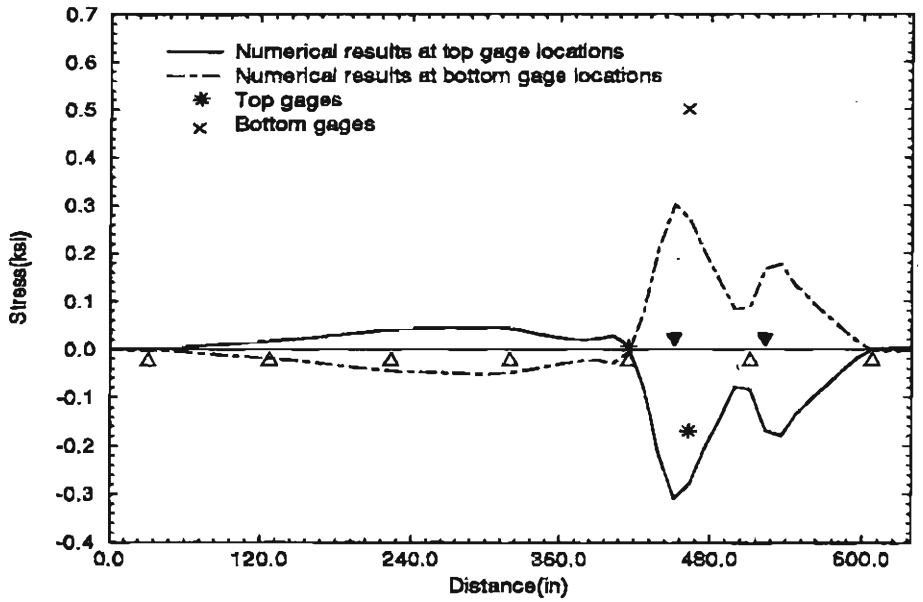

Figure F.4: Normal Stress in Transverse Direction along Gage Line 4 (Case 4C1)

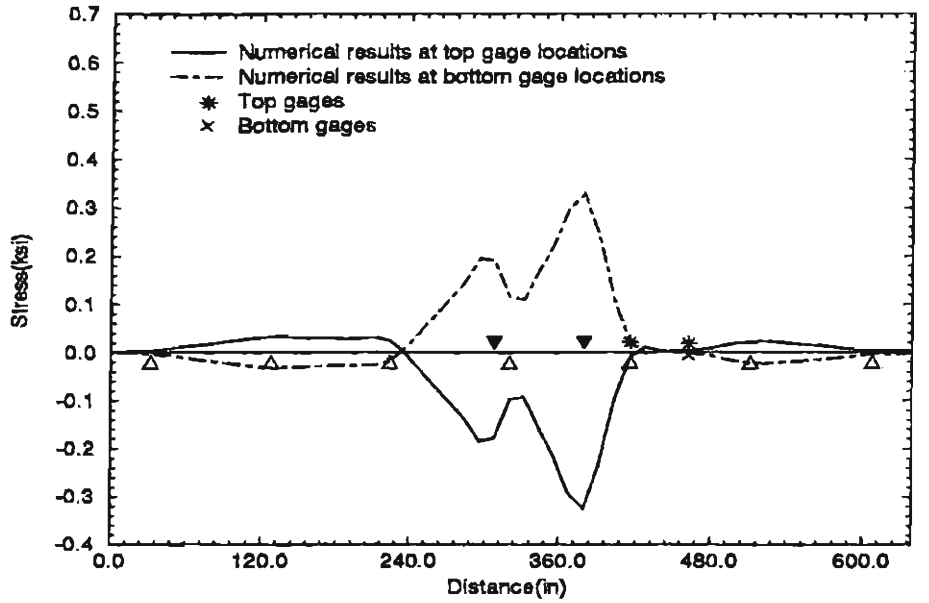

Figure F.5: Normal Stress in Transverse Direction along Gage Line 4 (Case 4C2)

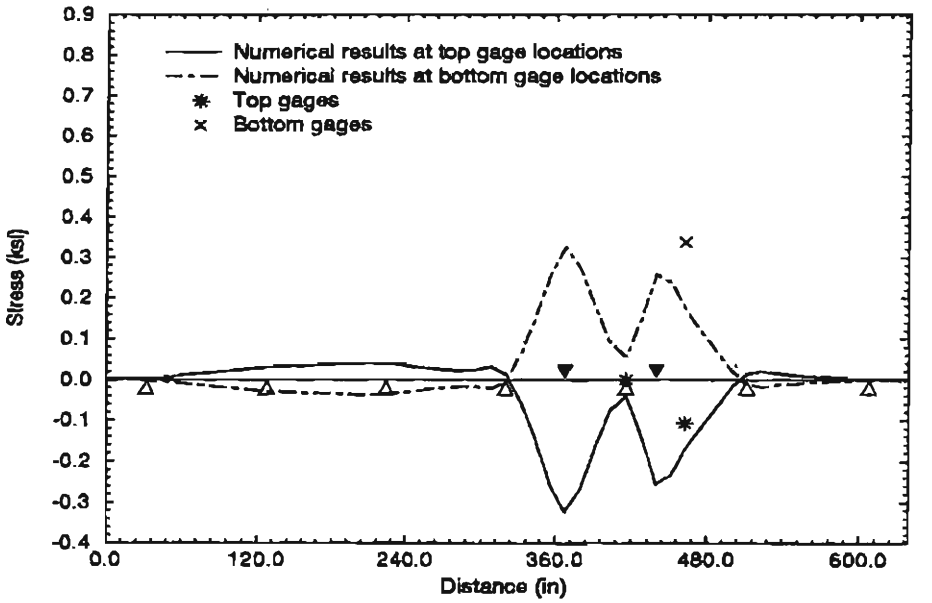

Figure F.6: Normal Stress in Transverse Direction along Gage Line 4 (Case 4D)

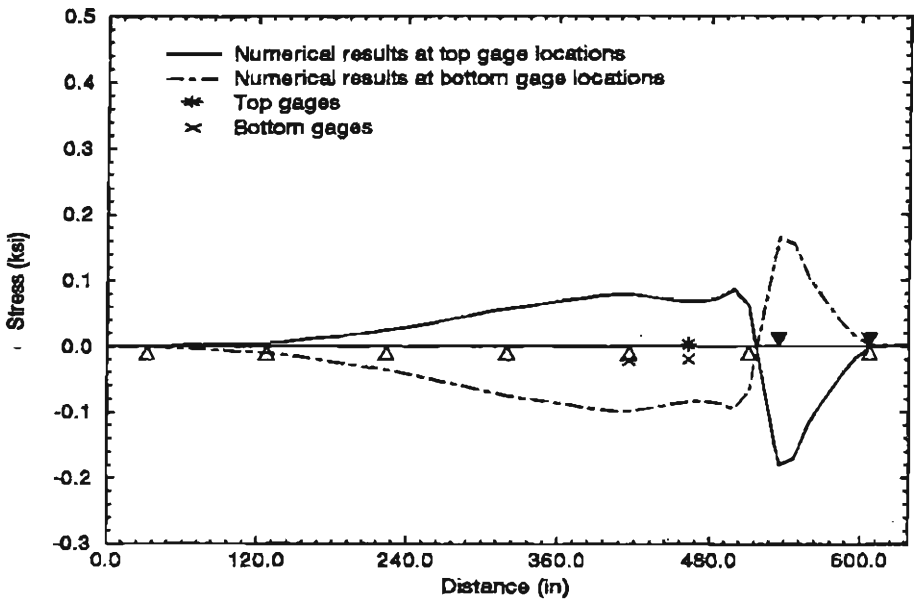

Figure F.7: Normal Stress in Transverse Direction along Gage Line 4 (Case 4E)

Appendix G

COMPARISON OF TEST AND NUMERICAL RESULTS FOR LOAD GROUP 5

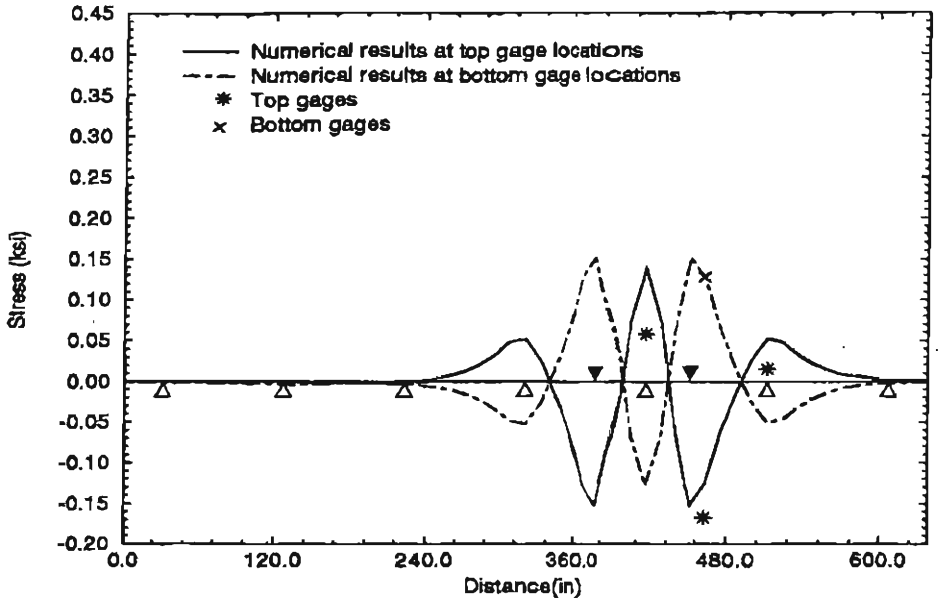

Figure G.1: Normal Stress in Transverse Direction along Gage Line 5, (Case 5A)

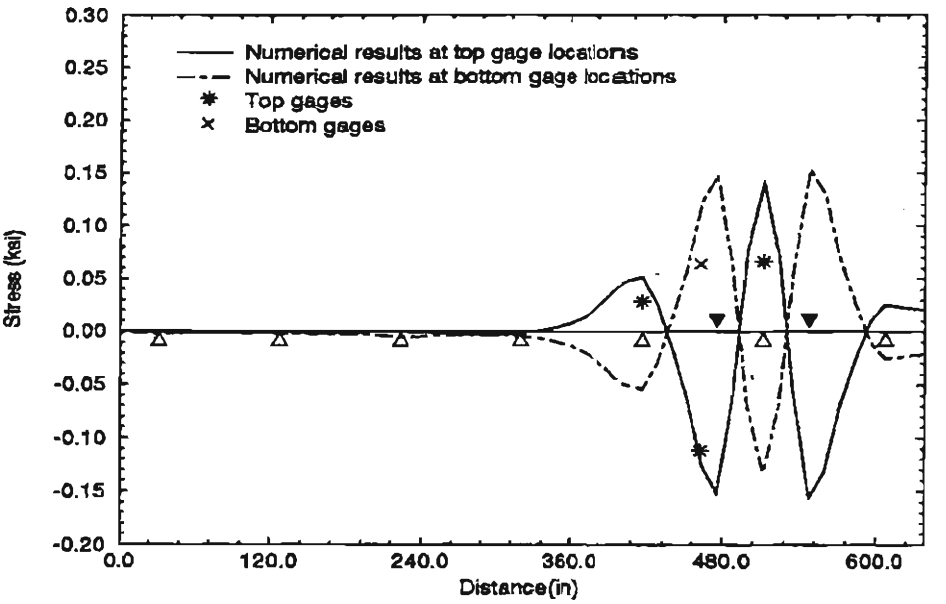

Figure G.2: Normal Stress in Transverse Direction along Gage Line 5, (Case 5B)

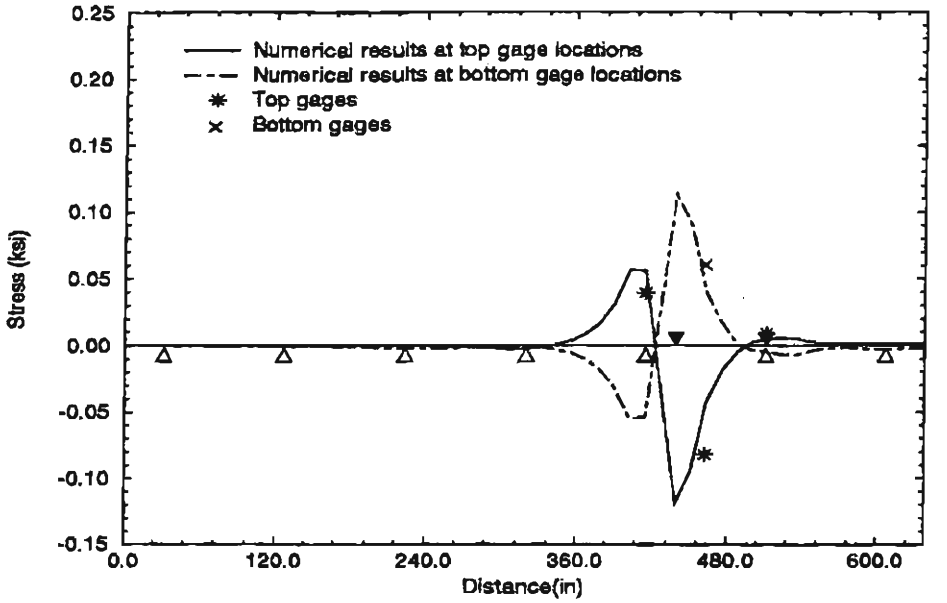

Figure G.3: Normal Stress in Transverse Direction along Gage Line 5, (Case 5C1)

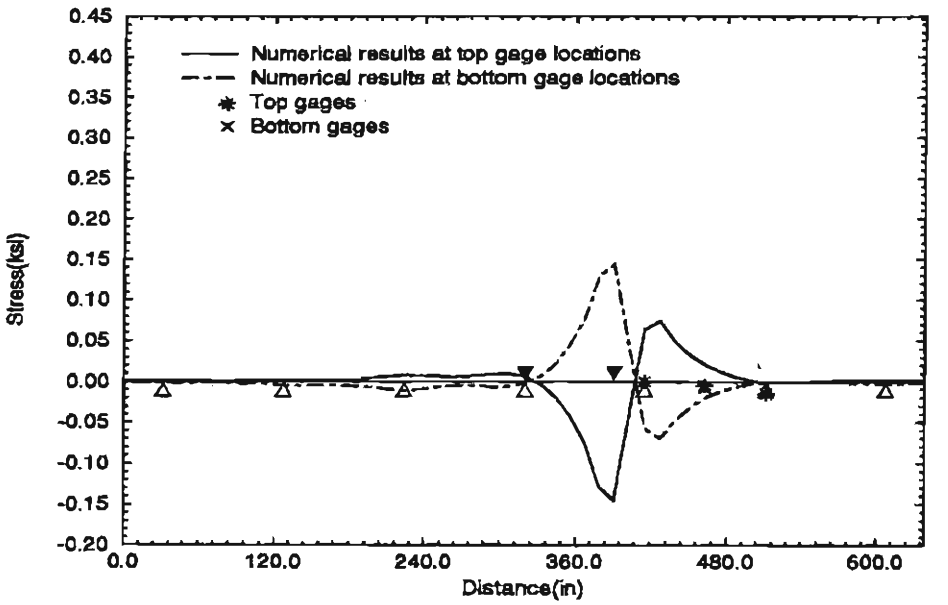

Figure G.4: Normal Stress in Transverse Direction along Gage Line 5, (Case 5C2)

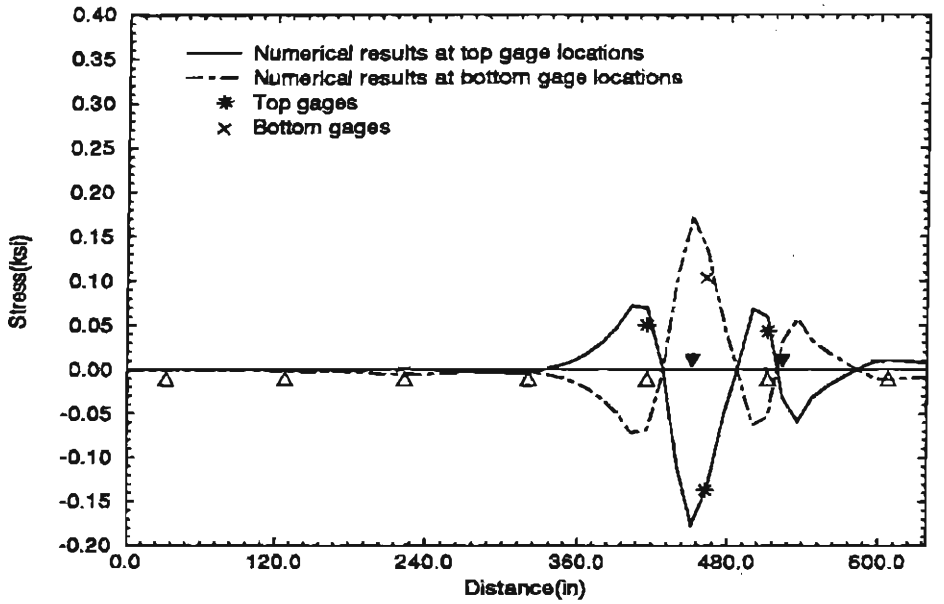

Figure G.5: Normal Stress in Transverse Direction along Gage Line 5, (Case 5D1)

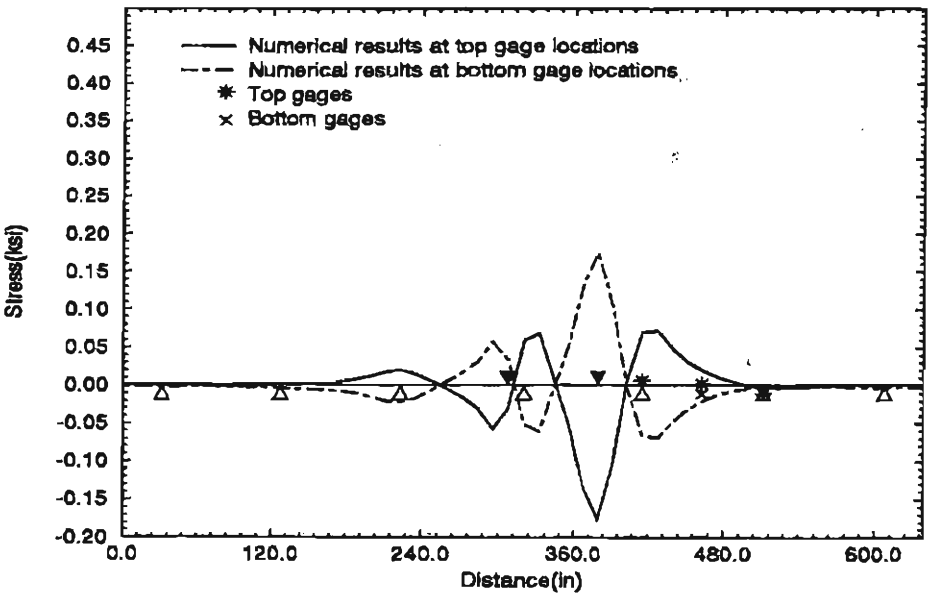

Figure G.6: Normal Stress in Transverse Direction along Gage Line 5, (Case 5D2)